Günter Allmaier

Masterarbeit

Monitoring of the encapsulation of a human rhinovirus in liposome vesicles

Ausgeführt am Institut für

Chemische Technologien und Analytik

der Technische Universität Wien

unter der Anleitung von

Assistant Prof. Mag. Dr. Victor Weiss

und

Univ.Prof. Mag. Dr. Günter Allmaier

durch

Stefan Kirnbauer, BSc

Rosa-Jochmann-Ring 34/2/4, 1110 Wien

Ort und Datum

Stefan Kirnbauer

Ich hoffe hier allen zu danken, die es sich wünschen.

Zuerst bedanke ich mich bei Prof. Günter Allmaier, der mir das Thema und die Arbeit vorgeschlagen und mich so in die Gruppe gebracht hat, sowie Prof. Martina Marchetti-Deschmann, dass ich die Arbeit in ihrer Arbeitsgruppe durchführen durfte. Sie hatte trotz vollen Kalenders immer ein offenes Ohr und Zeit für meine Anliegen, wofür ich ihr ebenfalls sehr dankbar bin.

Ich bedanke mich des Weiteren bei Dr. Victor Weiss, dessen Tatendrang und Anleitung mich durch die Arbeit geführt haben. Seine freundliche Art, unabhängig von guten oder schlechten Ergebnissen, war stets motivierend.

Der mittlerweile geschrumpften Arbeitsgruppe rund um Antonia, Stephi, Jessi, Sam, Vici, Edita, Martin, Cristian und Ernst danke ich, weil wir über die Zeit von Kollegen zu Freunden wurden. „Der Schmäh is' immer g'rennt", wie es so schön heißt.

Auch unser belgischer Kollege Michiel sei an dieser Stelle nicht unerwähnt, ich hoffe du kommst mal wieder vorbei.

Ich danke meinen Bubis, mit denen ich seit jeher viele Feierabende verbracht habe und gefühlt endlos viele Geschichten erlebt habe, dass ich bei euch immer abschalten konnte.

Mein Dank geht auch an Robert Plachy, schon allein, weil er auch mir in seiner Masterarbeit gedankt hat.

Zuletzt gehört mein Dank aber vor allem meinen Eltern Rudolf und Herta, sowie meiner Schwester Eva und meiner Großmutter Ingrid. Ihr habt mir das Studium ermöglicht, mir beigestanden und mich auf Schiene gehalten. Nun dürft ihr sagen: „Endlich ist er fertig".

Acknowledgements

Table of Contents

I

Abstract (Deutsch)

Die Erforschung von Viren und deren Infektionen führte über die letzten Jahrzehnte zu einer Vielzahl an Publikationen, darunter etwa die vor kurzem veröffentlichten Arbeiten zu den Risiken von potentiell krebsbegünstigenden humanen Papillomaviren (HPVs) [1], zoonotischen Viren wie der Vogelgrippe [2, 3] oder auch Viren, die für epidemischen Krankheiten wie Ebola [4] und Denguefieber [5] verantwortlich sind. Bei allen genannten Beispielen ist ein Verständnis des Infektionsprozesses ein potentieller Schritt, um Wirkstoffe zu entwickeln, die effektiv die Verbreitung des Viruses als auch die Infektionsgefahr unterbinden. In diesem Zusammenhang ist besonders die *in vitro* Rekonstruktion des Infektionsprozesses eine kostengünstige und ethisch vertretbare Alternative zu *in vivo* Tierversuchen. Ein mögliches Modelsystem für *in vitro* Versuche sind Liposomen, kleine Lipidvesikel die so erzeugt werden können, dass sie Viren enthalten. Diese Vesikel können dann dazu genutzt werden, den Infektionsprozess zu erforschen.

In dieser Arbeit wurden nun Liposomen verschiedener Größe bzw. Größenverteilungen erzeugt und dazu verwendet, humanes Rhinovirus Serotyp 2 (HRV-A2 bzw. HRV II oder RV-A2) zu verkapseln. Die Liposomen wurden dann unter Verwendung von „gas-phase electrophoretic mobility molecular analysis" (GEMMA) und Rasterelektronenmikroskopie (REM, engl. SEM) untersucht bzw. visualisiert. Die Aufreinigung der hergestellten Liposomen erfolgte durch Gradienten Zentrifugation / Flotation. Des Weiteren wurde eine Natriumdodecylsulfat-Polyacrylamid-Gelektrophorese (SDS-PAGE) sowie nachfolgend „Western Blotting" eingesetzt, um das Vorhandensein von viralen Proteinen zu bestätigen.

Der Prozess der Infektion mit humanen Rhinoviren, wie er *in vivo* nach der Aufnahme in Endosomen passiert, wird durch Acidifizierung induziert. Das synthethische Peptid GALA bildet unter bestimmten Bedingungen Poren in Lipidmembranen und würde so eine kontrollierte Azidifizierung der Liposomen durch Veränderung des äußeren pH-Werts ermöglichen. Als Vorarbeit zu dem künftigen Projektziel der Acidifizierung des Liposomeninnenraums wurden leere Liposomen mit GALA versetzt und mittels GEMMA deren Größe und deren Größenverteilung analysiert.

Neben dem Hauptziel der Arbeit, der Herstellung potentiell HRV-A2-enthaltender Liposomen und deren Charakterisierung und Veränderung mit GALA, wurden weitere Versuche mit grün-fluoreszierendem-Protein (GFP) gelabelten P22 virusartigen Partikeln (engl. VLPs) durchgeführt. Diese wurden ebenso in Liposomen verkapselt und mittels GEMMA wie oben analysiert. Ausserdem wurde der Grad der Fluoreszenz der geformten VLPs mittels eines planaren Fluoreszenzscanner ermittelt.

Abstract

Viruses have been investigated over decades and have inspired numerous publications, with recent work on the risks of viruses like cancer-risk-increasing human papillomaviruses (HPVs) [1], zoonotic viruses like avian influenza viruses [2, 3] or viruses that caused epidemics like Ebola virus [4] and Dengue virus [5]. In any case, a better understanding of infection processes, especially for viruses that cause diseases, is a potential first step of inventing vaccines that are more effective in preventing the spreading of infections or in the best case stopping the infection process itself. In this regard, a reconstruction of the process *in vitro* is a cost-efficient and more ethical alternative to studies involving animals or *in vivo* experiments on human subjects. One potential model system for *in vitro* experiments are liposomes, small lipid vesicles mimicking cell membranes or exosomes.

In this work, liposomes of different average sizes and size distributions were created and used to encapsulate human rhinovirus serotype 2 (HRV-A2 or HRV II or RV-A2). Ultimately, these vesicles are suggested to mimic the situation occurring *in vivo* upon uptake of virus particles in cells prior the transfer of the viral genome through the endosomal membrane and into the cytosol of the infected cell. Liposomes were then characterized via gas-phase electrophoretic mobility molecular analysis (GEMMA) and scanning electron microscopy (SEM). Purification of the prepared liposomes was done using a gradient centrifugation / flotation technique. Subsequently, sodium dodecyl sulfate polyacrylamide gel electrophoresis (SDS-PAGE) with subsequent Western Blotting was done to verify the presence of viral proteins.

The process of infection with HRV, like it occurs after the uptake in endosomes *in vivo*, is stimulated by the acidification of the endosome's core. As a pre-work to the future target of internal acidification of liposomes, empty liposomes were also mixed with the synthetic peptide GALA and analysed using GEMMA. This peptide forms pores in the lipid membrane under certain conditions and thus would enable a controlled acidification from outside the liposomes.

Besides the main aspect of this work, the creation of potentially HRV-A2-containing liposomes and their characterization and modification using GALA, additional efforts were made using green-fluorescent-protein (GFP) labeled P22 virus-like particles (VLPs) instead of HRV-A2 for encapsulation in liposomes to verify particle encapsulation within vesicles. These liposomes were then analysed by means of GEMMA. The fluorescence of the GFP-labeled P22 virus-like particles was also measured using a planar fluorescence laser scanner.

Introduction

Human rhinovirus (HRV)

Human rhinoviruses are the largest genus of the family *Picornaviridae* with more than 100 serotypes that were first described in the 1950s [6]. They are commonly known as "common cold viruses", as they are involved in infections of the respiratory system. Picornaviruses like HRV are made out of 60 copies each of the four capsid proteins VP1 through to VP4 with an icosahedral structure [7]. The proteins VP1, VP2 and VP3 are exposed at the viral surface, VP4 is found inside the shell in contact with the positive-sense, single-stranded RNA of approx. 7100 bases length [6, 7]. *Picornaviridae* are nonenveloped, which means that there is no viral envelope surrounding the proteinaceous capsid.

They can be classified into two groups depending on which receptor they use for binding to cells. There is the major group that binds to the intercellular adhesion molecule 1 (ICAM-1) receptor, while the minor group binds to the low-density-lipoprotein (LDL) receptor [6, 7]. Newer research has also identified Cadherin related family member 3 (CDHR3) receptors for host cell infection [8]. Rhinoviruses can be additionally classified into groups A and B depending on their sensitivity towards antiviral compounds [7].

The virus used in this work, human rhinovirus serotype 2 (afterwards denoted as HRV II or HRV- A2), belongs to the minor group and binds to the LDL receptor, and is included in antiviral group B [7]. It has a size of approx. 30 nm (based on cryo electron microscopy). The structure derived from x-ray crystallography at a resolution of 2.6 Å is shown in Figure 1.
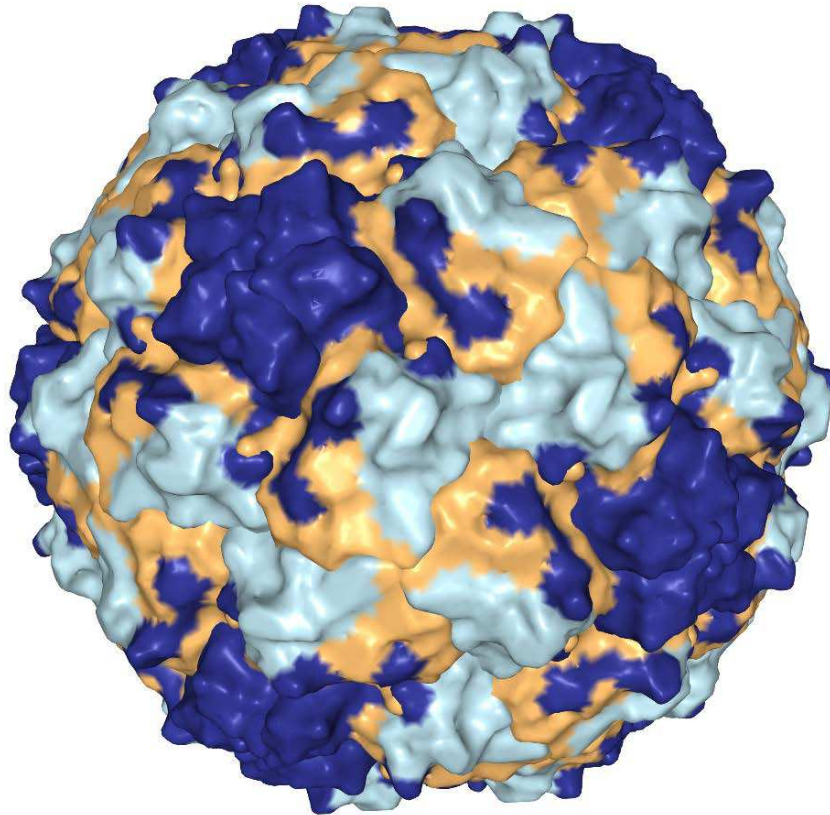
Figure 1: 3D model of human rhinovirus serotype 2. (Blue: VP1; Light blue: VP2; Orange: VP3) (https://www.rcsb.org/structure/1FPN, 26.11.2019 – 13:45).

Figure 2 shows the infection process *in vivo,* where virions are taken up via receptor-mediated endocytosis [8]. At first, the virus is binding to the LDL receptor at the cell surface. It is then taken up into the cell inside an endosome. The pH within endosomes is changing naturally as they ultimately become lysosomes. During the acidification from a pH of around 6.5 to 4.5, the uncoating of the virus is promoted and the transfer of its RNA through the endosomal membrane into the cytosol takes place to ultimately infect the cell. What remains inside the endosome is the empty viral capsid.

Figure 2: Scheme of the HRV-A2 infection process in-vivo. Acidification is foreshadowed by the intensification of the orange color of endosomal vesicles.

Liposomes

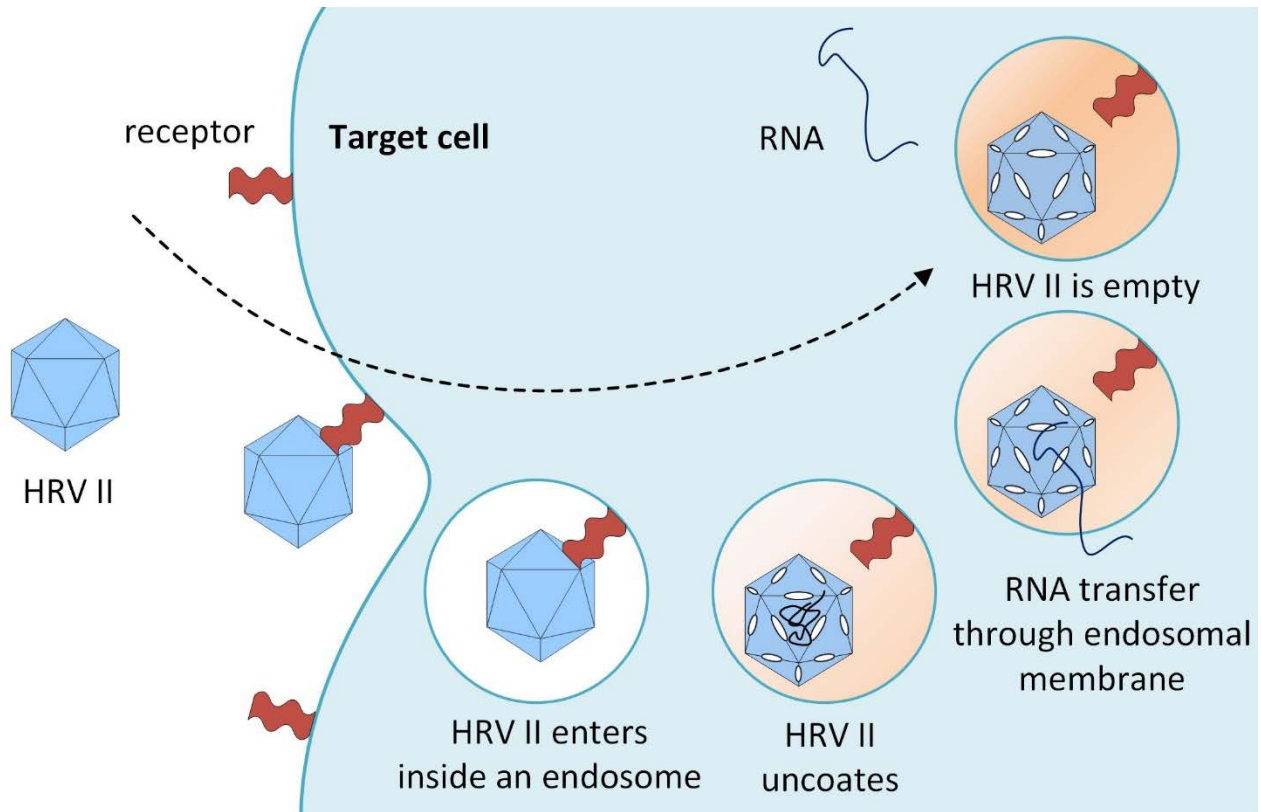Liposomes are vesicles made of one (unilamellar) or multiple (multilamellar) phospholipid bilayers with a diameter between 25 nm to several micrometers, depending on their source and way of formation [9, 10]. They were first described by Alec Bangham in a paper published in 1965 [11]. While his work focused on the diffusion of ions through the phospholipid membrane, the research on liposomes has since led to their use as drug carriers in medicine, cosmetics or nutraceutical applications [9]. An example of the advance and the opportunities of such liposomal carriers is provided by the development of tumor-targeting liposomes that are trigger-able by ultrasound to release an anticancer agent at the tumor site [12].

Besides their use as carriers, liposomes are also used as model systems, for example to gain a better understanding of the viral infection process [13] or viral-associated behavior of membranes [14].

Figure 3 shows a phospholipid bilayer found with liposomes. Figure 4 demonstrates one advantage of bilayer vesicles over monolayer vesicles (micelles): the presence of the inner hydrophilic core, which can be used to encapsulate bigger as well as hydrophilic molecules.
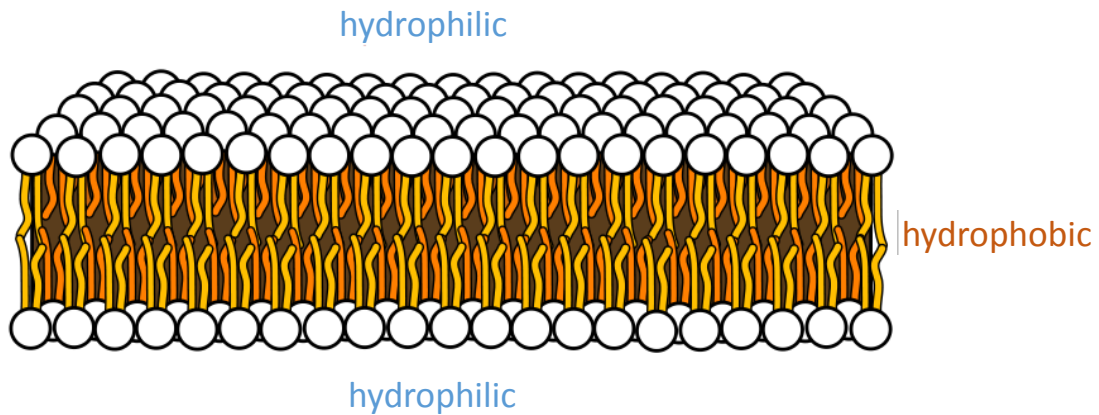

Figure 3: Phospholipid bilayer, schematic.
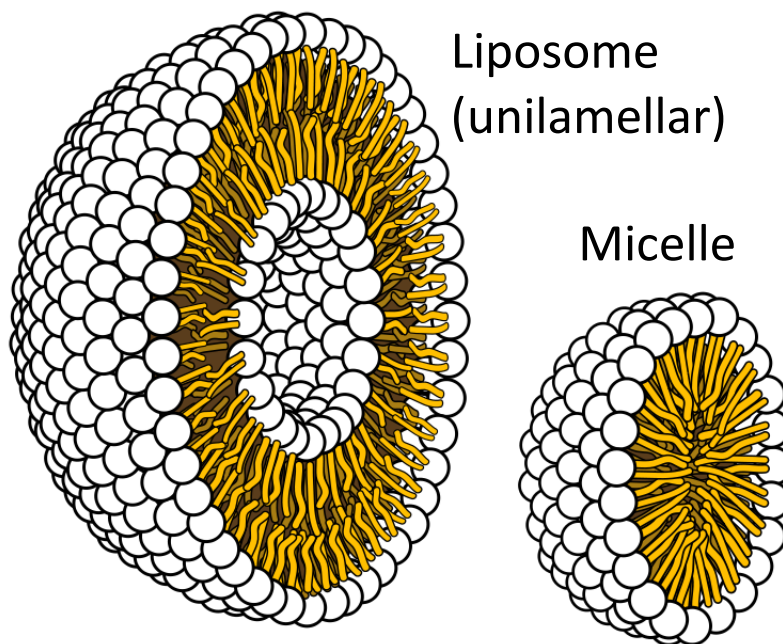(https://de.wikipedia.org/wiki/Liposom#/media/Datei:Phospholipide_in_Wasser.svg, 27.11.2019 - 13:45)

Figure 4: Liposomes (bilayer) in comparison to micelles (monolayer).
(https://de.wikipedia.org/wiki/Liposom#/media/Datei:Phospholipide_in_Wasser.svg, 27.11.2019 - 13:45)

For the creation of liposomes different methods are known and described in literature, like sonication, micro emulsification or lipid film hydration, to name a few. They all have four general steps in common [9]: Drying down lipids from organic solvent, dispersing the lipid in an aqueous media, followed by purification of the resulting liposomes and analysing the final product.

For this work, lipid film hydration was used to create the liposomes as described by Weiss et al. [15]. In short, first the lipid molecules are dissolved in a mixture of chloroform and methanol. Then the solvent is evaporated using a stream of nitrogen and a thin lipid layer is formed, which is then dried *in vaccuo* to remove remaining organic solvent. Finally, a dispersion in an aqueous solution is prepared. A scheme of the procedure is shown in Figure 5, the actual description of the preparation is found in the chapter Liposomes in the Materials and Methods section.
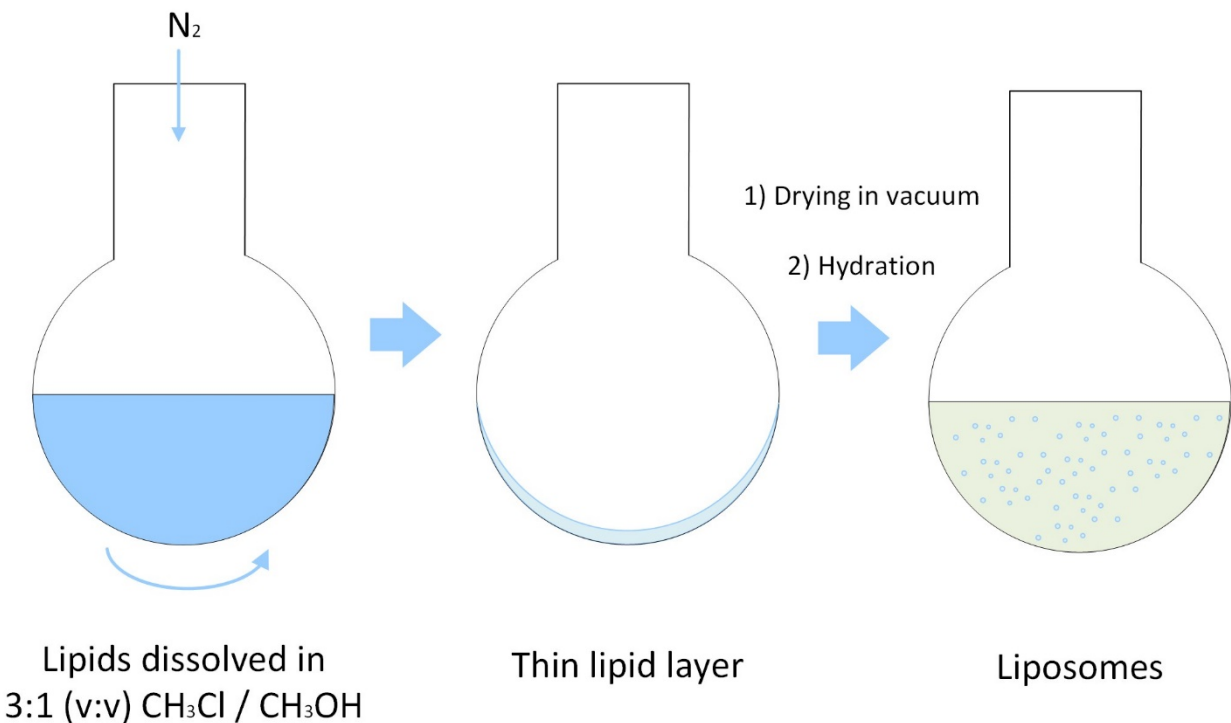
Figure 5: Thin lipid film hydration technique, scheme.

With this technique, liposomes of different sizes and lamellarity (multi- down to uni-) are formed. The liposomes are then extruded using a membrane of a specific pore size to receive unilamellar liposomes [16], whose average hydrodynamic diameter is close to the pore size of the filters [17]. For the extrusion, the solution containing liposomes is taken up into a syringe and mechanically pushed through the membrane for several times. Figure 6 shows an explosion sketch of an extruder as it was used during this work (without syringes).

Figure 6: Explosion sketch of the extrusion device.

(https://avantilipids.com/divisions/equipment-products/mini-extruder-assembly-instructions, 1.12.2019 - 10:42)

Gas-phase electrophoretic mobility molecular analysis (GEMMA)

Gas-phase electrophoretic mobility molecular analysis is a method to determine the electrophoretic mobility diameter (EM-diameter) of molecules, noncovalent complexes and (bio-) nanoparticles in the gas-phase. The EM-diameter is the diameter attributed to a particle based on its mobility in an electrical field, which is used to separate and measure the different particle sizes found with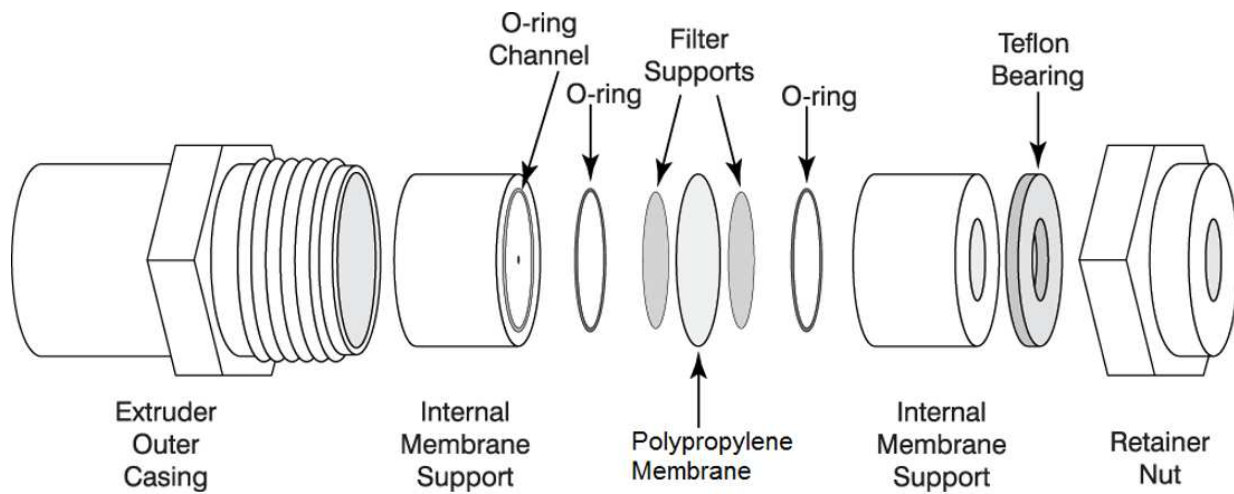in a sample (see Differential Mobility Analyser below). In case of a spherical particle, the EM-diameter corresponds to the actual surface-dry size of a particle [15].

GEMMA therefore is a possible alternative to the well-established methods of dynamic light scattering (DLS), atomic force microscopy (AFM) or electron microscopy (EM) for the size determination of nanoparticles. Moreover, it has some advantages over the aforementioned methods. In DLS, there is the problem that in heterogeneous samples, the mean particle diameter is strongly biased towards larger constituent sizes in the presence of larger particles [18], while AFM and EM demand a more expensive setup as well as a more time-consuming sample preparation. A general advantage of GEMMA is that due to the "soft ionization" and absence of harsh conditions (high temperature, high vacuum, etc.), proteins for example can be measured in a native state.

8

Additionally, efforts were made to create correlations of the EM-diameter to the molecular weight (MW) of the particles, as done for example for proteins [19, 20] or polysaccharides [21]. This makes it an alternative for the MW determination using for example size exclusion chromatography (SEC) or gel electrophoresis, making GEMMA a very versatile technique overall.

The GEMMA system consists of the following parts: (i) an electrospray unit with a chamber for charge reduction to form single-charged but otherwise native analytes, (ii) a differential mobility analyser (DMA) for classification of the polydisperse aerosol, i.e. separating the polydisperse aerosol into monodisperse fractions, and (iii) an ultrafine condensation particle counter (CPC) for the detection and quantification based on the particle number count. The result of the measurement is a spectrum of the size distribution against the counts per time.

Aside from analysing samples, as mentioned above, the GEMMA system can also be used to separate different particle sizes within a sample. By exchanging the CPC for a collection device (electrostatic precipitator, ENAS), selected particle sizes can then be collected.

The individual instrumental parts are described in detail in the following sections.
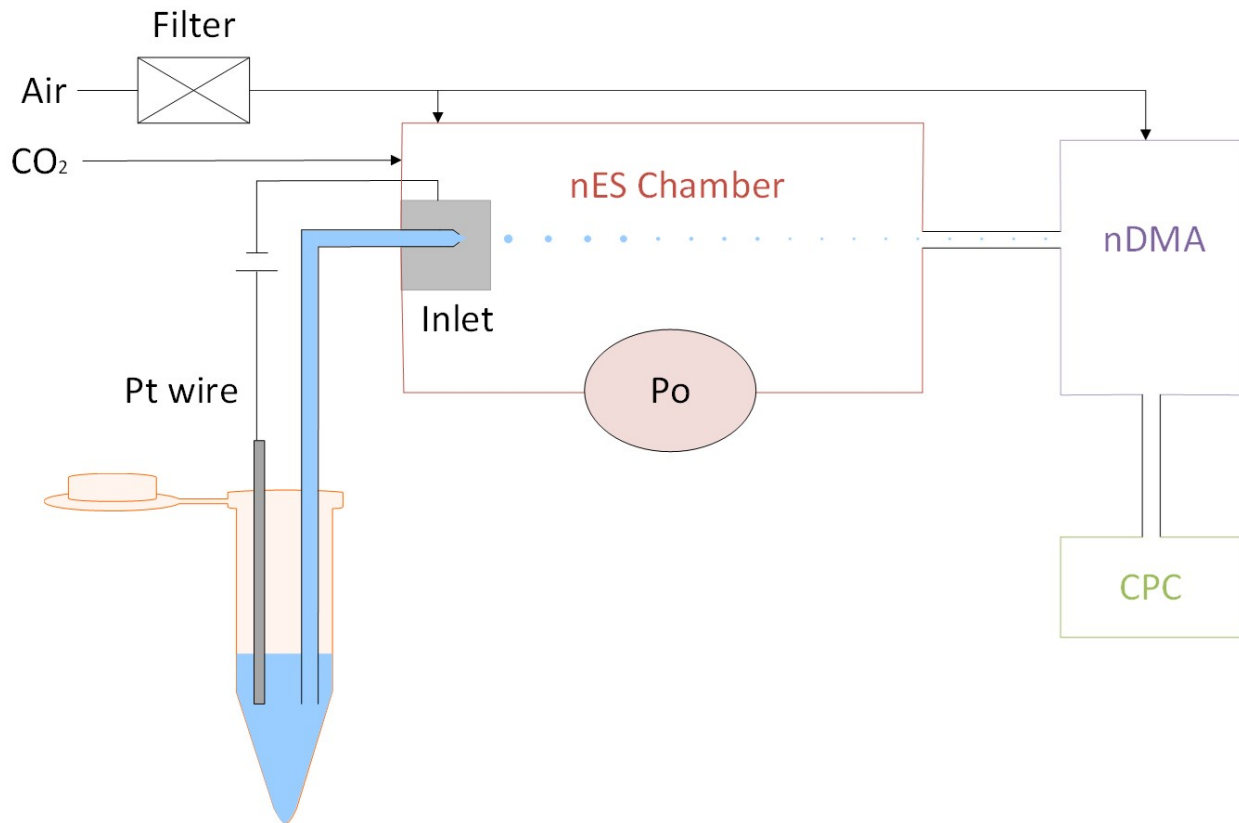

Figure 7: GEMMA setup, schematic.

Electrospray

The electrospray process is needed to create an ionized aerosol of polydisperse nanoparticles from a volatile electrolyte solution.

In a sealed sample chamber with the vial, a fused silica capillary and an electrode (platinum wire) are immersed in the liquid sample. The capillary connects the sample with a metal inlet, which acts as the second electrode and is screwed into the spray chamber.

A pressure difference (*capillary pressure drop*, overpressure in the sample chamber) is set between the sample and spray chamber. This way, the analyte solution is pushed through the capillary. Applying an electrical current between the immersed platinum wire and the target plate of the inlet leads to an electrical field at the tip of the capillary.

For analytes that are dissolved in a volatile liquid with a high number of ions (e.g. ammonium acetate) a conical spray is created at the tip. This spray can occur in different modes, like corona discharge (at high electrical field strengths) and dripping mode (low electrical field strength) or a variety of cone-jet modes, of whom the stable cone-jet is the preferred mode for practical use.

The small charged droplets that are created ideally contain only one analyte molecule each. The sprayed droplets are taken up in a gas stream of compressed, dried ambient air mixed with a low amount of CO_2 (which helps stabilizing the spray), where they effectively dry, leaving the particle in aerosol form.

The drying droplets would normally undergo disintegration processes as for example in an electrospray ionization (ESI) source of an ESI mass spectrometer (MS) [22]. Contrary to an ESI spray however, in GEMMA the creation of small multiply charged analytes is not wanted. Therefore, the particles are dried in a charge-reducing atmosphere.

Charge reduction

The charge reduction can be conducted in a variety of ways, for example using a corona discharge, soft X-ray radiation or α-radiation. For this work we used a source of α-radiation, Polonium (^{210}Po), which creates an atmosphere of bipolar ions.

Polonium is a naturally occurring element that emits α-particles, which are identical to a Helium nuclei, as it decays.

The ionization is induced through the high energy of these α-particles of about 5.3 MeV [23] upon collision with air molecules within the sealed chamber.

Although the α-particles may only travel a range of about 3.8 cm in 1 atm, they create approximately 10^5 ion pairs [24]. In this ionized atmosphere, the liquid droplets or solid nanoobjects effectively lose their surface charge.

As a result of the charge reduction, the droplets dry without the aforementioned fragmentation. Additionally, while the majority of analytes is then uncharged, a small fraction of molecules becomes singly charged (based on the work of Fuchs [25]) and even less become multiply charged (based on the equations of Wiedensohler [26]).

A table of the calculated charge fractions can be found in the Instructional Manual for the TSI 3480 Electrospray Aerosol Generator, Table B-2, p. B-6 from 2003. A part of that table is found below.

The mostly singly charged, airborne analytes are then entering the DMA through a tube that connects it with the spray chamber.

Table 1: Midpoint Particle Diameters and Fraction of Total Particle Concentration that carries n charges

Particle diameter (midpoint) [nm]	Fraction of Total Particle Concentration that carries this number of positive charges			
	+1	+2	+3	+4
10	0.0411	0	0	0
15	0.0638	0	0	0
21	0.0866	0.0001	0	0
28	0.1145	0.0007	0	0
38	0.1446	0.0027	0	0
48	0.1650	0.0056	0	0
59	0.1841	0.0105	0	0
74	0.2000	0.0180	0.0005	0
93	0.2113	0.0279	0.0016	0
104	0.2148	0.0339	0.0028	0
117	0.2167	0.0406	0.0046	0.0001
132	0.2167	0.0477	0.0072	0.0003
150	0.2149	0.0552	0.0105	0.0006
170	0.2113	0.0627	0.0149	0.0012

Differential Mobility Analyser

The DMA consists of a coaxial setup of electrodes, with an inner cylindrical electrode with a slit and a ring-like electrode surrounding it. The polydisperse sample aerosol is introduced in between those electrodes from the top.

A sheath flow is also introduced parallel to the sample aerosol. Because of the sheath flow, the aerosol is moving down between the electrodes. By then applying a potential between the electrodes, an electrical field is created. This affects the charged particles based on their mobility and thus their size.

The polarity of the electrodes is set so that the charged particles are attracted towards the central high-voltage electrode and the slit. For a given potential / electrical field, only particles within a narrow range of mobility (and thus size) might enter the slit. This way a monodisperse aerosol is received. This monodisperse aerosol is then entering the CPC.
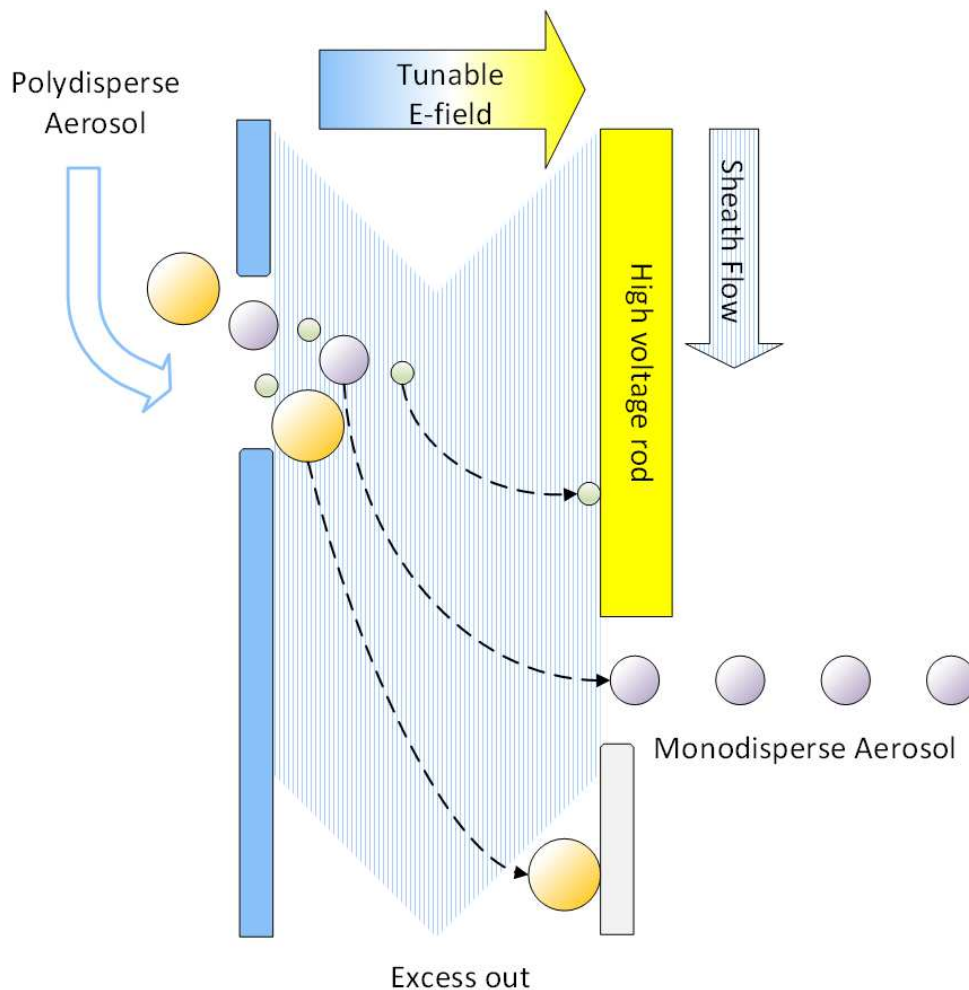

Figure 8: Differential mobility analyser, schematic.

Condensation Particle Counter

In the condensation particle counter the incoming, dry and singly charged nanoparticles from the DMA are artificially enlarged using butanol which enables the system to optically measure particles down to a size of around 3 nm. Normally, using only optical detection, nanoparticles are only measurable down to a size of approximately 100 nm [27].

First the nanoparticles enter a saturated n-butanol atmosphere inside the saturator part of the device.

The particles together with the butanol are then transported within the gas stream to the condenser part. There, the butanol vapor starts to condensate onto the particles (nucleation) as the temperature is reduced. The droplets are then passing an optical detection consisting of a laser and a photodiode. The measured scattering of the light from these particles is collected using a mirror and then measured using the photodiode.
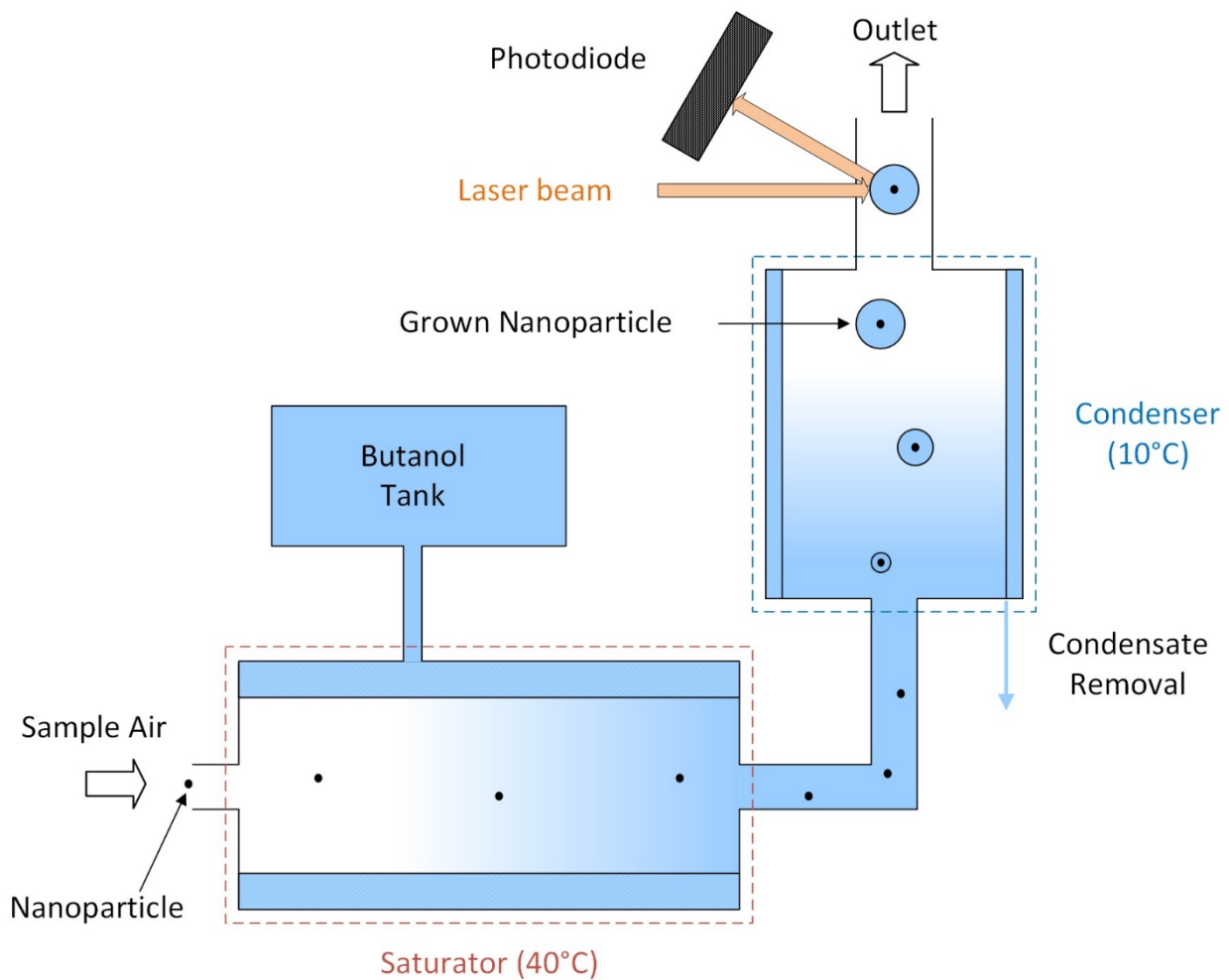

Figure 9: Condensation particle counter, schematic.

14

Collection device

For the collection of liposomes an electrostatic precipitator (also known as electrostatic nanoparticle sampler, ENPS, or electrostatic nanometer aerosol sampler, ENAS) was used.

The principle behind the device is that the singly charged and dry aerosol particle to be observed enters in a flowing gas stream and is deposited on a substrate (for AFM) or a sample holder (like a TEM grid, or glass slides [28]) by electrostatic attraction using an induced electrical field. According to the manufacturer of the precipitator used in this work [28], particles of a size between 2-100 nm can be collected.

Electrostatic precipitators are also commonly found in industrial gas cleaning [29, 30] as alternatives to scrubbers or filters. They are also used to collect aerosol particles for studies regarding for example air pollution in close proximity to freeways [31].

An electrostatic precipitator can be run as a one-stage system or two-stage system. The one-stage system combines the charging of the particles and the precipitation in one step. A two-stage system consists of a separated pre-charger (as in case of this work) and an electrostatic precipitator.

The two-stage system offers advantages over the one-stage system: The electric field in the collection stage can be higher than in an one-stage system due to the lack of sharp discharge points [30], thus increasing the collection efficiency. Specifically for the precipitator used in this work (TSI 3089 Nanometer Aerosol Sampler), the collection efficiency was found to increase with a higher voltage and decrease with the gas flow rate [31].

Techniques for the verification of the encapsulation

By using GEMMA alone, the encapsulation of the virus in liposomes is not detectable as shown later. Therefore, other techniques had to be used in order to provide viable information on the success of the encapsulation.

Scanning electron microscopy (SEM) was used in order to visualize the liposomes, and Western Blotting and SDS-PAGE to verify viral proteins.

Scanning electron microscopy

In electron microscopy (EM), a beam of electrons is used instead of light to examine and visualize a sample. The advantage over light microscopy is mainly based on the achievable resolution and thus the magnification possible due to the usage of electrons. The disadvantage on the other hand is that living organisms or cells are not measurable due to the high vacuum needed to prevent scattering of the electrons after contact with atmospheric atoms.

Depending on the measurement technique, scanning (SEM), transmission (TEM), scanning transmission (STEM) or reflection electron microscopy (REM) can be distinguished. Based on the technique, different interactions of the electrons are measured.

With SEM, which is used in this work, the electron beam is used to map the surface of the sample. Therefore, the energy of the beam does not have to be as high as in transmission techniques. The interaction of the electron beam with the surface results in many observable effects: The signal received is a composition of secondary electrons, backscattered electrons, x-rays as well as Auger electrons and heat radiation. Different detectors are used in conjunction to receive a final topographical image.

Methods of sample preparation are numerous. In this work metal sputtering together with negative staining was used. Sputtering is used to cover the surface with a conductive metal coating that prevents charging of the specimen, which would otherwise lead to artifacts. It also increases the amount of secondary electrons that can be detected from the surface of the specimen in the SEM and therefore increases the signal to noise ratio [32].

Negative staining is a technique where the analyte is embedded in a layer of an electron-rich heavy metal with high opacity, like uranyl acetate or phosphotungstic acid [33, 34]. Due to its high opacity, the layer around the specimen strongly reflects and absorbs the incoming electron beam while leaving the specimen (for example virus, bacteria) untouched. This results in a high contrast between the background and the specimen.

Sodium dodecyl sulfate polyacrylamide gel electrophoresis (SDS-PAGE)

SDS-PAGE is a technique to separate proteins based on their mass in an electrical field in the liquid phase.

For this technique polyacrylamide gels are used. The polymerized gel is made from acrylamide to cast the gel and bisacrylamide for cross-linking. Due to the cross-linking it acts like a sieve, with a pore size depending on the used composition of monomers.

For an SDS-PAGE the proteins are denatured using heat or chemicals together with SDS, which binds to amino acids and effectively shields their charge, while creating a constant negative charge across the protein. As a result, due to repulsion, the protein chain is linearized. Depending on the size and thus mass, the protein chain may pass the gel pores faster or slower. This results in a separation over time as the proteins pass the gel with different speed. The advantages of the denaturation is that the speed at which the proteins pass the gel is only dependent on their size (mass), resulting in single bands for specific protein species, and that the proteins are all moving in the same direction due to the constant negative charge.

Mostly, discontinuous systems are used, meaning that the gel consists of the *stacking* part (bigger pore size) followed by a *separating* part (narrow pore size). Additional to the different gel areas, two different buffers systems are used. The most commonly used buffer system is the Tris-HCl / Tris-Glycine system, with a lower molarity Tris-HCl solution at pH 6.8 as loading buffer for the stacking gel, and a higher molarity Tris-HCl solution at around pH 8.8 as running buffer.

The sample is applied on the stacking part of the gel. Because SDS is used, the mobility is only dependent on the size. The highest mobility ions have low electrical field strength (chloride) and lowest mobility ions have a high electrical field strength (glycine) when an electrical field is applied. Between these ions, an electrical field gradient is created. This results in the stacking of the different proteins in between the ions in order of their mobilities and a slower diffusion into the gel with less agglomeration and a concerted entry of the protein fractions into the separating gel.

When they enter the separation part of the gel, they are suddenly retarded by the frictional resistance due to the smaller pore size of the gel.

Glycine, because of its small size, is not that affected by the frictional resistance and can overtake the proteins. This neutralizes the field gradient, and the proteins leave the stack to pass through the separation gel as long as an electrical field is applied.

After the separation the gel can be stained to visualize the proteins. There are different methods for the staining of polyacrylamide gels, in this work silver staining was used.

The staining process using silver for proteins in polyacrylamide gels has been introduced by the end of the 1970s by Switzer et al. [35], who used cupric-silver compound for staining. Today, the most common used compounds are silver nitrate and ammonia silver complexes [36]. They stain the protein after reducing the silver ions that are binding to the protein, preferably at negatively charged side chains of the amino acids (Asp, Glu, His, Cys, Lys), to metallic silver. With silver staining, the detection limit of proteins is within the range of 1-10 ng, while it is around 50-100 ng for the popular Coomassie blue staining [37].

The basic steps for silver staining are 1) fixation of the proteins at their spot on the gel (while removing SDS) using mixtures of ethanol and acetic acid, 2) sensitization to increase the sensitivity using a so-called sensitizer like sodium thiosulfate [36, 37], 3) incubation with the silver compound and 4) development using formaldehyde, which reduces the silver and thus gives the protein spots a brownish to black color. When the development has progressed to a satisfying coloration, the development is stopped using acetic acid.

There is also research using fluorescent complexes, where silver binds to the proteins and then a fluorescent probe is added that binds to silver, thus omitting the reduction step in the traditional staining procedures [38].

Western Blotting

Western blotting was first described by Towbin et al. in 1979 [39]. It is a method where a protein can be specifically detected using antibodies.

For this method, first a SDS-PAGE is used to separate the proteins present in the sample. Depending on preliminary sample preparation, the sample may contain a high or low number of different proteins, resulting in more or less bands on the gel.

After the separation on the gel, the proteins are immobilized onto a membrane using an electrophoretic transfer [40]. This step is followed by the blocking of the free area on the membrane to avoid non-specific binding of the antibodies used. Afterwards follows the first incubation using an antibody that specifically binds to the protein of interest. Excess antibody is then removed by washing the membrane.

Then a second antibody, which is a conjugate with an enzyme, isotope or a fluorophore [40], is added for detection. The second antibody binds to the first antibody, resulting in a protein: antibody: antibody complex. Depending on the conjugate used, either fluorescence or chemiluminescence are used for detection.

For chemiluminescence, the most common conjugate is an antibody with horseradish peroxidase attached to it [40]. The peroxidase can, in presence of a peroxide-based reagent, catalyse the oxidation of luminol, which is added to the membrane in a solution. The oxidation of luminol then leads to the detectable emission of light.

Fluorescence on the other hand is based on the excitation of a fluorophore using light at a specific wavelength (mostly from a laser source). When the excited fluorophore returns to its basic energy state, it emits photons of a specific wavelength that can be detected.

Either method can be used to qualitatively and quantitatively detect the specific protein, as the signal is proportional to the protein on the membrane [40].

Other analytical methods of low importance will be discussed briefly in the Appendix.

GALA

GALA is a peptide consisting of 30 amino acids with a glutamic acid – alanine – leucine – alanine repeat. It was created in an attempt to produce a peptide similar to viral proteins that are actively supporting the escape of the viral genes from endosomes into the cytosol [41]. The characteristic of GALA is that depending on the pH value, it is either has a random coil structure and is water-soluble (pH 7.0) or is an amphipathic α-helix that binds to bilayer membranes (pH 5.0) [42]. Amphipathic α-helices are found in different biologically active peptides and proteins, like in polypeptide venoms, polypeptide antibiotics, hormones like endorphin and certain transmembrane proteins [42, 43]. The distinct characteristic of an amphipathic α-helix is that along the long axis, one face of the helix consists mainly of nonpolar amino acids and thus is hydrophobic, while the other face consists mainly of polar amino acids and is hydrophilic.

The interaction of GALA with the membrane induces membrane fusion, fragmentation and / or the formation of transmembrane peptide pores. These pores are comprised of approximately 10 (± 2) GALA α-helical monomers, who together array themselves perpendicular to the plane of the membrane [42]. Due to the pore formation, leakage was found for membrane vesicles treated with GALA as shown in the literature [14, 44]. This leakage can be used to either release entrapped molecules from the liposomes, but also to allow for the interaction with the liposomal environment, as in case of this project to possibly change the pH after encapsulating the virus.

GALA pores (10±2 helices)
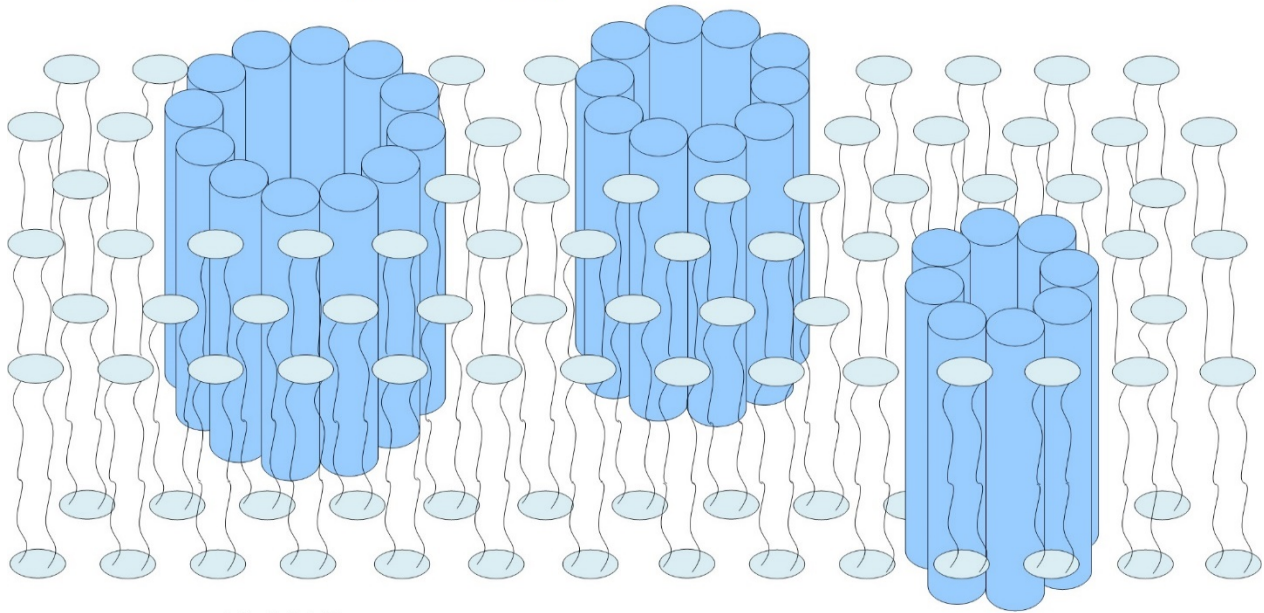
Lipid bilayer

Figure 10: Schematic of pore formation in a phospholipid bilayer (with the polar *head* as turquoise ellipses, and nonpolar *tails* in black) at acidic pH. Each GALA helix (blue) is depicted as a cylinder.

Materials and Methods

Chemicals

The general chemicals used in the laboratories of the working group of Prof. Martina Marchetti-Deschmann at the TU Wien are found in Table 2.

Table 2: Chemicals

Chemical	Formula	Producer	Purity	Molecular Weight [g/mol]
Acetic acid	CH_3COOH	Honeywell Specialty Chemicals Seelze (Seelze, Germany)	≥99.8 %	60.05
Ammonium acetate	NH_4COOCH_3	Sigma-Aldrich (St.Louis, MO, USA)	>99.99 %	77.08
Ammonia (aqueous solution)	NH_4OH	Sigma (St.Louis, MO, USA)	28.2 %	17.03 (gas)
Boric acid	H_3BO_3	Merck (Darmstadt, Germany)	≥99.5 %	61.83
Chloroform	$CHCl_3$	Sigma (St.Louis, MO, USA)	≥99.9 %	119.38
Cholesterol		Avanti Chemicals (Alabaster, AL, USA)	98 % from ovine wool	386.65
Dithiothreitol (DTT)	$C_4H_{10}O_2S_2$	Sigma (St.Louis, MO, USA)	≥99.5 %	154.25
1,2-Distearoyl-sn-glycero-3-phosphoethanol-amine (DSPE)		Avanti Chemicals (Alabaster, AL, USA)	>99 %	748.07
Formalin, 35%	CH_2O	Merck (Darmstadt, Germany)		
GALA, Pore-forming Peptide, lyophilisate	WEAALAEALAE ALAEHLAEALA EALEALAA	AnaSpec (Fremont, CA, USA)	≥95 %	3032.7

Chemical	Formula	Producer	Purity	Molecular Weight [g/mol]
hydrogenated L-α-phosphatidyl-choline from soy (Hydro-Soy PC)		Avanti Chemicals (Alabaster, AL, USA)	>99 %	783.77
Methanol	CH_3OH	Merck (Darmstadt, Germany)	≥99.9 %	32.04
Silver nitrate	$AgNO_3$	Merck (Darmstadt, Germany)	≥99.8 %	169.87
Sodium carbonate	Na_2CO_3	Sigma (St.Louis, MO, USA)	≥99.8 %	105.99
Sodium hydroxide	$NaOH$	Merck (Darmstadt, Germany)	≥98 %	39.99
Sodium thiosulfate	$Na_2S_2O_3$	Sigma-Aldrich (St.Louis, MO, USA)	≥99.5 %	248.18
Sucrose	$C_{12}H_{22}O_{11}$	Serva (Heidelberg, Germany)	>98 %	342.3

The water used for general work and preparing the solutions was of so-called "ultrapure" grade with a resistivity of 18.2 MΩcm (25 °C) derived from a MilliQ filter system (Merck Millipore, Burlington, MA, USA).

The lyophilized GALA (1 mg) was dissolved in 1 mL ultrapure water. This 320 µM stock solution was split into aliquots of 100 µL each. The aliquots were stored at -80 °C. GALA was added to the liposomes directly before the measurement, followed by 10 min of incubation.

The aqueous buffers were filtered through 0.2 µm Sartorius Minisart SFCA syringe filters (Göttingen, Germany) before use to remove particles.

The following chemicals were used based on the standard methods applied at the Vienna Biocenter.

Table 3: Chemicals (Vienna Biocenter)

Chemical	Formula	Molecular Weight [g/mol]
Ammoniumperoxidisulfate (APS)	$(NH_4)_2S_2O_8$	228.18
Disodium hydrogen phosphate	Na_2HPO_4	141.96
Glycine	$C_2H_5NO_2$	75.07
Methanol	CH_3OH	32.04
Polysorbate 20 (Tween)	$C_{58}H_{114}O_{26}$	1.227.54
Potassium chloride	KCl	74.55
Potassium dihydrogen phosphate	KH_2PO_4	174.2
Phosphotungstic acid (PTA)	$H_3PW_{12}O_{40}$	2880.2
Sodium Chloride	$NaCl$	58.44
Sodium dodecyl sulfate	$NaC_{12}H_{25}SO_4$	288.37
Tetramethylethylenediamine (TEMED)	$C_6H_{16}N_2$	116.21
Trehalose	$C_{12}H_{22}O_{11}$	342.30
Tris-(hydroxymethyl)-aminomethane (Tris)	$C_4H_{11}NO_3$	121.14

nES GEMMA

The used setup consisted of the following devices from TSI (Shoreview, MN, USA): a TSI 3480 Electrospray Aerosol Generator with a ^{210}Po source, a TSI 3080 Electrostatic Classifier, a TSI 3085 nano Differential Mobility Analyser, an n-butanol driven TSI 3776 Ultrafine Condensation Particle Counter and a TSI 3089 Nanometer Aerosol Sampler (aka ENPS).

The first four devices were used for analytical measurements, while the Aerosol Sampler was used only for the collection of liposomes on silicon wafers.
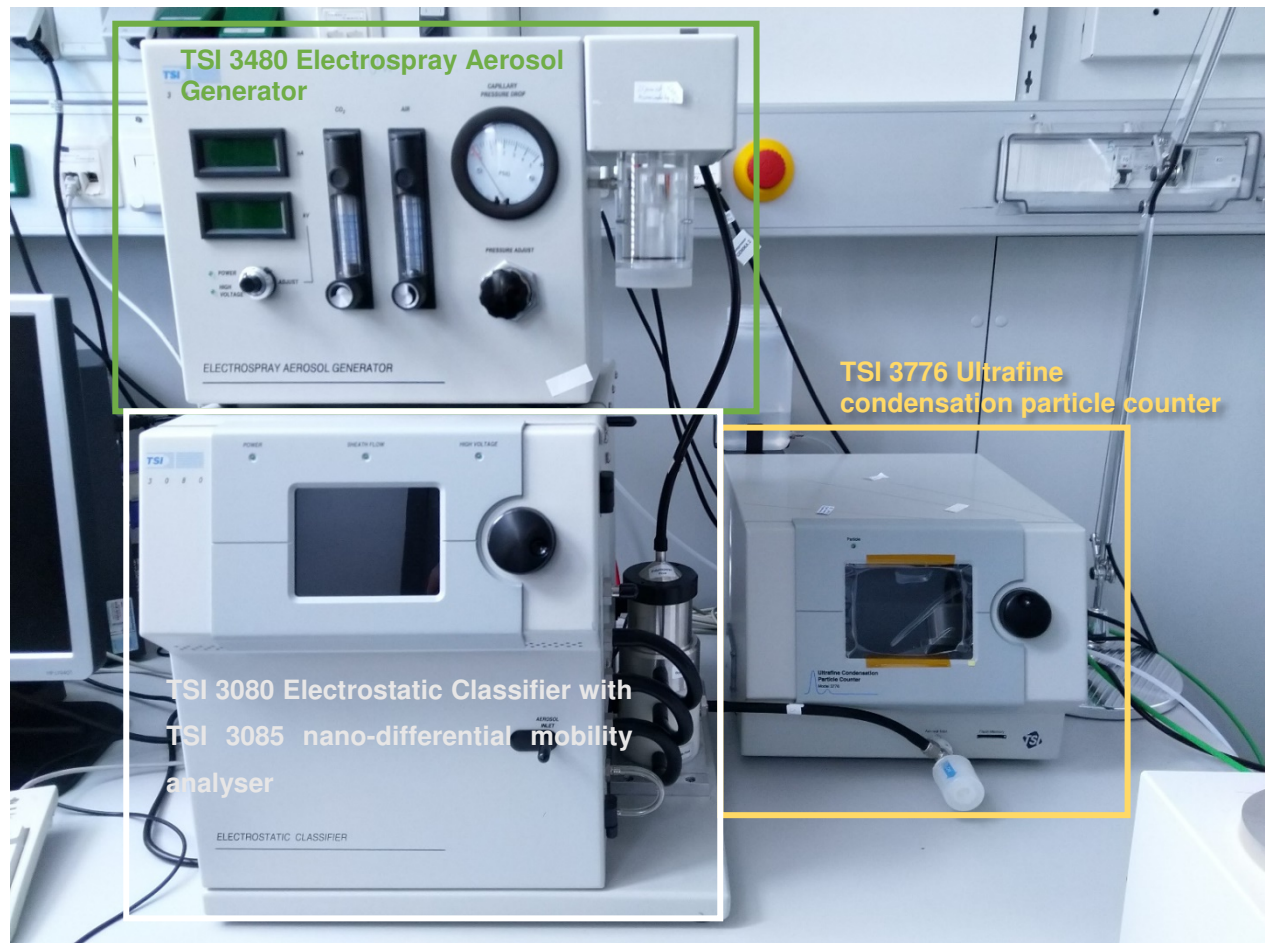
Figure 11: GEMMA, actual setup.

The fused-silica capillaries used were polyimide coated with an inner diameter of either 25 µm or 40 µm as indicated and an outer diameter of 150 µm and were purchased from Polymicro Technologies (Phoenix, AZ, USA). 25 µm inner diameter capillaries were mainly used during early stages of the work. However, since these were more prone to being clogged by proteins (GALA, viruses) later experiments focused on 40 µm inner diameter capillaries. The tips of the capillaries were ground using a homemade grinding device based on the work by Tycova et al. [45]. Before usage and for storage the capillaries were flushed with a 1:1 [v:v] mixture of ultrapure water and isopropanol to prevent microbial growth.

The voltage and pressure drop applied across the capillary varied based on the inner diameter of the capillaries, but were also affected by the position of the capillary tip or the shape of the tip. The nDMA sheath flow was low for liposome samples to cover a wider measurable size range (with a lower peak resolution) from 4.85 nm up to 185.2 nm, as the measurable size range decreases with higher sheath flows. For the smaller particles (i.e. virus) however it was set to higher values, thus giving a higher peak resolution, as only a part of the coverable size range was of interest. For the virus the measurable size range was from 1.95 nm to 65.2 nm.

Table 3: General settings of the GEMMA for the different capillaries used.

Capillary inner diameter [nm]	Voltage [kV]	Pressure drop [PSI]	CO_2 In [l/min]	Air In [l/min]	nDMA Sheath flow [l/min]
25	1.7-2.0	3.8-4.2	0.1-0.2	1	2.5 (Liposomes)
40	1.6-1.9	3.4-3.8			15 (Virus/VLPs)

nES GEMMA measurements relate the number of particles per volume unit counted in the ultrafine CPC to a given voltage setting of the nDMA. Based on the voltage settings of the applied electrical field of the nDMA, the electrophoretic mobility diameter (EM-diameter) of these particles is calculated.

A nES GEMMA spectrum therefore shows the plot of total number of particles against the EM-diameter.

For visualization, the total count number detected is sometimes not useful, for example when comparing higher and lower dilutions. In these cases, the relative count number was used instead.

$$Relative\ counts\ [0;1] = \frac{Counts\ at\ specific\ EM-diameter}{Maximum\ of\ measured\ counts\ across\ EM-diameter\ range}$$

Equation 1: Calculation of the relative count number based on total counts

Important to note is also, that the spectra shown later in this work are medians of at least 5 single measurements.

Virus

Two aliquots of HRV-A2 virus were prepared by the Max F. Perutz Laboratories of the Medical University of Vienna (Vienna Biocenter, Vienna, Austria) according to standard protocols [46, 47]. The first aliquot (20 µL) was in 50 mM HEPES, the second one (12 µL) in 50 mM Tris-HCl (pH 7.4) including 25 mM sodium chloride, both with a virus concentration of 10 mg/mL. The solvent of both aliquots was exchanged (see Solvent Exchange and Desalting) to 40 mM ammonium acetate at pH 8.4. In doing so, the virus stocks were diluted 1:50 [v/v]. After checking their purity using GEMMA, the two aliquots were united to create around 1.6 mL of desalted virus solution.

Liposomes

As mentioned in the introductory chapter (Liposomes), the liposomes were created using the thin lipid layer hydration technique.

The liposomes consisted of hydrogenated L-α-phosphatidylcholine from soy (Hydro-Soy PC), Cholesterol, and 1,2-Distearoyl-s_n-glycero-3-phosphoethanolamine (DSPE) in a molar ratio of 4:3:3 (i.e. 3.135 mg HSPC, 1.160 mg Cholesterol, 2.244 mg DSPE per mL dispersion). These were weighed into a 50 mL round-bottomed flask using a scale from Sartorius (Göttingen, Germany). To remove unwanted substances in the flask, the flask was cleaned prior to weighing using a mixture consisting of 25 % chloroform and 75 % methanol [v:v]. The flask was then dried for 10 min in a desiccator under vacuum at room temperature.

After weighing, the solids were dissolved in the same mixture of chloroform and methanol. The solvent was evaporated using a slight stream of nitrogen applied through a tube while constantly rotating the flask. This results in a thin lipid layer on the inner glass surface. The lipid layer is then dried for two hours in a vacuum desiccator to remove traces of chloroform and methanol.

Afterwards 1 mL of 40 mM ammonium acetate was added resulting in a 10 mM lipid dispersion. The flask was constantly shaken using a vortex shaker and the lipid layer slowly depletes as the liposomes are formed. Heating of the flask up to around 50-60 °C increased the depletion speed.

The mixture is transferred to gas-tight syringes for extrusion as soon as the lipid layer had completely detached from the flasks surface. The extrusion was performed using a kit by Avanti Polar Lipids (Alabaster, AL, USA). Figure 12 shows the used set after assembling.

The membranes used were Whatman Nucleopore Track-Etch (GE Healthcare, Chalfont St. Giles, United Kingdom) made of polypropylene with a pore diameter of 0.1 µm, 0.2 µm and 0.4 µm.

Two filter membranes were used per extrusion. They were sandwiched between two filter supports in order to improve the resistance of the filters against mechanical stress and thus avoid ruptures. The filters and filter supports were also pre-wetted using ultrapure water before assembling.

The system was then tested for tightness by extruding ultrapure grade water. Afterwards the lipid solution was extruded 21 times. Then the hazy solution was transferred into brown 1 mL flasks and stored at 4 °C.

The same procedure with slight variations was used to create liposomes containing virus.

Instead of adding 1 mL of 40 mM ammonium acetate to create the liposomes a mixture of 500 µL of desalted virus solution and 500 µL of 40 mM ammonium acetate with a pH of 8.4 was added. The pH was afterwards measured and set to 8.4 using an aqueous solution of ammonia ($NH_3 \cdot H_2O$). Heating of the flask to facilitate lipid film detachment was avoided in order to avoid virus degradation.

Figure 12: Extruder used to create the liposomes.

For measuring, the liposomes were diluted 1:5, 1:10 or 1:25 using 40 mM ammonium acetate to a final volume of around 100 µl.

Density gradient centrifugation / flotation

Density gradient centrifugation was performed on liposomes containing HRV-A2 for the separation of the filled liposomes from the empty liposomes and free virus. For most centrifugations the samples were applied in the bottom phase resulting in the liposomes moving into the upper phases during separation, making the procedure a centrifugation / flotation. In the following segments however, this procedure will be referred to as 'centrifugation'.

For the density gradient centrifugation / flotation a Sigma 3-30K centrifuge (Sigma Laborzentrifugen, Osterode am Harz, Germany) was used.

The density difference was created using layers of sucrose in 40 mM ammonium acetate of different mass percentages. The different layers were prepared by dilution of a 67 % [w/v] sucrose stock solution.

The rotors used were a fixed-angle rotor 12110 (Sigma Laborzentrifugen) with 1.5 mL and 2 mL centrifugation tubes (Eppendorf, Hamburg, Germany) and a swing-out rotor 11390 with beakers 13152 and 15 mL tubes (VWR, Radnor, PA, USA).

Two different general approaches were tested as seen in Figure 13. The densities of the phases were taken from an on-line table [48]. A summary of the centrifugations made is found in Table 4.

Centrifugations were always made at least in duplicates with the same parameters.

For the first approach the analyte was added in the bottom phase. During the first centrifugations, 20 µL of liposomes containing HRV-A2 (in 40 mM ammonium acetate at pH 8.4) was mixed with 180 µL of 67 % sucrose solution, resulting in a 60 % sucrose solution (centrifugations number 1- 6). During later centrifugations (centrifugations number 11- 16), the volume of liposome solution was increased to 50 µL, resulting in a 50 % sucrose bottom phase. In total there were three layers consisting of 600 µL 0 %, 600 µL 30 % sucrose solution and 200 µL 50 % or 60 % sucrose solution (each [w/v]). For the runs with the 15 mL tubes the volume of the 0 % phase was increased to 10 mL while the other volumes remained unchanged.

For the second approach the analyte was added in the top phase with 0 % sucrose (centrifugations number 7-10) based on the work by Sánchez-López et al. [10]. 60 or 80 µL of liposomes containing HRV-A2 were mixed with 100 µL of 40 mM ammonium acetate solution. The number of different layers was increased to 7, each with a volume of 180 µL.
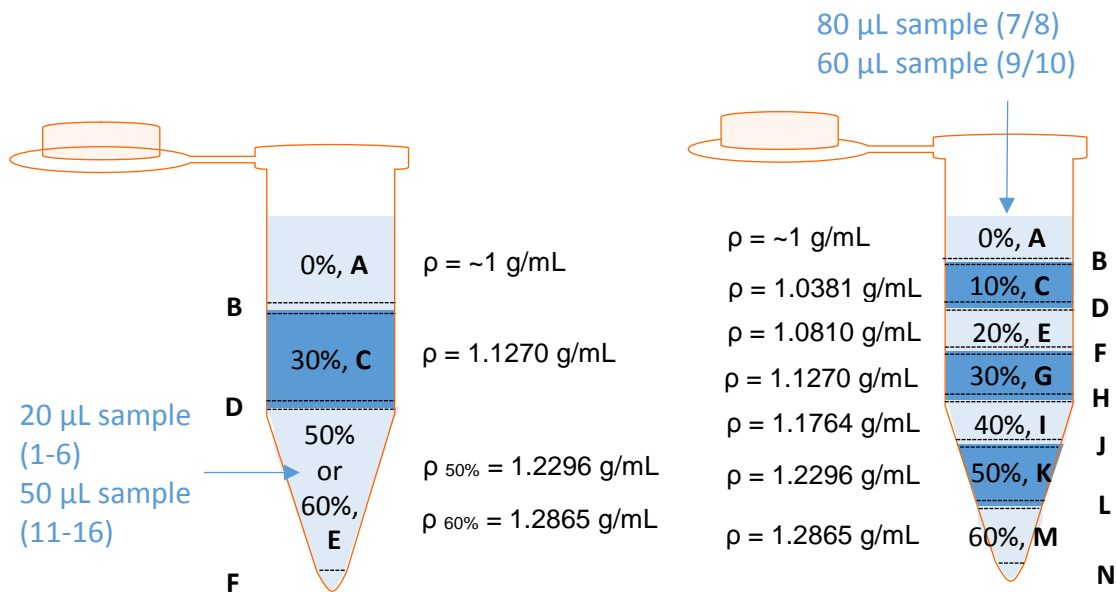
Figure 13: The two general approaches for the density centrifugation of liposomes containing HRV-A2. The sample was either applied on top (centrifugation) or bottom (flotation) using either 3 phases (left) or 7 phases (right). The phases and interphases are given letters in consecutive order starting from the top with A for 0% sucrose, B for the first interphase, etc..

After the centrifugation the different phases and interphases were collected separately. The collection was done using a 200 µL pipette (Eppendorf, Hamburg, Germany), by carefully removing the liquid from the top.

In general, the fractions were collected based on the volumes of the phases. The interphase was assumed to have a volume of 50 µL between the different sucrose layers. Additionally, the bottom 25 µL were collected as a fraction as well. This results in a total of six fraction samples for the approach with 3 layers: The first fraction on top with 575 µL, then 50 µL of interphase between 0 % and 30 % sucrose concentration, then 550 µL of the 30 % sucrose phase, 50 µL of second interphase between 30 % and 60 % sucrose concentration, 150 µL of the 60 % sucrose phase and 25 µL from the bottom.

The same alternating procedure was done for the approach with 7 layers, where a total of 14 fractions was received.

For some centrifuged samples of the first approach, a visible phase border was found in between the 0 % and 30 % sucrose layers after the centrifugation. In this case the visible phase border was collected entirely, and the volume of the following fraction adapted to a lower amount (i.e. 100 µL of interphase, followed by 500 µL of 30 % sucrose). During later centrifugations (11 onwards), the volume of the bottom phase was increased to 50 µl while the volume of the 60 % sucrose phase was decreased to 125 µl.

Table 4: Density gradient centrifugations and their settings (The centrifugations with orange background were made using the second approach)

Centrifugation number	Sample applied	Relative centrifugal force, RCF [xg]	Temperature [°C]	Time [h:mm]	Rotor	Centrifugal tube
1 / 2 / 3 / 4	20 µL from bottom	25000	4	3:30	12110	1.5 mL Eppendorf tubes
5 / 6	20 µL from bottom	1500	4	5:30	11390	15 mL Falcon centrifugal tubes
7 / 8	80 µL from top	20000	4	0:35	12110	2 mL Eppendorf tubes
9 / 10	60 µL from top	20000	4	2:00	12110	2 mL Eppendorf tubes
11 / 12	50 µL from bottom	25000	4	1:30	12110	1.5 mL Eppendorf tubes
13 / 14	50 µL from bottom	25000	4	2:30	12110	1.5 mL Eppendorf tubes
15 / 16	50 µL from bottom	25000	4	3:30	12110	1.5 mL Eppendorf tubes

Solvent Exchange and Desalting

For exchanging the solvents of samples, 10 kDa molecular weight cut-off centrifugal filters made of modified polyethersulfone (VWR, Radnor, PA, USA) and a Sigma 1-14K centrifuge with a model 12092 fixed-angle rotor (Sigma Laborzentrifugen, Osterode am Harz, Germany) were used. This procedure was done for analytes that were dissolved in solvents that needed to be exchanged for the nES GEMMA measurement, as for example with sucrose-rich phases after density gradient centrifugation because of nES incompatible solvents.

The analyte in the original buffer solution was pipetted on a tared filter membrane. The weight of the analyte solution was noted. It was then mixed and diluted with 40 mM ammonium acetate at pH 8.4 to a total volume of around 500 µL. After centrifugation at 9.0×10^3 g only a small amount of liquid remained on the filter. The time needed for this varied between 2-2:15 min (liposome fractions, HRV-A2 in Tris) and 6 min (HRV-A2 in 50 mM HEPES, GFP-labeled P22). The flow- through was discarded and 500 µL of 40 mM ammonium acetate was added on top of the membrane for the next centrifugation cycle.

This step was repeated between 3 to 7 times depending on the original solvent and/or the signals received using nES GEMMA. After the last centrifugation step, the remaining liquid on the filter was transferred into a tared 0.5 mL centrifugation tube. The weight was again noted.

An additional amount of ammonium acetate was added based on the difference of final weight and original weight to receive the final (mass-based) dilution.

Alternatively, the dilution was based on the volume of liquid applied to the filter. This was the case when the density of the original solvent was not comparable to the final solvent, for example with the sucrose fractions from the density centrifugation.

The diluted samples were stored at 4 °C.

Electron microscopy (SEM)

For measuring the liposomes containing HRV-A2 by means of the electron microscope, they were spotted on a vacuum-dried carbon-coated copper grid. 12 µL of sample were applied per spot. The sample comprised of 1.2 µL analyte, 8.8 µL of 40 mM ammonium acetate pH 8.4 and 2 µL of 60 % aqueous trehalose solution. The trehalose should prevent the liposomes from drying out and help to visualize their shape. Afterwards the samples were stained using a 2 % phosphotungstic acid (PTA) solution.

The carbon grid was then sputtered in a BAL-TEC SCD005 Cool Sputter Coater (BAL- TEC, Balzers, Liechtenstein) in argon atmosphere at 10^{-1} mbar and with a current of around 20 mA.

The EM measurements were performed using a FEI Morgagni 268 Transmission electron microscope (FEI, Eindhoven, Netherlands) at 10^{-7} mbar with an acceleration voltage of 80 kV and a 110x magnification.

Sodium dodecyl sulfate polyacrylamide gel electrophoresis (SDS-PAGE)

For SDS-PAGE precast NuPAGE® 10 % Bis-Tris Mini Gels (Invitrogen, Carlsbad, CA, USA) were used. The samples were mixed with 2.5 µL NuPAGE® 4x LDS sample buffer,1 µL of 0.5 M DTT, 4 µL to 6.5 µL of analyte and up to 2.5 µL of ultrapure water for a final volume of 10 µL. The mixture was then heated for 5 min at 90 °C in a ThermoMixer (Eppendorf, Hamburg, Germany). As marker we used the Novex Sharp Pre-stained Protein Standard (ThermoFisher Scientific, Waltham, MA, USA). The migration pattern of proteins on the gel as well as the protein bands in the protein standard can be found in the Appendix.

The running buffer was 1x MES buffer (Invitrogen, Carlsbad, CA, USA), which was diluted from a 20x stock by mixing 50 mL of 20x MES with 950 mL of ultrapure water. The diluted buffer was prepared on the day of usage.

Some samples used for SDS-PAGE had to be concentrated, for which a Univapo 100H vacuum concentrator centrifuge from UniEquip (Planegg, Germany) was used.

The samples were carefully inserted into the pockets of the gel using a 20 µL pipette (Eppendorf, Hamburg, Germany). The outmost pockets were not used due to possible band distortion (smiling effects). Empty pockets were filled with blank samples containing 4 to 6.5 µl 40 mM ammonium acetate instead of analyte.

The gels ran vertically, with 200 V of voltage and 120 mA of current applied. The electrophoresis chamber (Invitrogen) was kept in an ice bath in order to prevent thermal effects on the gel during the run. Afterwards, the gels were stained for visualization of the protein bands using a silver staining protocol from Shevchenko et al. [37]. During every step, the gel was slowly shaken using an orbital shaker. Some of the steps had to be repeated, by exchanging the solution used for the step with a fresh one.

Table 5: Silver staining protocol

Step	Incubation time [min]	Amount [mL]	Composition
Fixation	20	50	50 % [v/v] EtOH
			5 % [v/v] CH_3COOH
			45 % [v/v] Ultrapure water
Washing	10	50	50 % [v/v] EtOH
Washing	20 (3x)	50 (3x)	Ultrapure water
Sensitivation	1	50	0.01 g $Na_2S_2O_3$
			50 mL Ultrapure water
Washing	1 (2x)	50 (2x)	Ultrapure water
Incubation	20 (in fridge)	50	0.05 g $AgNO_3$
			50 mL Ultrapure water
Washing	1 (2x)	50 (2x)	
Development	Until bands are visible	50 (2x)	3 g Na_2CO_3
			60 µL Formalin (min. 35%)
			150 mL Ultrapure water
Stopping	5 (3x)	50 (3x)	5 % [v/v] CH_3COOH
			95 % [v/v] Ultrapure water
Conservation	- (at 4 °C)	100	1 % [v/v] CH_3COOH
			99 % [v/v] Ultrapure water

Western Blot

Before the Western Blotting the samples had first to be separated by SDS-PAGE. Afterwards, the gel was blotted and stained fluorescently prior measurement.

The SDS-PAGE and Western Blotting was done according to a protocol from the Max F. Perutz Laboratories (Medical University of Vienna, Vienna). The parts taken from the protocol are found in italic letters. In Table 6 the composition of the SDS gel is found.

For the SDS-PAGE, *the samples were mixed with a 5x sample loading buffer, containing 250 mM Tris-HCl pH 6.8, 1 g SDS, 30 % [v/v] Glycerol, 5 % ß-mercaptoethanol and 0.1 % bromphenol blue. The electrophoresis separation was done in a chamber filled with 1x running buffer, containing 25 mM Tris, 192 mM glycine and 0.1 % SDS for 30 minutes at 120 V.*

Table 6: SDS Gel, taken from a protocol of the Max F. Perutz Laboratories

Chemicals	Separating gel	Stacking gel
H_2O	7.4 mL	6 mL
30 % Acrylamide/Bis	9 mL	1.35 mL
3 M Tris	5.625 mL	-
0.5 M Tris	-	2.5 mL
10 % APS	0.225 mL	0.1 mL
TEMED	0.0225 mL	0.01 mL

For the blotting*, a PVDF (polyvinylidene difluoride) membrane was activated in methanol for 5 seconds and then equilibrated for 2 minutes in Transfer buffer (25 mM Tris, 190 mM glycine, 20 % methanol, 0.1 % SDS). The membrane was covered in six filter papers (three per side). These filter papers were also equilibrated in the same Transfer buffer for 5 minutes.*

The transfer was done for 15 minutes at 1.3 ampere using a Trans-Blot Turbo System (Bio- Rad Laboratories, Hercules, CA, USA). After the transfer, the membrane was blocked using a solution of 5 % milk in phosphate buffer saline (PBTS), containing additionally 137 mM NaCl, 2.7 mM KCl, 10 mM Na_2HPO_4, 1.8 mM KH_2PO_4 and 0.05 % Tween.

After the blocking, the membrane was washed with PBTS, and then the antibody 8F5 VP2 (derived from mice) with a dilution of 1:1000 was added. The membrane was thereafter incubated for 1 hour in the solution. After an additional washing step with PBTS, anti-mouse horseradish peroxidase (an antibody with peroxidase attached to it) in a dilution of 1:10000 was added and again the membrane incubated for 1 hour. After washing the membrane with PBTS, 1.5 mL of the colouring agent SuperSignal West Pico PLUS Chemiluminescent Substrate (ThermoFisher Scientific, Waltham, MA, USA) was added.

The fluorescence of the blotted membranes was measured using a Biotek Synergy H1 (BioTek Instruments, Winooski, VT, USA) at an excitation wavelength of 562 nm and a temperature of 25 °C.

Results

The target of this work was to encapsulate HRV-A2 in liposomes to create a model system that is comparable to naturally occurring infections, where virus is encapsulated in endosomes when taken up into cells. During the *in vivo* infection process, acidification takes place inside the endosomes which leads to uncoating of the virus, i.e. transfer of its RNA genome through the lipid membrane.

For this work, liposomes were created in different variations as said before. First they were created in different sizes using membranes with different pore sizes. Afterwards they were created with a pH of 5 and GALA added, where GALA should be forming pores that can be utilized to acidify the aqueous lumen of the liposomes. Finally, liposomes were created using a mixture of ammonium acetate and a virus stock solution. After measuring the liposomes putatively containing virus and the virus stock and comparing the results, it was found that a purification of the liposome preparation is needed to remove free virus and virus bound to the membrane. This was done by sucrose gradient centrifugation / flotation.

For the evaluation of the created liposomes the two main techniques used were GEMMA and EM. The results of the measurements are found below starting with GEMMA.

Afterwards, the results of the Western Blot and stand-alone SDS-PAGE are shown. Both techniques were used for verifying the presence of viral proteins in fractions obtained after centrifugation / flotation.

GEMMA

This chapter will contain the results of the GEMMA measurements on empty liposomes and the liposomes putatively containing virus.

Empty liposomes

Liposomes extruded with different membrane pore sizes and at different dilutions were measured, and their GEMMA spectra are shown in Figure 14. An overlay of GEMMA spectra for vesicles extruded at different membrane pore sizes at a dilution of 1:10 is found in Figure 15.

The size maximum for all the liposomes remains at around 100-120 nm, but with strongly different size distributions when using different membrane pore sizes as visible in Figure 15. While the size maximum for the liposomes extruded with a 0.1 µm membrane pore size is 96 nm with a full width at half maximum (FWHM) of 67 nm, it is 103 nm with a FWHM of 86 nm using a 0.2 µm membrane pore size and 120 nm with a FWHM of 133 nm using a 0.4 µm membrane pore size.

37

As seen in Figure 14, the number of liposomes on the other hand decreases with an increasing pore size, due to the amount of lipids necessary to form larger vesicles.

Visible in both figures is that there are two peak regions, one around 10-40 nm and a second one starting after 50 nm, as well as a baseline of over 50 counts/nm found with every liposome sample.

As a result of these initial measurements, a membrane pore size of 0.1 µm was chosen for later experiments, as the number of liposomes is higher and the diameter for the encapsulation of 30 nm diameter virus particles is thought to be high enough. The peak maximum did not change significantly within three months (not shown), therefore the liposomes are seemingly stable in solution for at least that time.
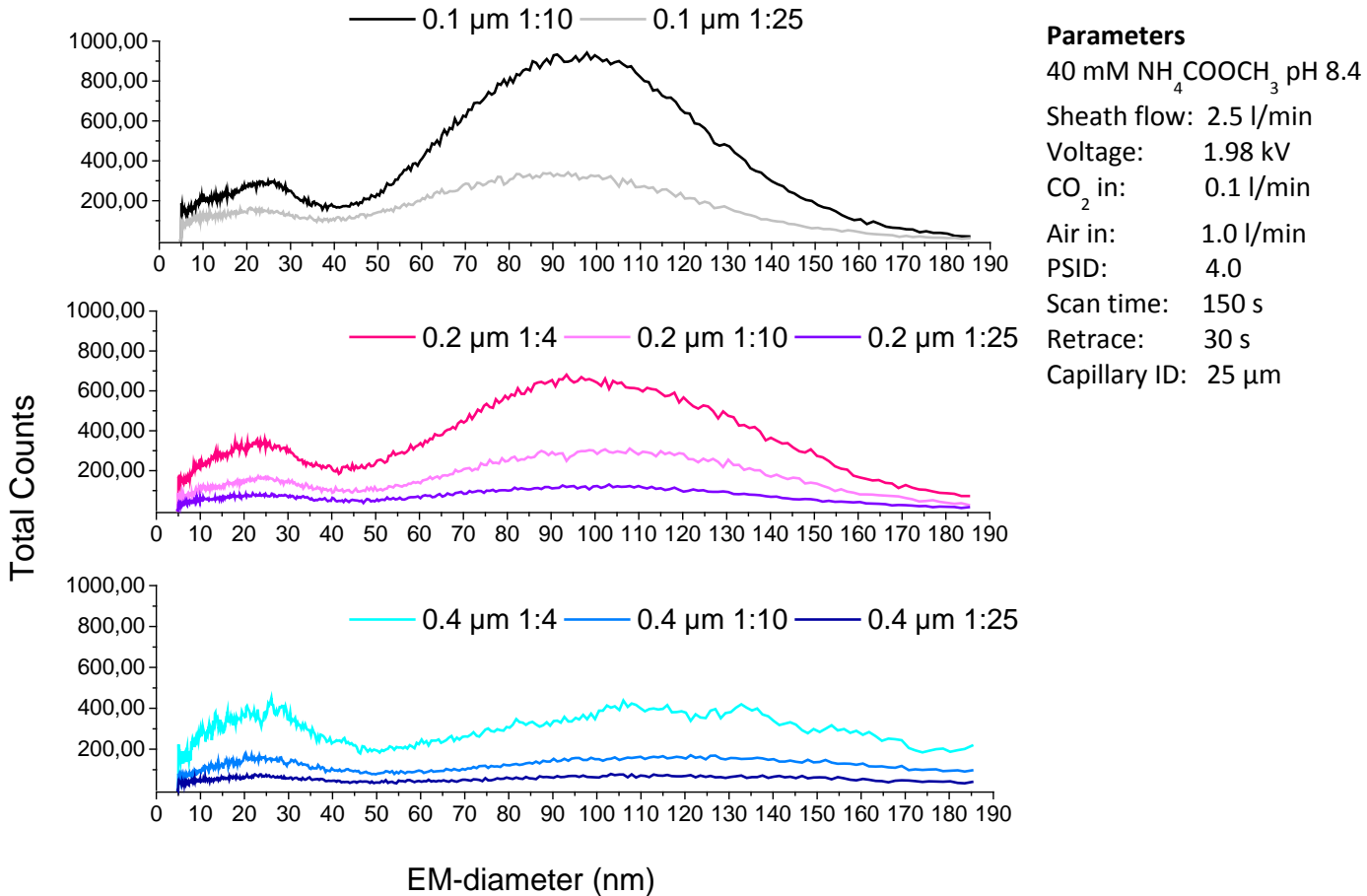
Figure 14: GEMMA spectra of liposomes extruded with different membrane pore sizes (top: 0.1 µm, middle: 0.2 µm, bottom: 0.4 µm) and with different dilution factors of a 10 mM lipid stock.
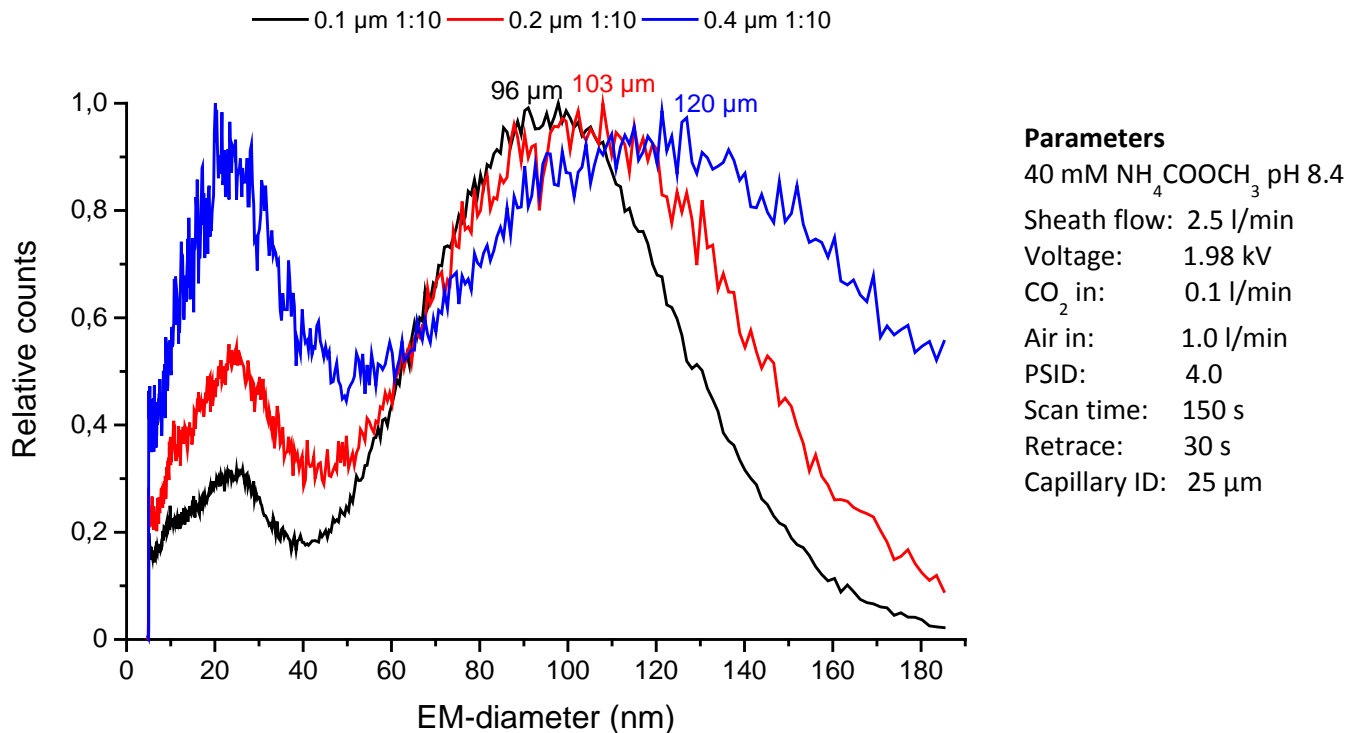
Figure 15: Overlay of GEMMA spectra of liposomes extruded through filters with different pore sizes analysed at a 1:10 dilution of a 10 mM lipid stock solution.

Empty liposomes with added GALA

GALA as stated in the introductory chapter is adhering to membranes and forming pores through the lipid membranes of liposomes when in acidic environment. Therefore, the liposomes were prepared using a 0.1 µm membrane pore size and 40 mM ammonium acetate with a pH of 5. GALA, as previously said in the Materials and Methods chapter, was added before the measurement with a 10 min incubation time. Afterwards the liposomes were measured with a dilution of 1:10.

Figure 16 shows the GEMMA spectra of the treated liposomes overlaid by the GEMMA spectra of liposomes that were created using 40 mM ammonium acetate at pH 8.4. The curve is different between the samples, with a higher number of liposomes in the pH 8.4 sample at around 100 nm versus a slightly higher number of particles found in the first peak area around 10-40 nm in the pH 5 sample. These differences can be a result of the preparation of the sample or the dilution for the GEMMA analysis.
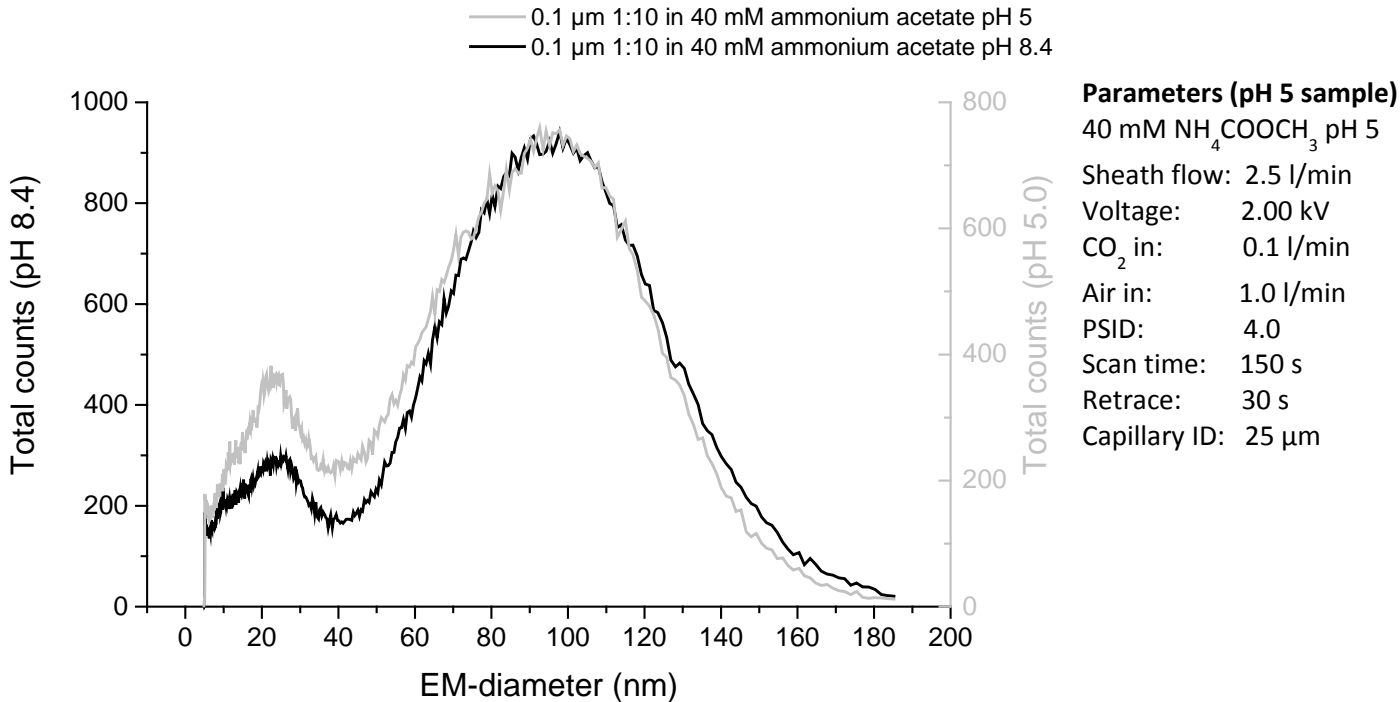
Figure 16: Comparison of the measured empty liposomes at pH 5 with liposomes at pH 8.4.

Tests on the effect of GALA were made using the liposomes at pH 5 and different concentrations of GALA added. The amount added was based on previous leakage tests done by Weiss et al. [14]. As they have shown, even ratios of 0.1 peptide to lipids should lead to induced leakage.

A GEMMA spectrum using a concentration of 10 µM GALA can be found Figure 17. The addition of GALA seemingly altered the liposomes, as there is a high peak at the start of the spectrum (4.85 nm) that was not observed before. It was assumed that this peak is a result of disintegrated liposomes, or aggregation and cluster formation of the GALA peptide.

Also, the first peak region is higher than before, while the second one decreased and its maximum was shifted towards smaller diameters compared to the original sample at pH 5. The shift in the count maximum in the peak area around 100 nm, from 92.6 nm in the untreated sample to 88.6 nm in the GALA-treated sample, could be explained with an increased shrinkage of the liposomes during the GEMMA process. Liposomes that do not possess pores may not loose liquid from their core, while it can evaporate from inside the liposomes possessing pores. The decreased maximum is possibly a result of the before-mentioned liposome disintegration.
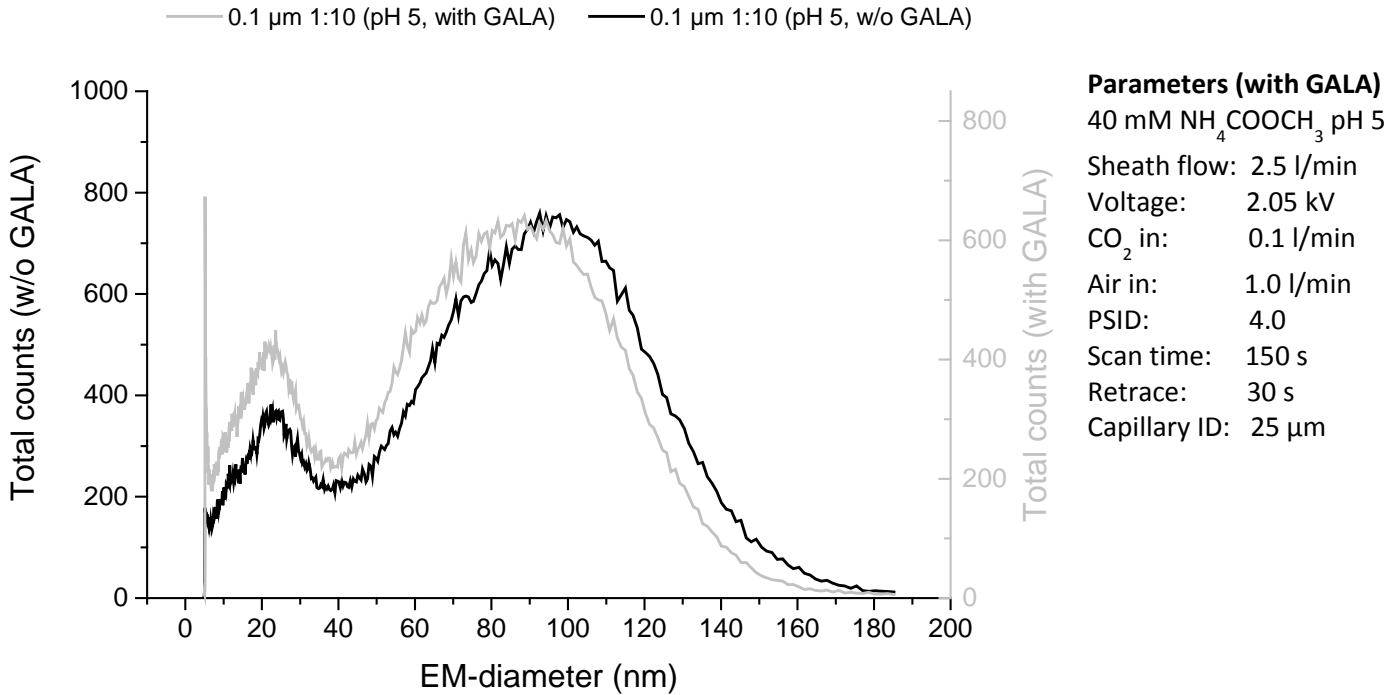
Figure 17: Overlaid GEMMA spectra of empty liposomes with and without 10 µM GALA added to the liposome dispersion, initial test.

In a second attempt, the concentrations of GALA added were varied. The result is found in Figure 18, for better comparability shown in relative counts. There is no obvious difference between the different concentrations of GALA added visible in the GEMMA spectrum, however, using higher concentrations of GALA (>10 µM) lead to fast clogging of the capillary and resulted in an unstable spray within a few minutes of use. Cleaning the capillary manually after every measurement with a syringe and pure ammonium acetate helped to counter the problem. As a result, lower concentrations of GALA added are favorable as the size shift is comparable to higher concentrations while also avoiding clogging of the capillary.
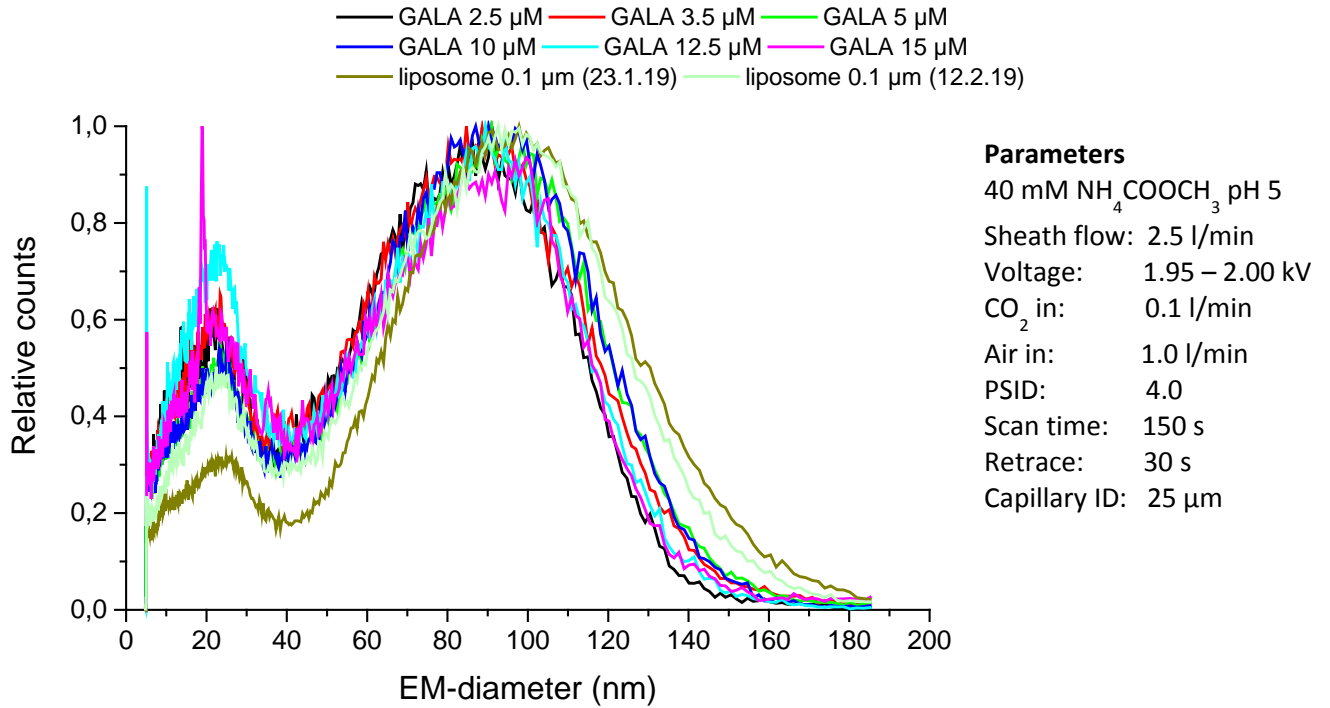
Figure 18: Overlaid GEMMA spectra of empty liposomes with varying GALA concentration.

In Figure 18 there are also two spectra made on different days of the same liposome preparation (extruded with 0.1 µm pore size membranes). These spectra show no size shift as it is found with the GALA samples. This leads to the conclusion that the size shift is a result of the addition of GALA and not the possible degradation of the liposomes over time.

Liposomes with HRV-A2
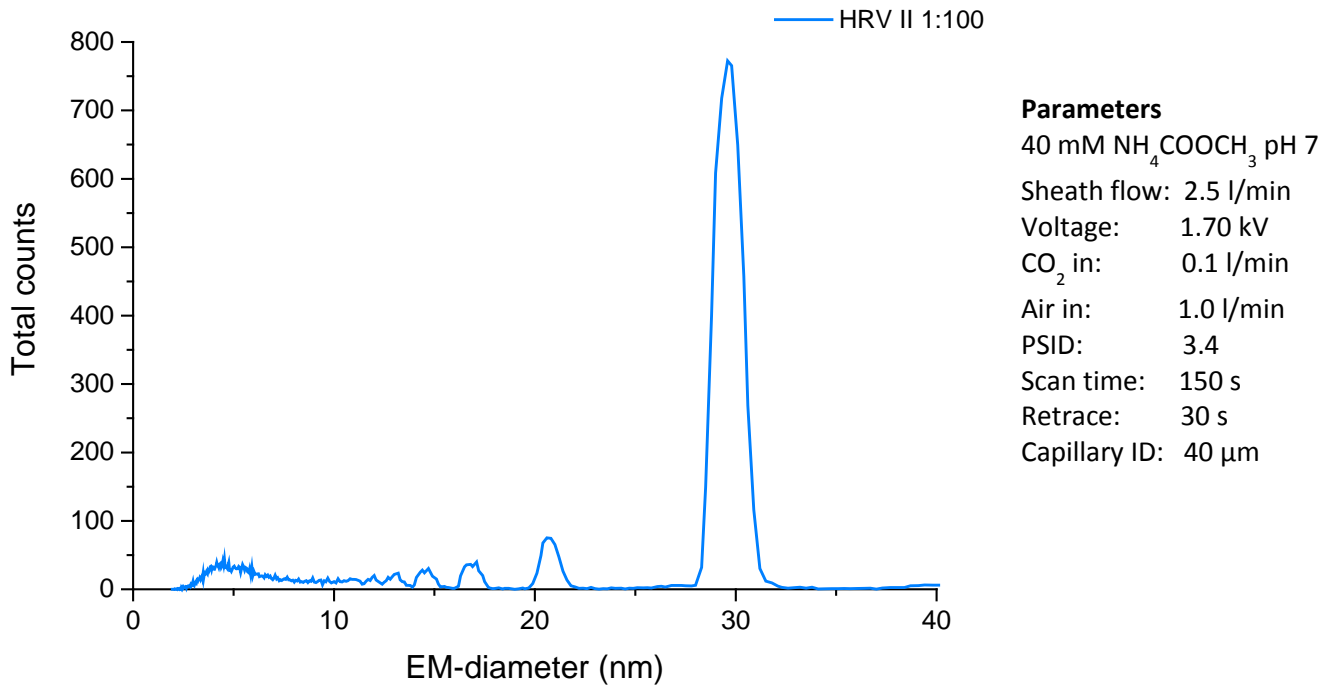
Figure 19: GEMMA spectrum of human rhino virus serotype II, united aliquots.

Figure 19 shows the spectrum of the HRV-A2 stock used for encapsulation with a dilution of 1:100 (1:2 from the 1:50 stock). There are 3 distinct peaks. The first one at around 16 nm, the second one around 20 nm and the main peak at 29.8 nm. As it was found in an unpublished work using AFM measurements on collected fractions of these peaks, they all originate from virus particles of the same size. It was therefore concluded that the size shift is a result of different charge states ($[M]^{2+}$ and $[M]^{3+}$ M, intact virus) of the virus.

Parameters (Liposome sample)
40 mM NH_4COOCH_3 pH 8.4
Sheath flow: 2.5 l/min
Voltage: 1.83 kV
CO_2 in: 0.1 l/min
Air in: 1.0 l/min
PSID: 3.4
Scan time: 150 s
Retrace: 30 s
Capillary ID: 40 µm
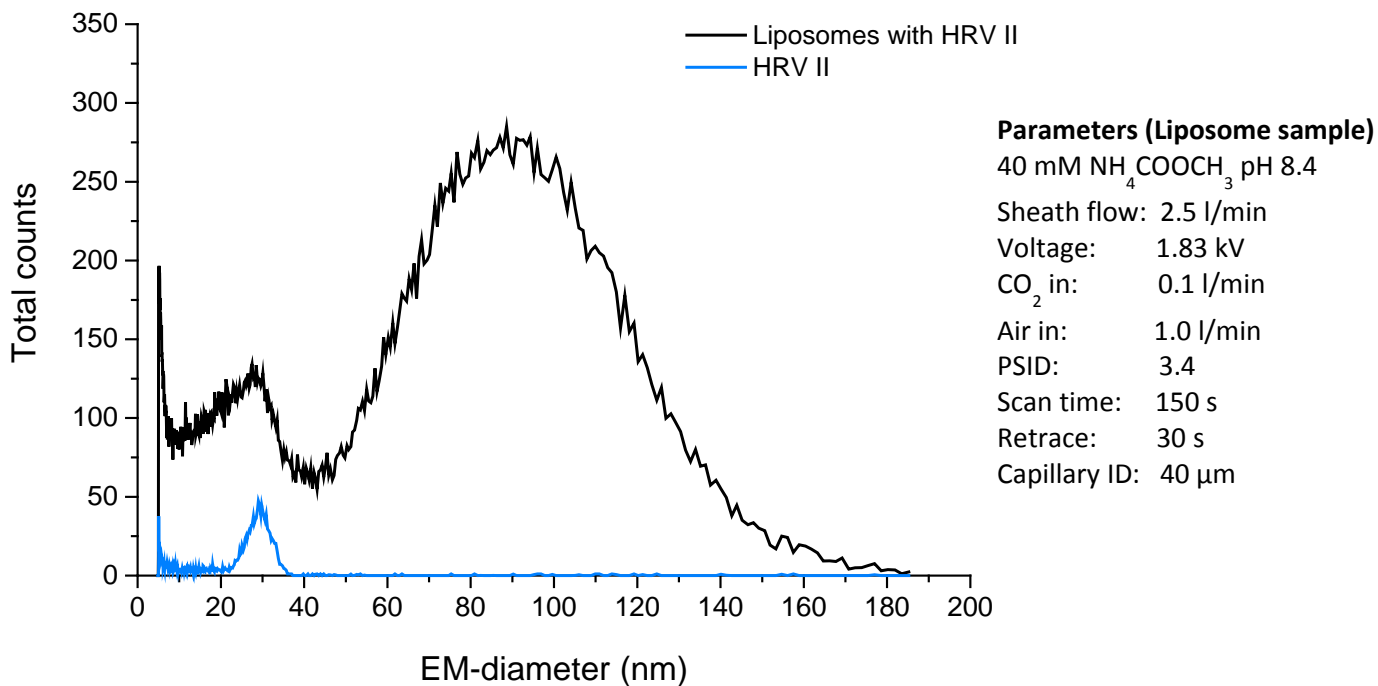
Figure 20: Liposomes created with added HRV-A2, plotted against HRV-A2 stock.

Figure 20 shows the liposomes, extruded using a 0.1 µm membrane pore size, that were prepared by using a mixture of ammonium acetate and virus stock in a plot together with the HRV-A2 stock. The virus was measured with a dilution as it is present in the liposome sample. The measurement shows that the virus in the liposome sample would not be detectable using GEMMA as it lies below the liposome signal. Hence, removal of non-encapsulated virus particles prior measurement is a necessary prerequisite.

Liposomes after density gradient centrifugation

In total 16 density centrifugations were performed as said before and listed in Table 4, using liposomes containing HRV-A2 (see Figure 20).

Of these, the spectra of centrifugations number 1, number 14 and number 7 are shown in this chapter. Spectra of the other centrifugations can be found in the Appendix (Density gradient centrifugation – Additional centrifugations). Additional figures created to describe and compare the centrifugations are also found in this chapter.

Figure 21 shows an overlay of the spectra from the collected fractions of centrifugation number 1 after removing the sucrose using centrifugal filters (procedure see Solvent Exchange and Desalting). The count number of liposomes in the region of 80-100 nm is relatively low, especially compared to the peak in the area of 4.85 nm – 40 nm region that represents residual sucrose.
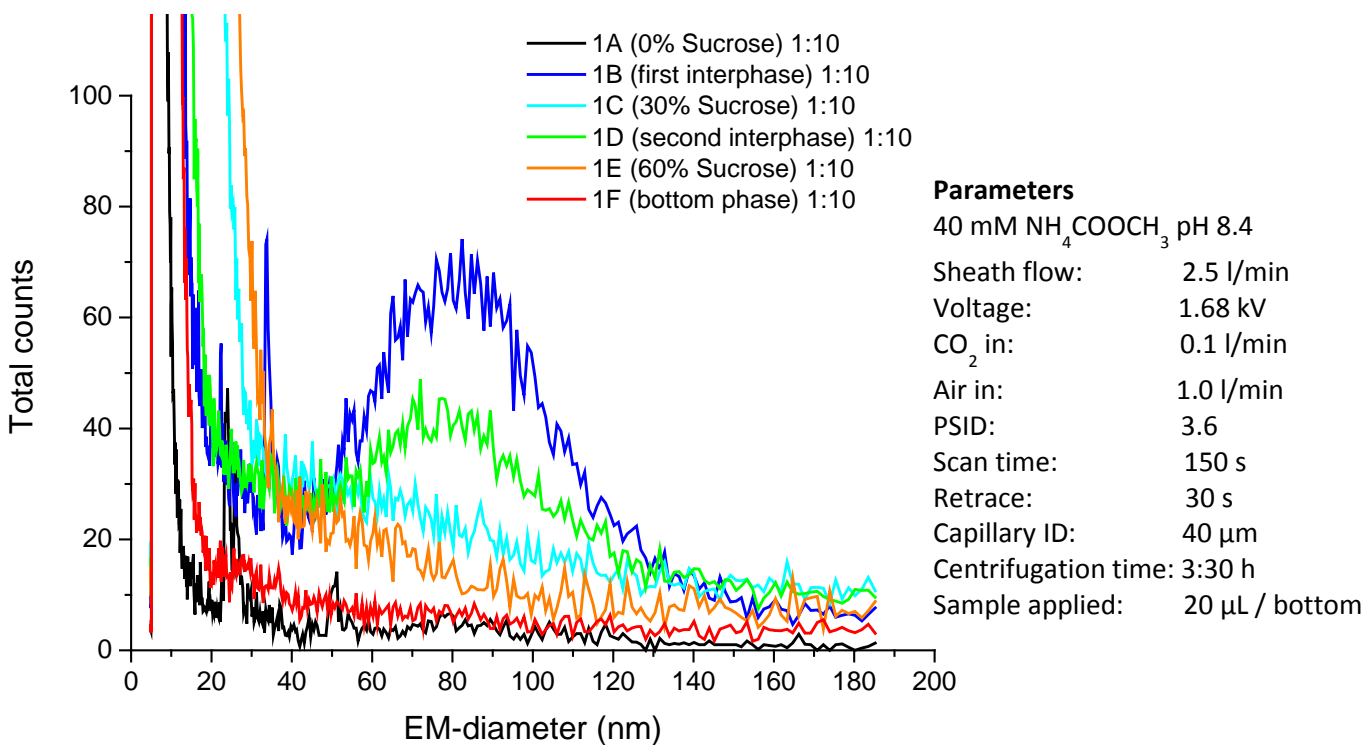
Figure 21: Density gradient centrifugation number 1, fractions after solvent exchange.

Figure 22 shows an overlay of the spectra from the collected fractions of centrifugation number 14 after desalting.

For this centrifugation there was more liposome sample added (increased from 20 µL to 50 µL), more cycles of solvent exchange were done (increased from 3 to 7), and the sample was measured less diluted in comparison to centrifugation number 1 above. As a result, a higher number of liposomes was found throughout the fractions and the sucrose peak decreased in relation.

As the figure shows, there are liposome peaks found in all phases, albeit in different concentrations. The highest numbers of liposomes are found in the first interphase as well as in the second interphase and the 50 % sucrose phase. Since the interphases are of less volume than the %-phases, the liposomes are potentially higher concentrated in the interphases.

Direct comparisons between interphases and phases are therefore not useful based on this figure. What can be said however is that in the 0 % sucrose phase a lower number of liposomes is found than in the 30 % sucrose phase and 50 % sucrose phase. This is contrary for the interphases, where the highest number of liposomes are found in the first interphase, decreasing towards the bottom phase.

Additionally, the overlay shows a shift in the size of the liposomes towards smaller liposomes from top to bottom phase.
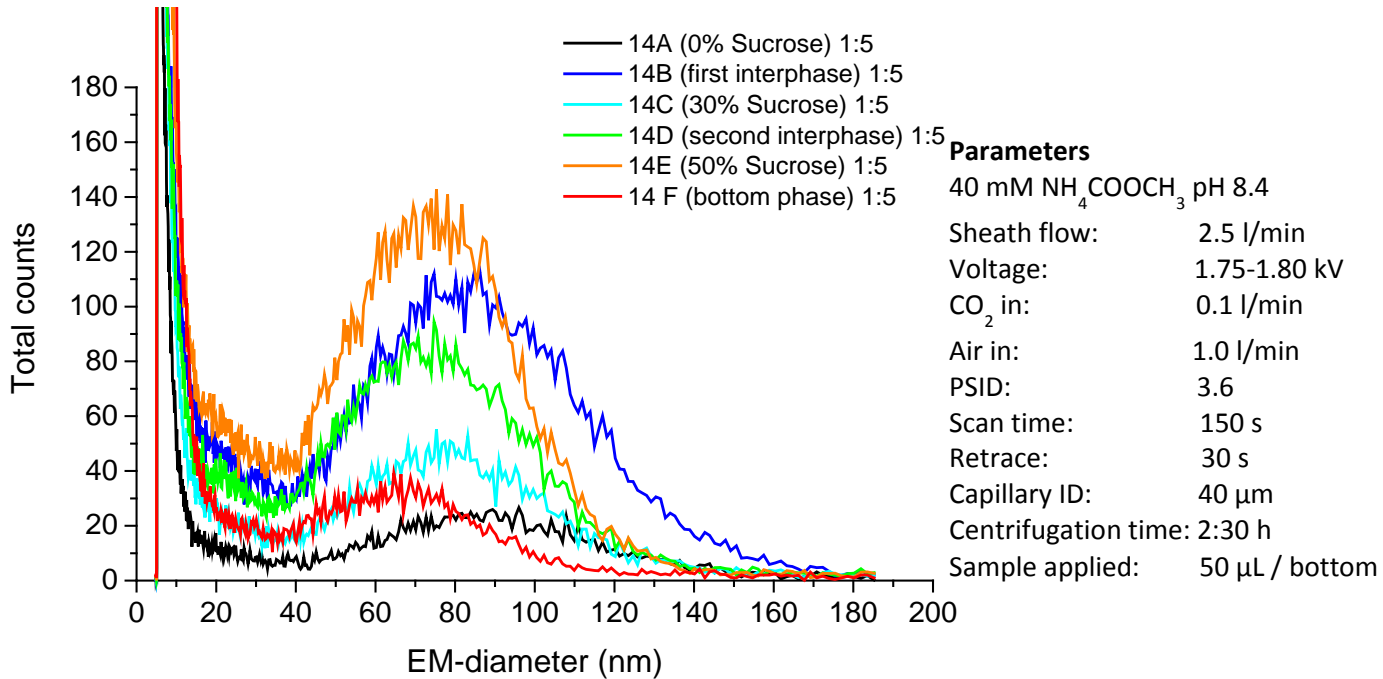
Figure 22: Density gradient centrifugation number 14, fractions after solvent exchange.

A centrifugation with a different approach than the former two that were shown is number 7. For this centrifugation the sample was applied in the top phase. The centrifugation sample consisted of 7 phases, resulting in the collection of a total of 14 fractions of phases and interphases. However, after the third interphase 7F no liposomes were detectable using GEMMA. The spectrum of the overlay of the collected fractions that contained liposome peaks is shown in Figure 23.

The spectrum shows that there is a size shift between the 0 % sucrose phase and the first interphase. This has been observed in a similar way in centrifugation number 14 as well.

The highest number of liposomes is found in the top phases here, potentially because of the short centrifugation time of 35 min compared to the 150 min of centrifugation number 14. An increased centrifugation time did not improve the separation as seen in Figure 57 (see Appendix), which is the spectrum of the measurement from centrifugation number 9. This centrifugation is identical to number 7, except for a longer centrifugation time.
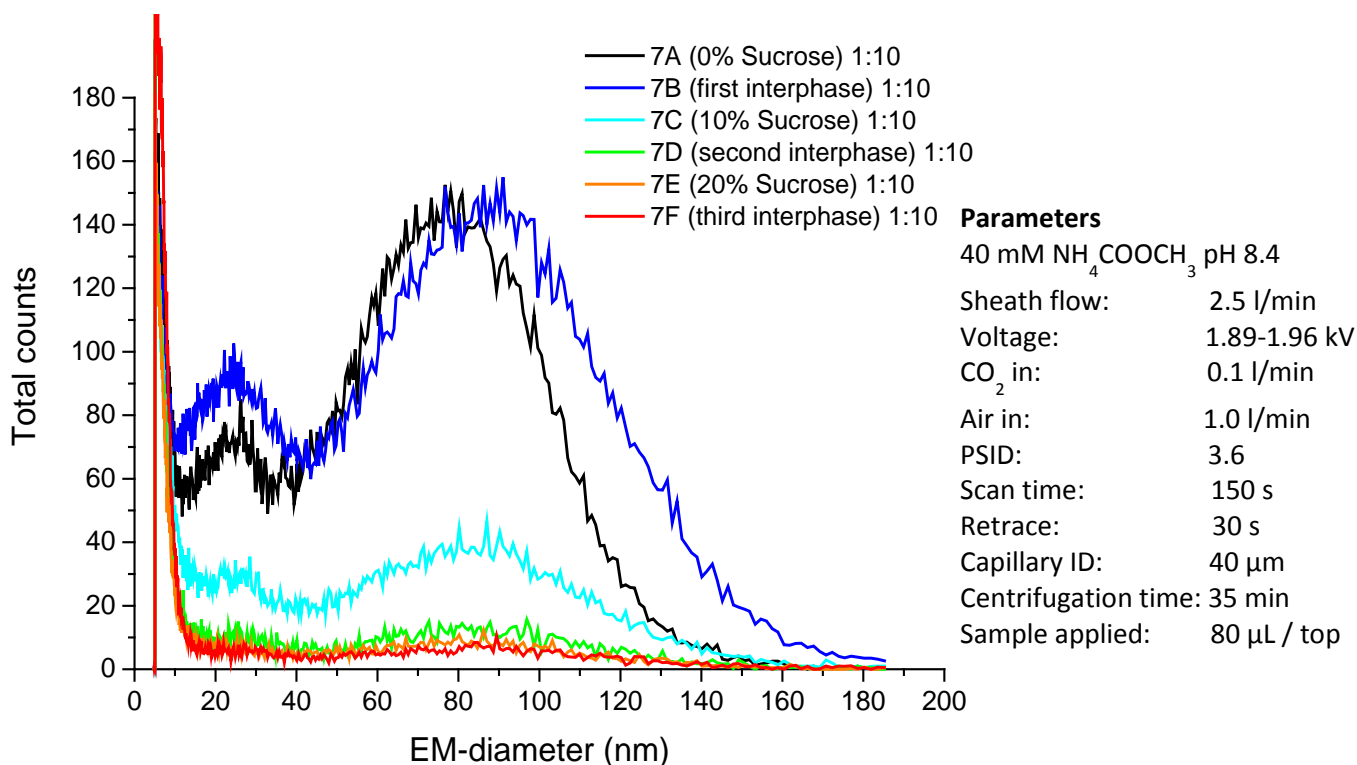
Figure 23: Density gradient centrifugation number 7, fractions containing liposomes after solvent exchange.

A visualization of the separation that also allows for a comparison between the phases of each centrifugation and for a comparison of the different centrifugations was done in the following figures. In these figures, the volumetric count maximum (count maximum/volume) of each fraction and its EM-diameter are plotted together with the density of the phase. The count maximum and its EM-diameter were found using the *MAX* function in Microsoft Excel on the raw counts within the range of 50 to 130 nm. The volumetric count maximum was received by dividing the count maximum by the volume of the collected centrifugation fraction. The densities were taken from an online table [48].

The figures were made for all centrifugations where liposomes were found, i.e. 1, 7, 9, and 11 to 16. For centrifugation number 7 and 9, where 14 fractions were collected, only the fractions up to the third interphase are shown. The fractions thereafter (30 % Sucrose and onwards) did not show any liposome signals.
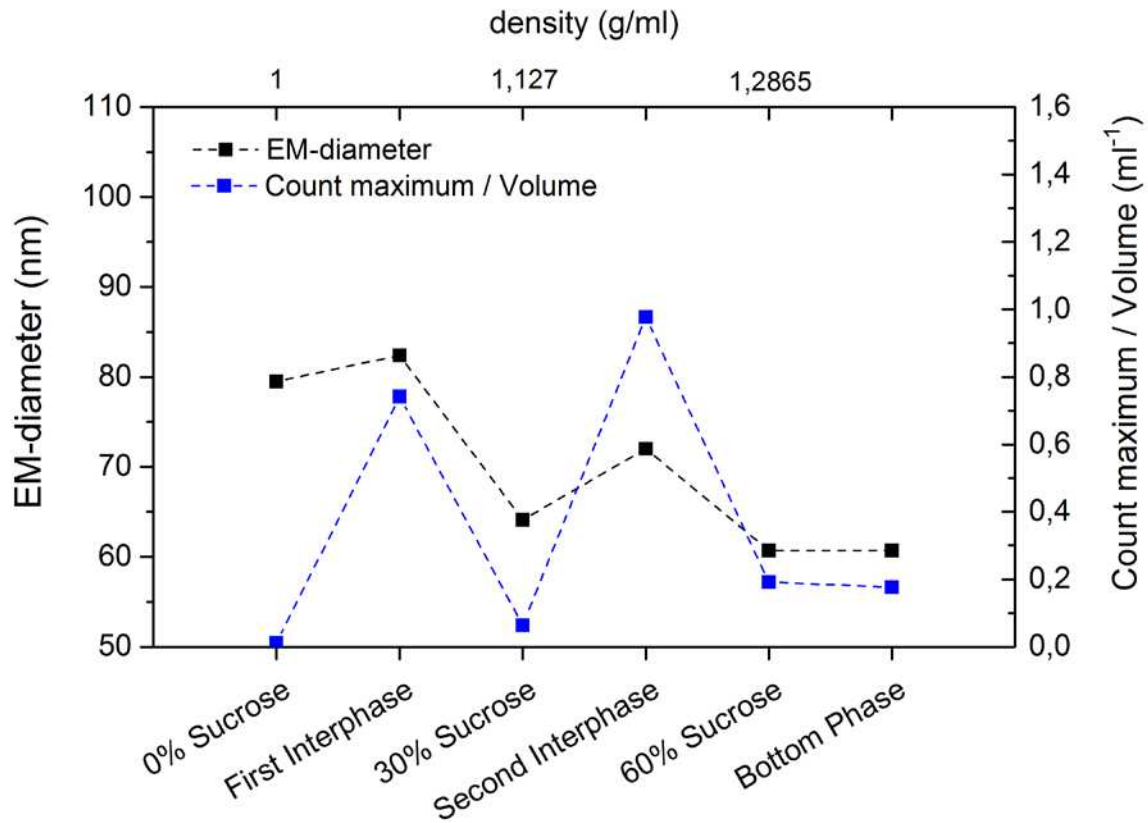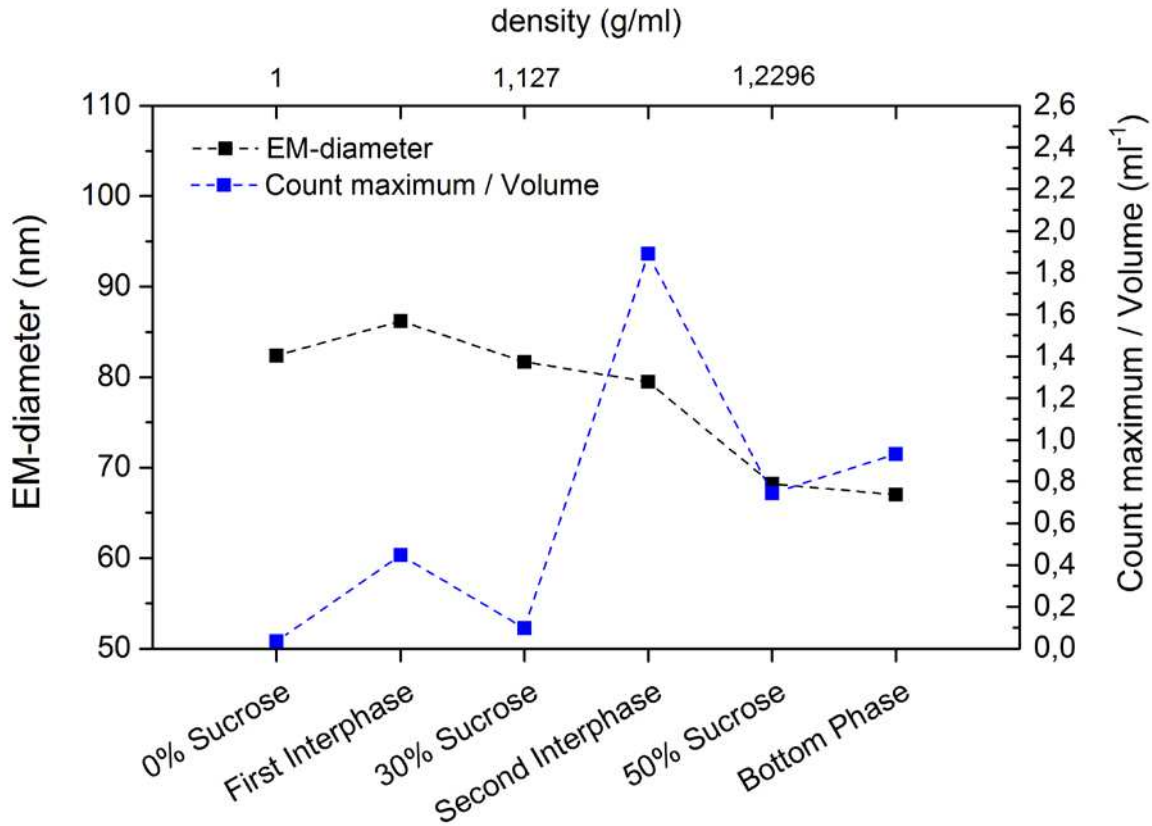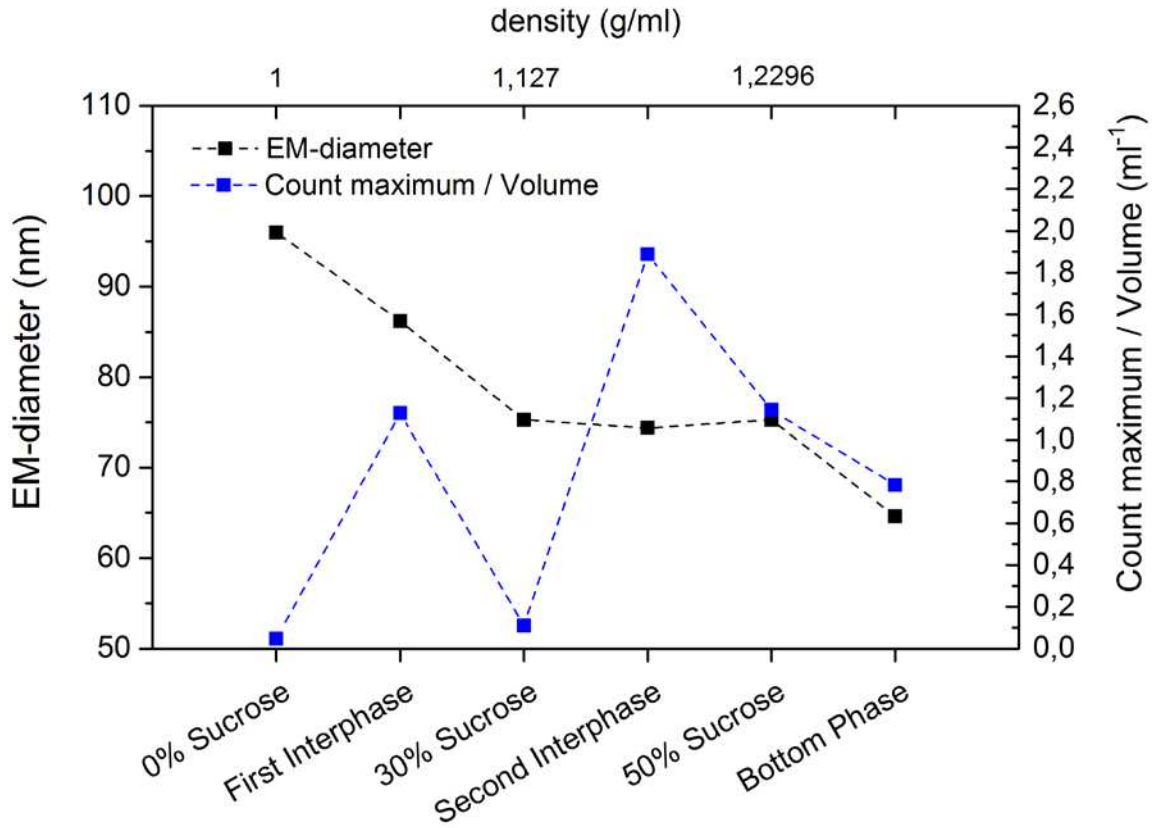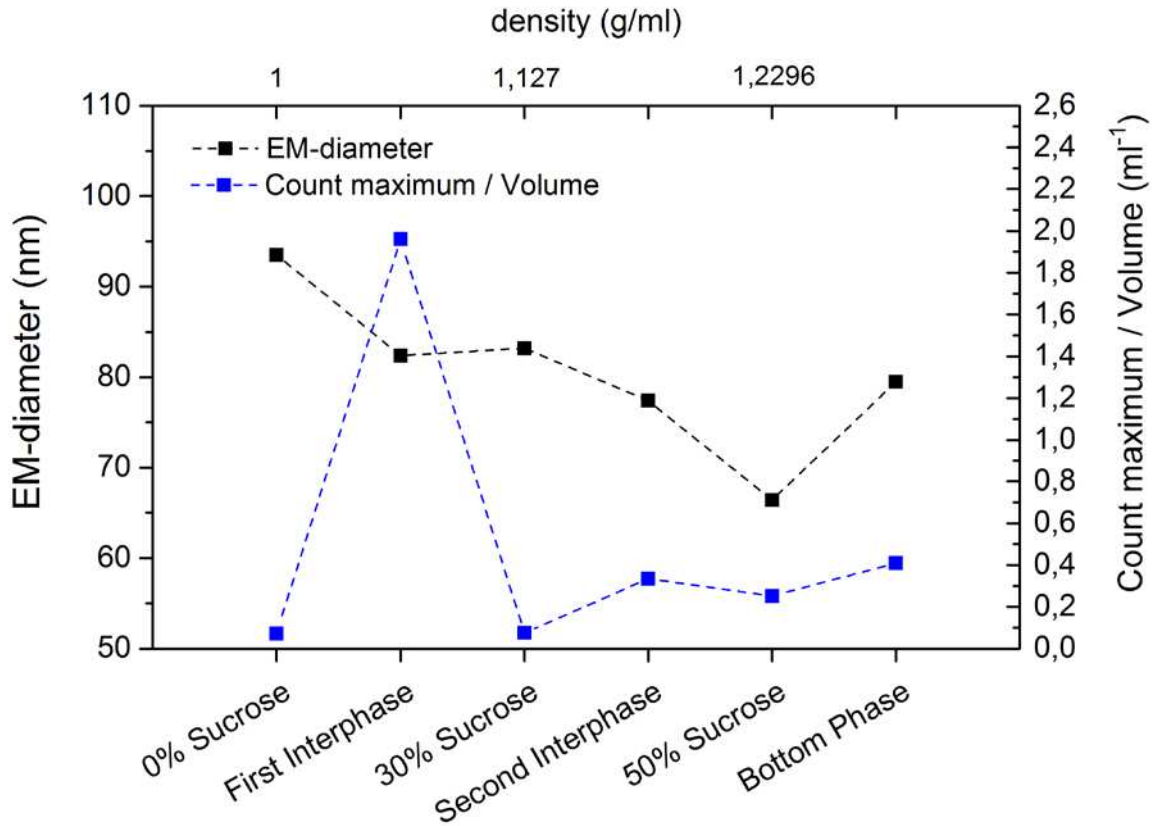

Figure 24: Density gradient centrifugation number 1, EM-diameter and volumetric count maximum against fractions and density.

Centrifugation number 1 shows two prominent peaks for the volumetric count maximum, which are separated by at least one phase, which means that a separation of two groups of particles was accomplished. It was assumed that these groups are empty liposomes in the first interphase that should be less dense and filled liposomes in the second interphase with a higher density.

The EM-diameter, as visible in the figure decreases from the top phase to the bottom phase. This additionally indicates that the liposomes in the interphases are not identical.
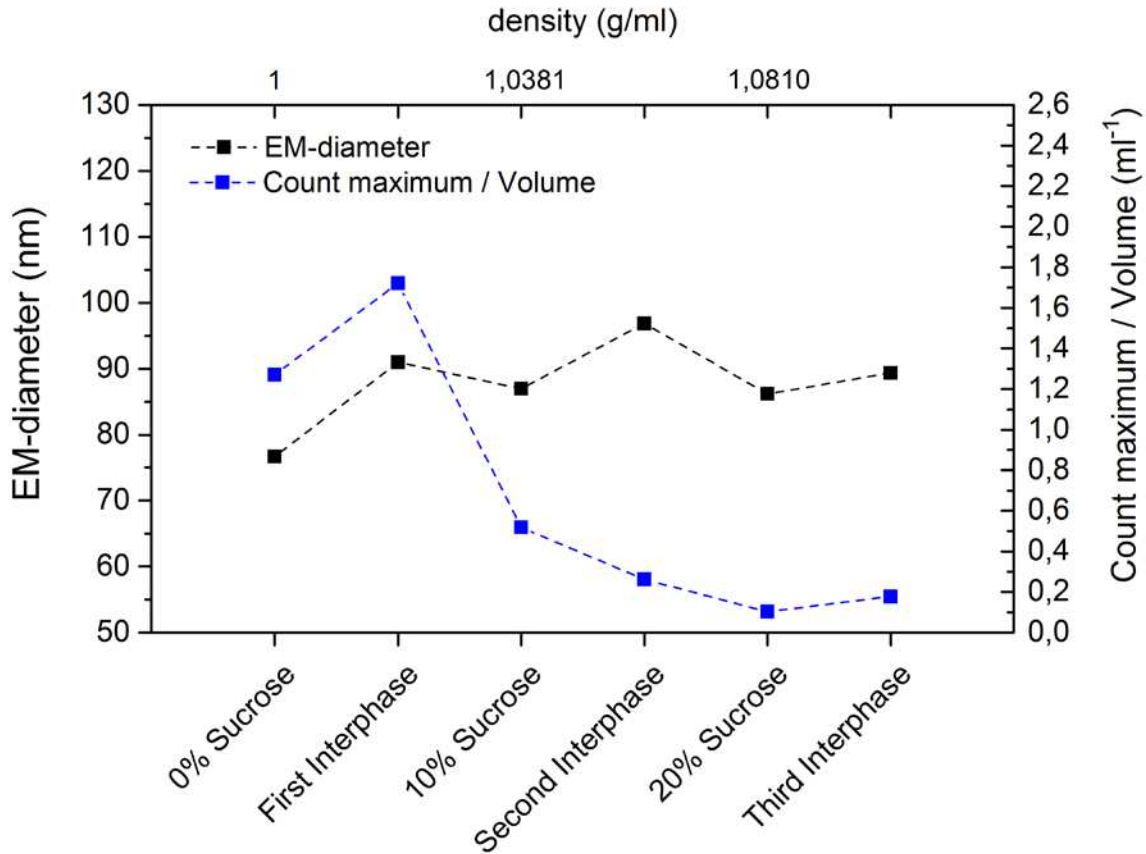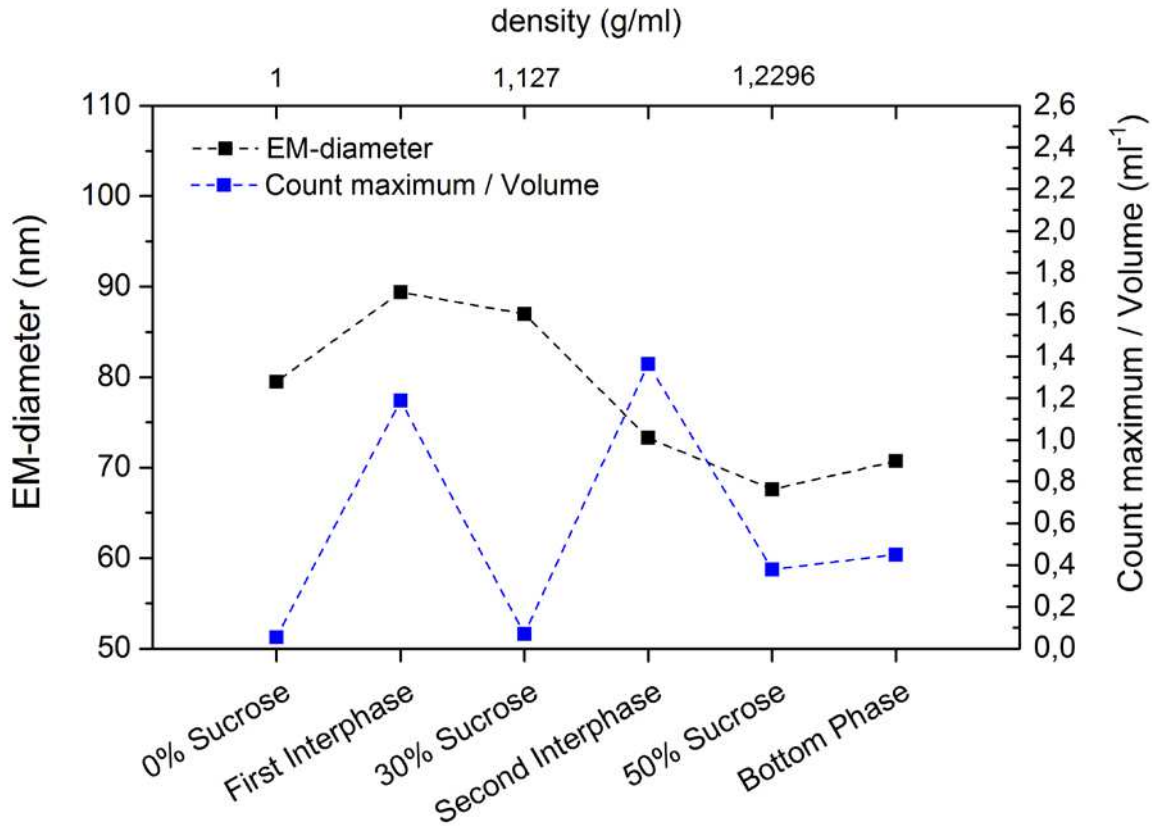
Figure 25: Density gradient centrifugation number 7, EM-diameter and volumetric count maximum against fractions and density.

Centrifugation number 7 shows a high volumetric count maximum in the first two phases, which decreases towards the bottom phase. It seems that the liposomes did not have enough time to reach the sucrose phases in this centrifugation. The separation into groups of liposomes is also not seen here like it was in centrifugation number 1.

The effect of a decreasing EM-diameter is also not found in this centrifugation, meaning that the maximum in counts was found at about the same particle size in the different phases. That also underlines that there is no clear separation of the different liposomes as found in centrifugation number 1.
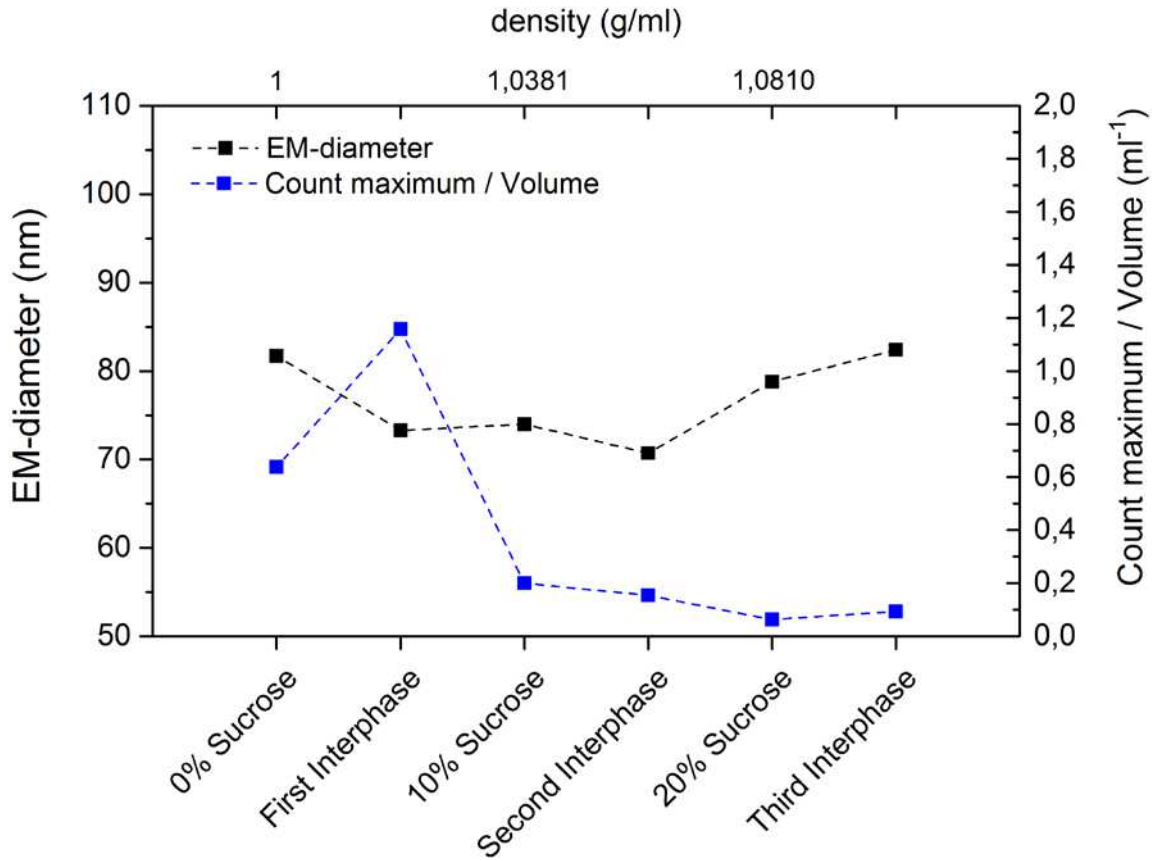
Figure 26: Density gradient centrifugation number 9, EM-diameter and volumetric count maximum against fractions and density.

The graphs derived from the data of centrifugation number 9 resemble the ones from centrifugation number 7 although obtained after significantly increasing centrifugation time. That means that the same statements that were made above for centrifugation 7 are also valid for this centrifugation and that there is no clear separation of the liposomes.
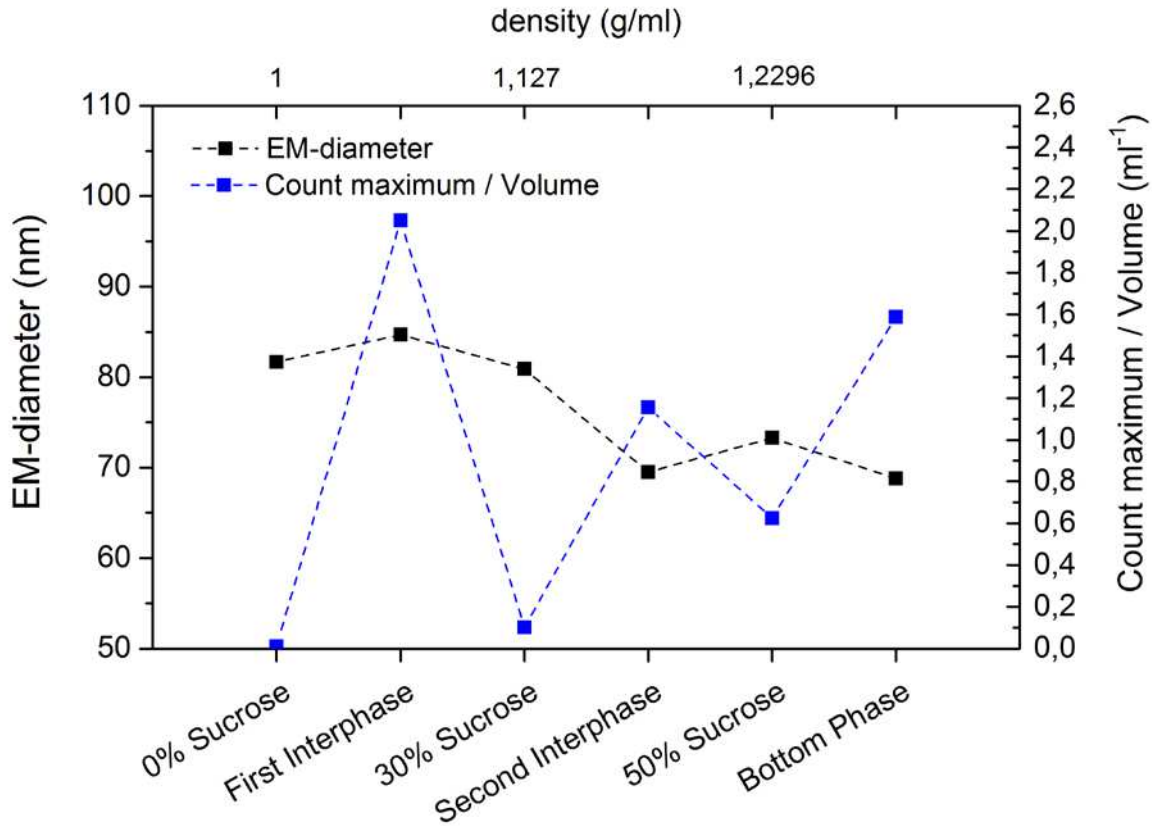
Figure 27: Density gradient centrifugation number 11, EM-diameter and volumetric count maximum against fractions and density.

Centrifugation number 11 and onwards were repeats of centrifugation number 1 with increased sample volume and varying centrifugation times. Centrifugation number 11 (centrifugation time of 1:30 h) is also comparable to centrifugation number 1 (centrifugation time 3:30 h) when comparing Figure 24 and Figure 27. The volumetric count maximum in comparison is higher in Figure 27 since the sample volume and thus the number of liposomes is higher. The main difference however is that the volumetric count maximum is relatively high in the bottom phase, which was not found in centrifugation number 1.

It seems here as well that a separation took place, as the volumetric count maximum is low in the 30 % sucrose phase. This separation of different liposome groups is again also indicated by decreasing EM-diameter from the top phase to the bottom phase.
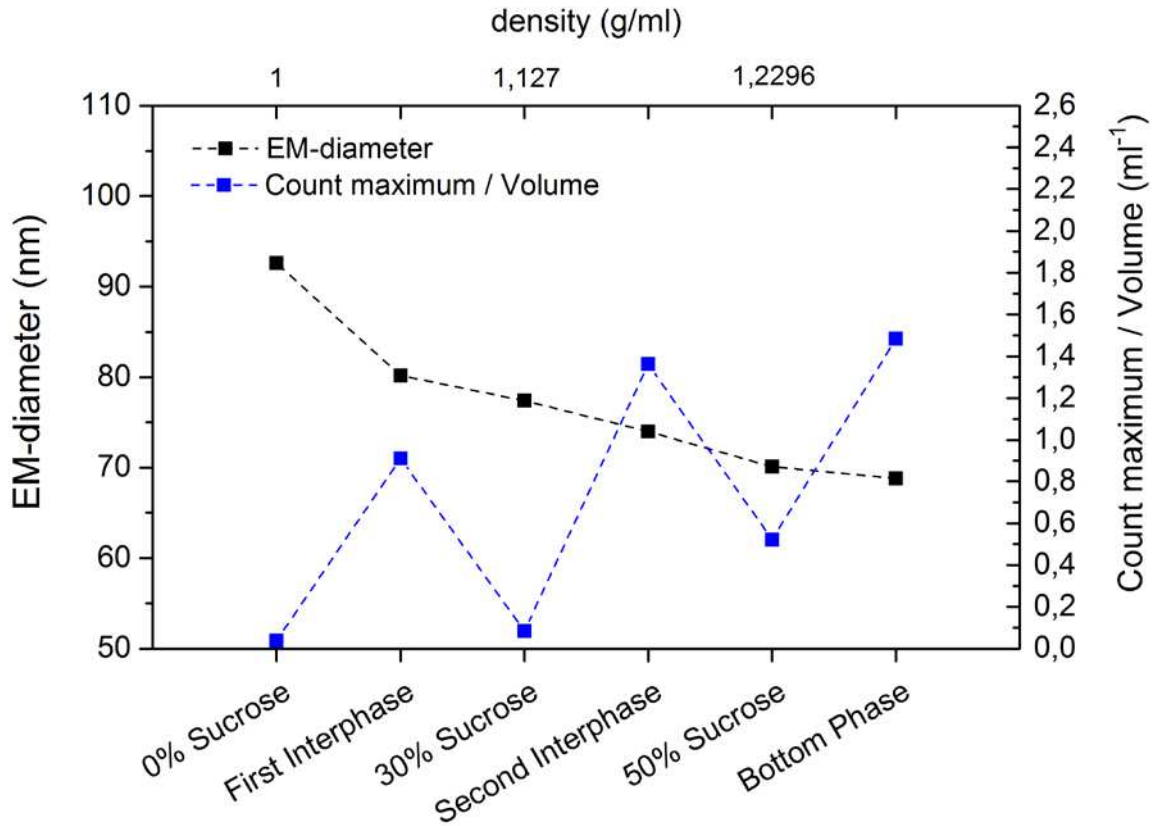
Figure 28: Density gradient centrifugation number 12, EM-diameter and volumetric count maximum against fractions and density.

Centrifugation number 12 is the duplicate of centrifugation number 11. The two centrifugations are comparable, both have peaks for the volumetric count maximum in the interphases. This indicates a separation. The decrease of the EM-diameter is even more pronounced here than it was for centrifugation number 11, also indicating a separation.

Figure 29: Density gradient centrifugation number 13, EM-diameter and volumetric count maximum against fractions and density.

Centrifugation number 13 had a centrifugation time of 2:30 h. Compared to the centrifugations with centrifugation times of 1:30 h (numbers 11 and 12), the volumetric count maximum is relatively low in the first interphase, but high in the second interphase. This could mean that more filled liposomes where present. Since the liposomes are floating from the bottom upwards until they reach a phase of near equal density, it can be assumed that the reason for the higher number of liposomes in the second interphase is not a result of liposomes that settled from the upper phases.

The EM-diameter is comparable to centrifugation 11. Therefore, also here a separation seems to have taken place.

Figure 30: Density gradient centrifugation number 14, EM-diameter and volumetric count maximum against fractions and density.

Centrifugation number 14 is comparable to its duplicate, centrifugation number 13, except that here the volumetric count maximum is decreasing after the second interphase until the end. Also, the decrease of the EM-diameter is more pronounced.

Figure 31: Density gradient centrifugation number 15, EM-diameter and volumetric count maximum against fractions and density.

Centrifugation number 15 had a centrifugation time of 3:30 h. The highest number of liposomes per volume was found in the first interphase here, where the empty liposomes are assumed to be found. There is an increase in the volumetric count maximum in the bottom phase as it was found for centrifugation number 11. A separation seemingly was accomplished.

Figure 32: Density gradient centrifugation number 16, EM-diameter and volumetric count maximum against fractions and density.

Centrifugation number 16, the duplicate of number 15, shows a separation of different liposome groups just like centrifugation number 1. The EM-diameter is decreasing again from the top to the bottom phase, even though there is a relatively low value of the EM-diameter in the 0 % sucrose phase. This is a result of the low number of liposomes found in this phase, with the maximum count number at a relatively low diameter. Therefore, the assumption of a decreasing EM-diameter is still valid.

To summarize the outcome of the gradient centrifugation, it seems that there was a separation of different liposome groups in the centrifugations number 1 and number 11 to 16. It also seems that the influence of the centrifugation time (based on the results of Figure 27 to Figure 32) is not as high as possibly expected, with similar results for all centrifugation times tested. Reproducibility is an issue, due to the fact of preparing the overlay of the sucrose phases, where mixture might occur if not done slowly, and collecting the phases afterwards with the pipette.

The approach where the sample is added to the bottom phase seems to be favorable over the addition of sample to the top phase.

Electron microscopy

Electron microscopy was first done using liposomes that were prepared with virus (GEMMA spectra see Liposomes with HRV-A2) as seen in Figure 33. Liposomes are visualized as structures in different shades of grey, while virus is seen as rounded particles with a dark border. Some of these virus particles seem to be in native state (glowing white), while others seem to have undergone structural changes already (greyish color). There is virus visible underneath and adhered to the liposomes, but also free and next to no liposomes which is unwanted. The pictures below also show that the liposomes lost their integrity in the vacuum although they were covered in trehalose.
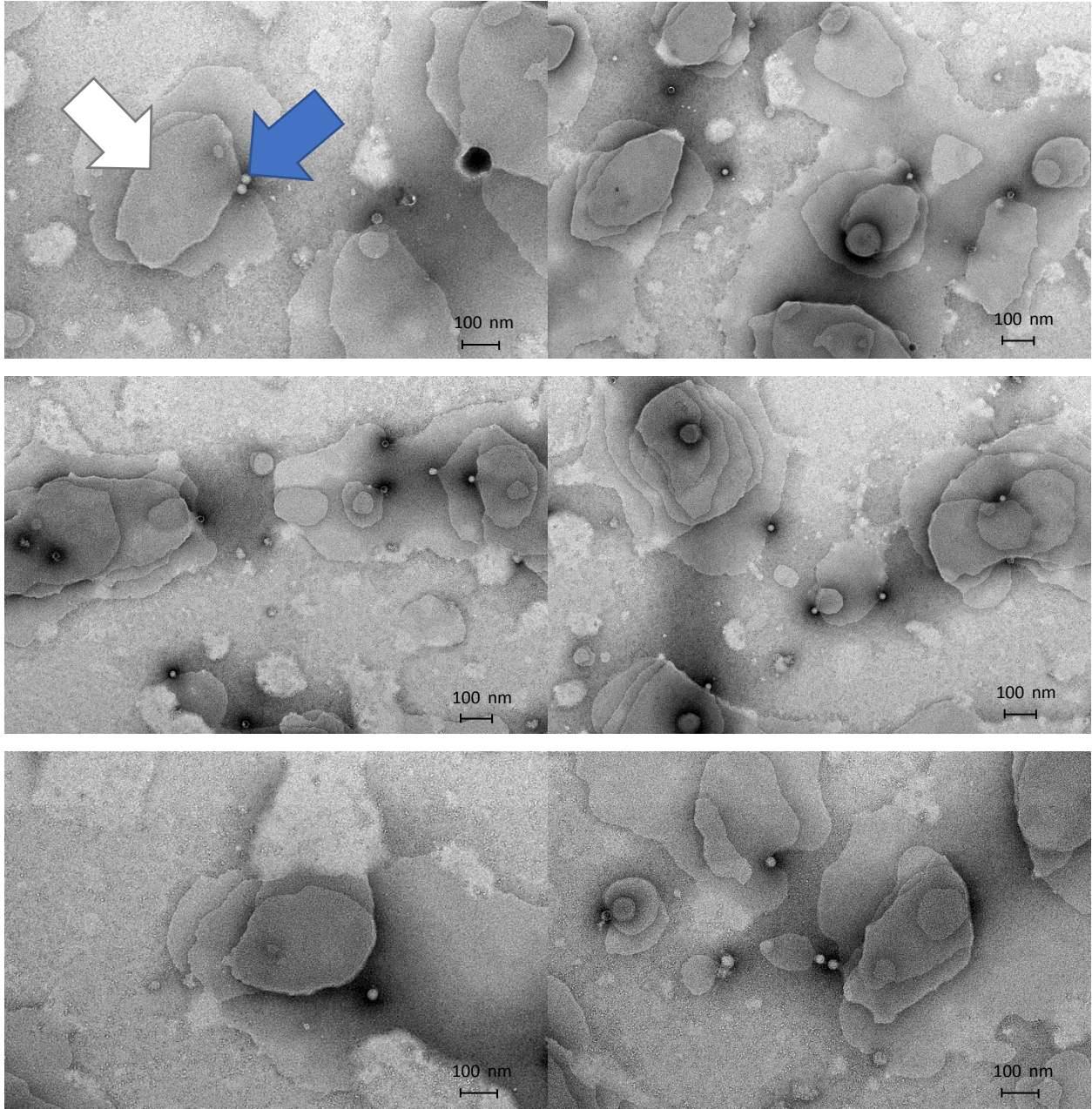
Figure 33: Electron microscopy pictures from liposomes (white arrow) prepared with HRV-A2 (blue arrow) prior centrifugation.

Based on the outcome of the above made pictures, it was decided to perform the gradient density centrifugation to remove free virus and unfilled liposomes as said before. It was also tested whether the sucrose from the gradient centrifugation could have an influence on the stability of the liposomes during the electron microscopy.

As visible in the figures below with added sucrose, the liposomes kept their spherical shape, which is an improvement over the previous electron microscopy pictures. These pictures again show free virus and virus attached to the liposome surface, thus indicating the need of the purification.
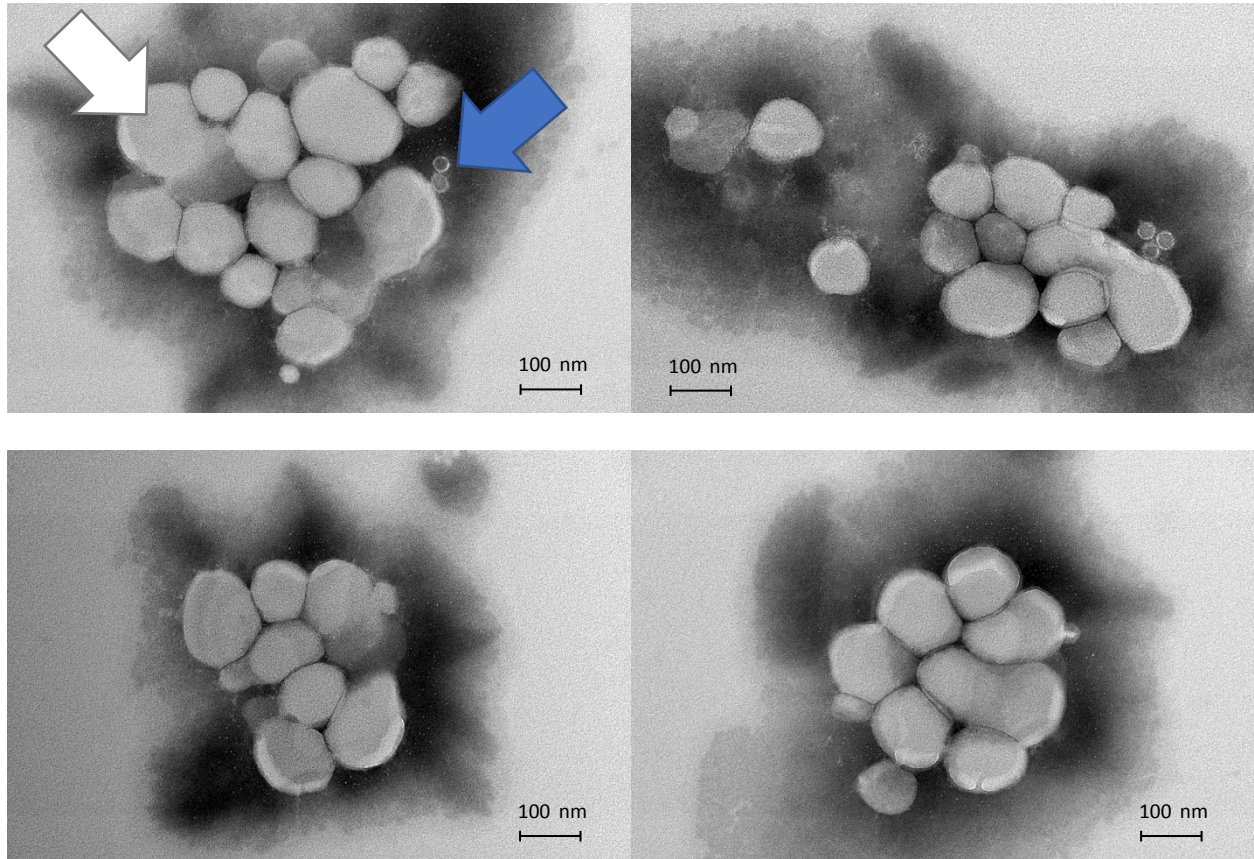
Figure 34: Electron microscopy pictures from liposomes (white arrow) prepared with HRV-A2 (blue arrow) with added sucrose (30 m%) before centrifugation.

Electron microscopy was repeated using centrifugation samples 1B / 1D and 7A and 7B (Figure 35 to Figure 36).

Figure 35 shows 1B, which is the first interphase between the 0 % sucrose phase and the 30 % sucrose phase of centrifugation number 1, and 1D, the second interphase between the 30 % and 60 % sucrose phase. In these phases, liposome signals were found using GEMMA, and the electron microscopy pictures verify the presence of liposomes. In both cases no free virus was found in the pictures made. The initial aim of removing free virus thus seems to be fulfilled. Whether the separation of empty liposomes and liposomes containing virus was successful on the other hand cannot be verified by these pictures, as the electrons penetrate the liposomes only to a very small extent in scanning electron microscopy.

In the bottom right-hand picture of Figure 35, virus that is potentially bound to the inner liposome surface can be seen in the bottom-right liposomes as a dark stain (marked by an asterisk).
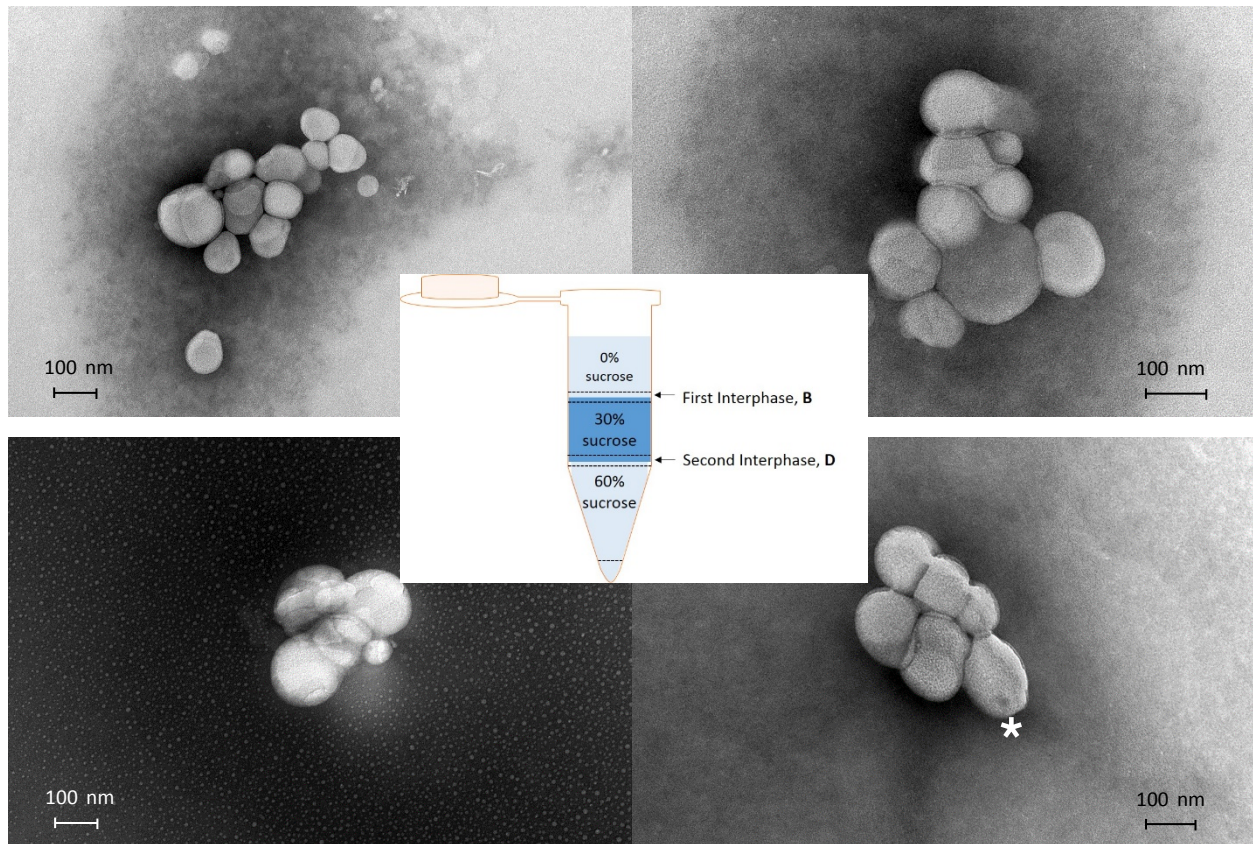
Figure 35: Electron microscopy pictures of sample 1B (top left / top right) and 1D (bottom left / bottom right).

The electron microscopy pictures of the 0 % sucrose phase of centrifugation number 7 (7A) and the first interphase (7B) both show free virus present, thus the separation target was not fulfilled with this (top down) centrifugation.
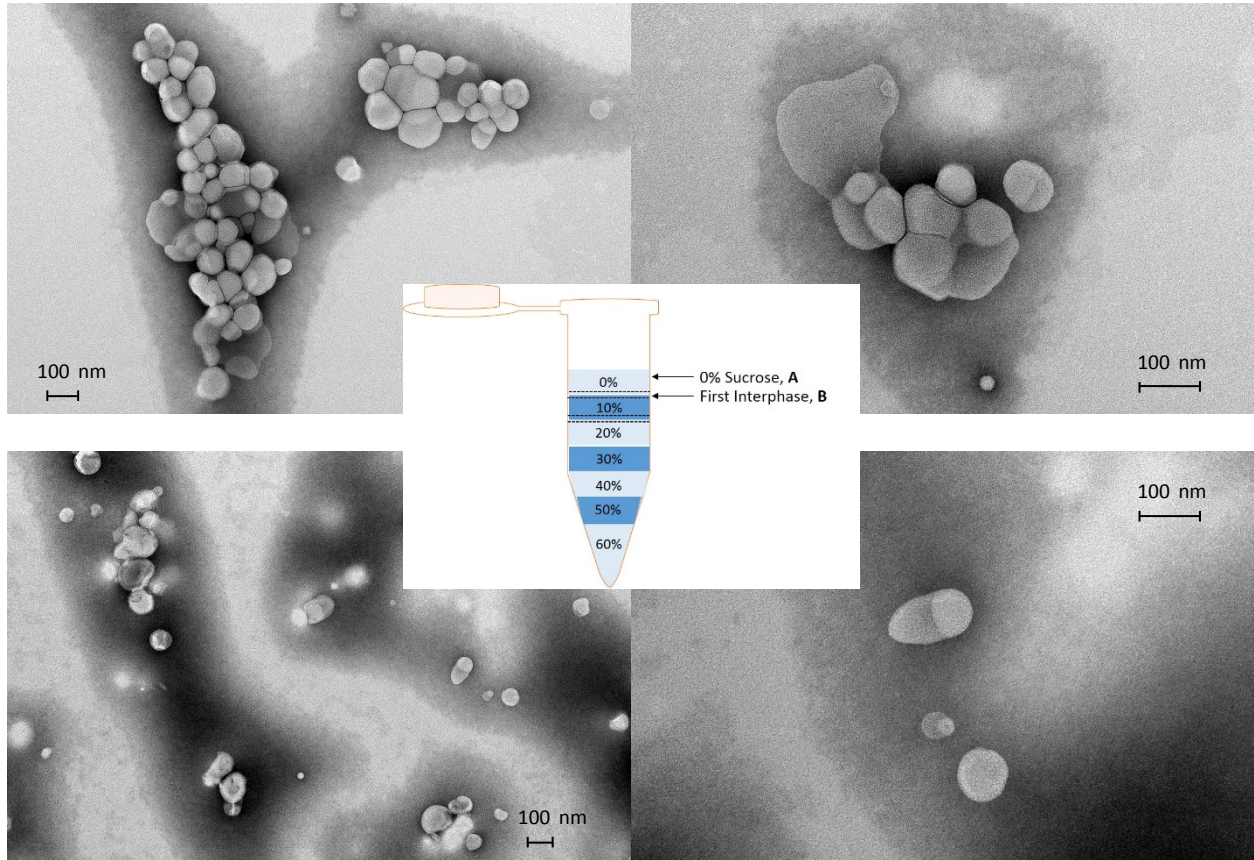
Figure 36: Electron microscopy pictures of sample 7A (top left / top right) and 7B (bottom left / bottom right).

Western Blot

The Western Blot was done using samples 1B and 1D and fractions of centrifugation number 7 after electron microscopy. The used antibody 8F5 VP2 is specific to the native VP2 capsid protein in HRV-A2 [49, 50]. Additional blocking of the membrane using BSA should avoid false positive identifications. Pictures of the chemiluminescent membranes are shown in Figure 37 and Figure 38.

Each fraction besides 1B showed a positive identification for proteins that are bound to the membrane. Since a specific antibody for VP2 of HRV-A2 was used, the bands should originate from that capsid protein. A possibility for additional bands is the presence of VP0, a precursor that is cleaved into VP2 and VP4 upon maturation [46]. Another possibility could be the formation of dimers or multimers of VP2, but this explanation needs further verification.

61
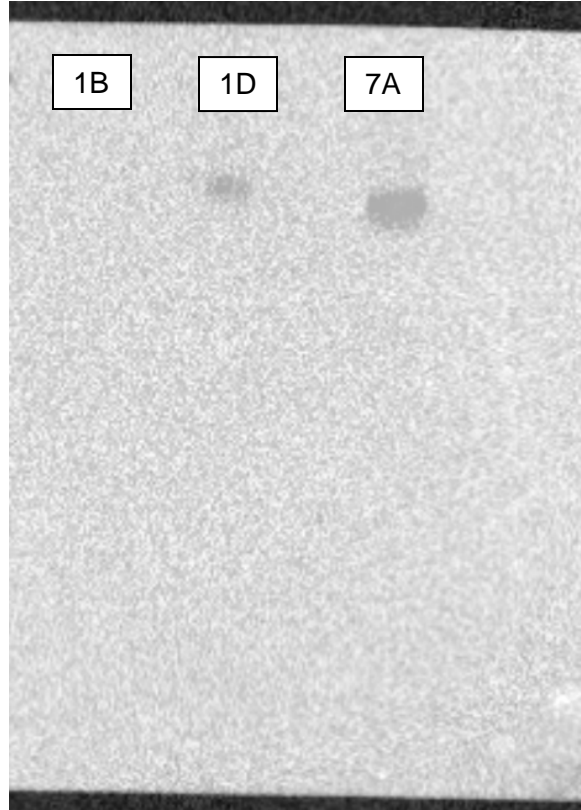
Figure 37: Blotted membrane with fractions 1B / 1D / 7A.
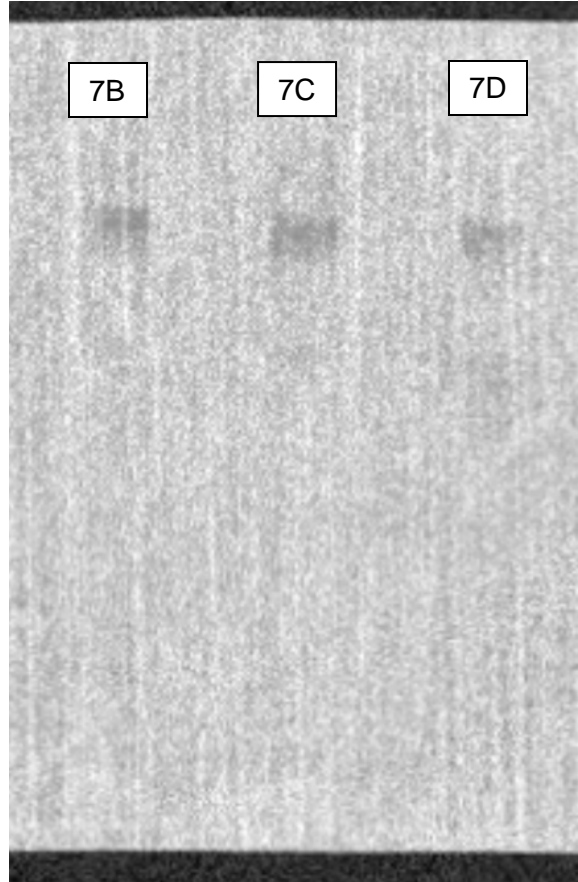
Figure 38: Blotted membrane with fractions 7B / 7C/ 7D.

Sodium dodecyl sulfate polyacrylamide gel electrophoresis (SDS-PAGE)

The SDS-PAGE that was done before the Western Blot did not show viral protein bands after blotting. To verify the presence of viral protein in addition to the blotted membrane two separate SDS-PAGEs with subsequent silver staining were done as described in the chapter of the same name in the Material and Methods section.

The first gel made is shown in Figure 39 and the second one in Figure 40. Table 7 and Table 8 list the samples applied to the gels. The dilution factor relates to the HRV-A2 stock, which itself is a dilution of 1:50 from the received aliquot, meaning that a 1:100 dilution is equal to a 1:5000 dilution of the original aliquot (concentration 10 mg/mL).

The first gel was stained for an excessive amount of time, but as Figure 39 shows there were no measureable amounts of protein in the samples. In the second gel (Figure 40) however, there are bands of proteins found in the undiluted virus stock, with two double bands at around 35 kDa and 25 kDa and a weak band at around 6 kDa. These bands represent the different viral capsid proteins VP1 (~32.9 kDa), VP2 (~29.0 kDa), VP3 (~26.1 kDA) and VP4 (~7.4 kDa) and VP0 (precursor protein which is cleaved into VP4 and VP2 upon virus maturation, ~36.4 kDa), as it has been shown for HRV-A2 before [46, 51].

The above made gels indicate that virus in the liposome samples would not be detectable using silver staining, as neither the quantities found in the samples after centrifugation nor the further diluted samples after solvent exchange (which equals the dilution of 1:1400) produced visible bands.

Table 7: Sample applied on SDS-PAGE gel in Figure 39

	Lane										
1	2	3	4	5	6	7	8	9	10	11	12
-	Ladder	-	HRV-A2 1:100	-	HRV-A2 1:1400	-	1B	-	1D	-	-
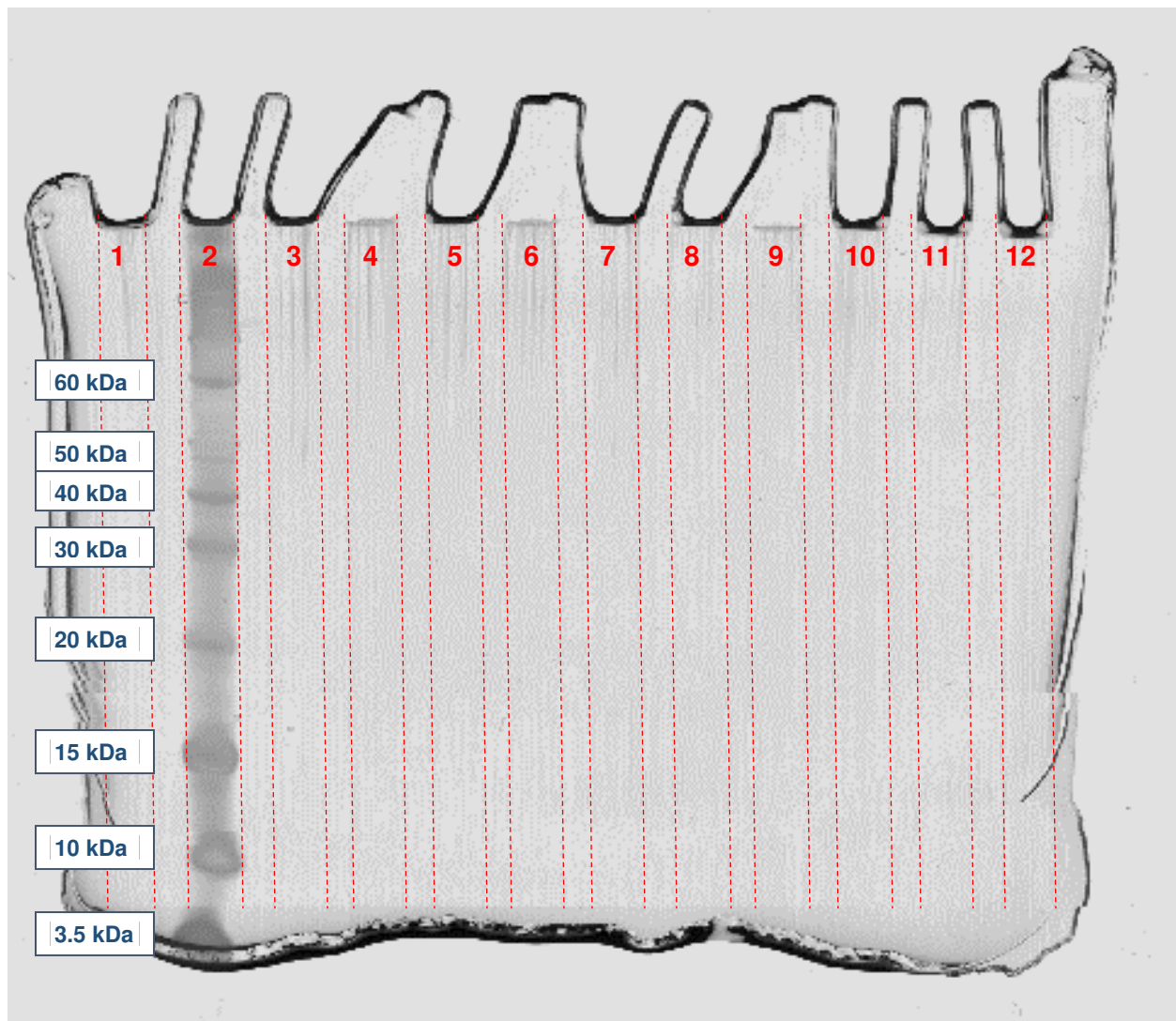
Figure 39: SDS-PAGE of centrifugation samples 1B/1D and HRV-A2.

Table 8: Sample applied on SDS-PAGE gel in Figure 40

Lane											
1	2	3	4	5	6	7	8	9	10	11	12
-	Ladder	-	1B	-	1D	-	HRV-A2 1:50	-	HRV-A2 1:1400	-	-
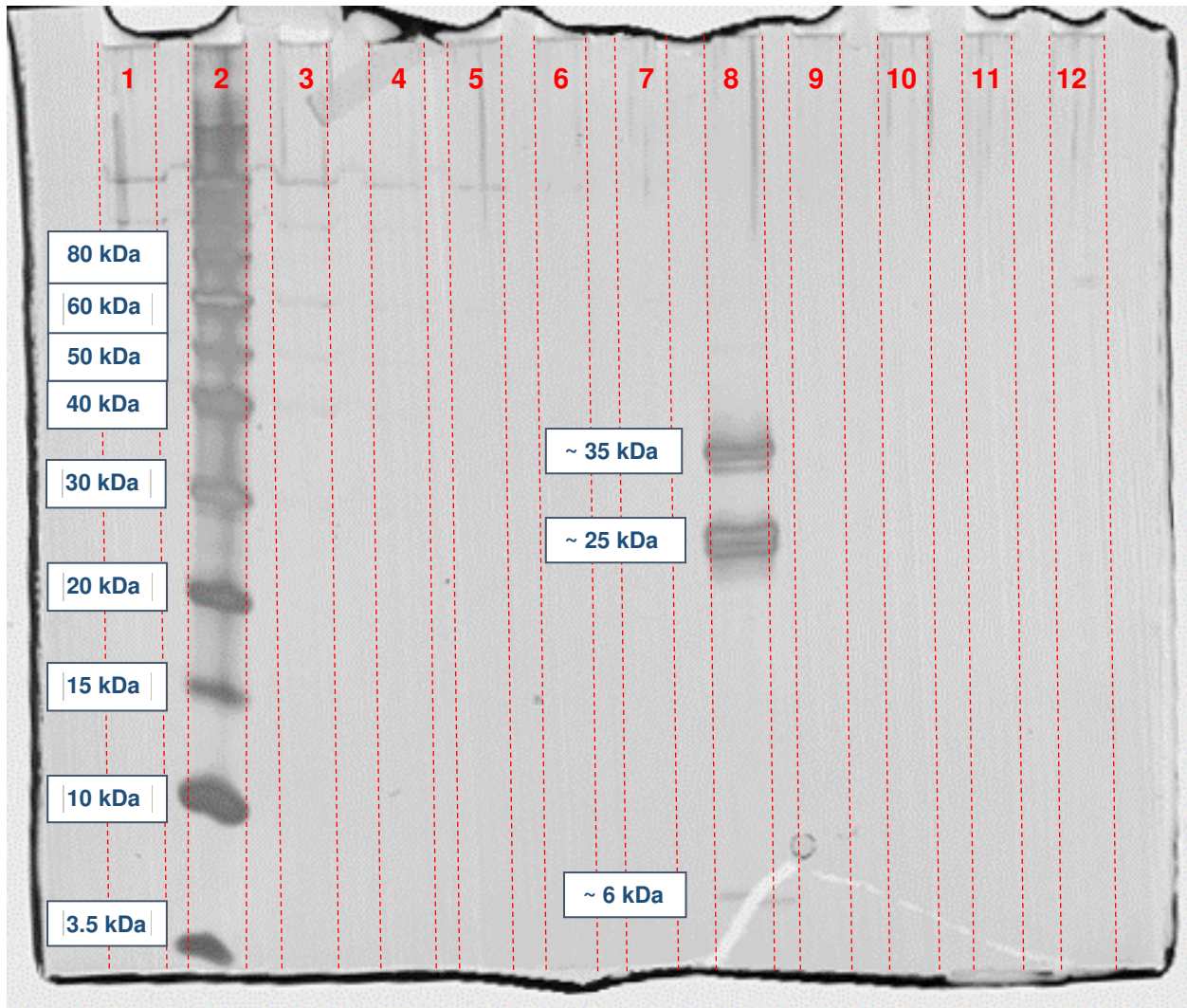
Figure 40: SDS-PAGE of centrifugation samples 1B/1D and HRV-A2, repetition.

Conclusion and Outlook

In this work, liposomes of different size distributions were created by extrusion using different membranes with different pore sizes. It was shown that the membrane pore size has an effect on the size distribution of the liposomes by measuring on the GEMMA system. Liposomes were also created without and with HRV-A2 and measured using GEMMA, showing that the virus is not detectable in the liposome dispersion in the free form.

Electron microscopy was performed on the putatively virus containing liposomes for visualization of the liposome dispersion. The method was improved by adding sucrose to the samples, which resulted in intact, spherical liposomes that with the old method of preparation were disintegrated flat surfaces. It was shown that the prepared liposomes (with HRV-A2) featured virus bound to the outer virus surface and free virus. An irrefutable verification that virus was enclosed inside the liposomes with this method is not possible however, as scanning electron microscopy was performed instead of cryo electron microscopy. In a future work, the liposomes prepared could be measured using a cryo EM.

Due to the free and surface bound virus present in the liposome preparation with HRV-A2, sucrose density gradient centrifugation / flotation was done for purifying the sample. Two different approaches were tested. The first approach (sample applied in the bottom phase) proved to be superior in comparison to the second approach (sample applied in the top phase) as shown in Figure 24 to Figure 32. An overall issue of the method is that it lacks reproducibility. The different centrifugations showed varying concentrations of liposomes across the fractions. This issue might be derived from collecting the fractions, variations in sample preparation and producing the overlay of phases, the solvent exchange using centrifugal filters or other random factors. For this work this was not as much of an issue, as no quantitative separation was targeted but only the question whether the fractions that are collected are different from one another and a separation takes place. Such a separation of different liposomal fractions, with different EM-diameters, was accomplished at least with centrifugation number 1 and 11 to 16. For future centrifugations, an improvement over the current instrumentation, which only allows up to 2.5×10^4 g, could be an ultracentrifugation with up to 100×10^4 g. However, under these conditions, liposome stability might be an issue.

Further tests are needed to verify the presence of virus inside the liposomes and the effectiveness of the purification. The Western Blot had visible bands in samples using a VP2 specific antibody. SDS-PAGE using silver staining was not sensitive enough for the amounts of virus present after the purification and desalting procedure, but the method in general worked as a band was found with undiluted virus stock.

The addition of the synthetic peptide GALA lead to a visible shift in the size distribution of untreated and treated liposomes that were either prepared with or without HRV-A2 when using GEMMA. In a future work, these GALA treated liposomes could be visualized by electron microscopy.

Appendix

Pre-Tests

The pre-tests covered in this chapter comprise of experiments with GFP-labeled P22 VLPs that were done before working with HRV-A2. The aim of these tests was to determine whether fluorescence labeling is a viable option for the verification of virus encapsulated in liposomes.

Virus-like particles (VLPs)

Two aliquots of virus-like particles P22 labeled with green-fluorescent-protein (GFP, 2.3 mg/mL VLPs) were received from Indiana University (Bloomington, IN, USA). The aliquots' solvent (50 mM sodium phosphate, 100 mM sodium chloride, 200 ppm sodium azide, pH 7.0) were also exchanged using centrifugal filters (see Solvent Exchange and Desalting) and furthermore diluted in a ratio of 1:3 [m/m] using 40 mM ammonium acetate with a pH of 7.0.

The VLP stock was used for encapsulation in liposomes just as HRV-A2, with an analogous procedure of creating the liposomes, although with different ratios of stock to pure ammonium acetate: 50 µL of VLP stock was mixed with 950 µL of 40 mM ammonium acetate at pH 8.4 when performing the lipid film hydration, followed by extrusion. For the extrusion, membranes with a pore size of 0.2 µm and 0.4 µm were chosen. The pH was afterwards set to 8.4 using an aqueous solution of ammonia ($NH_3 \cdot H_2O$).

GEMMA: VLPs and Liposomes with VLPs

A GEMMA spectrum was made from the desalted VLPs (Figure 41). It shows multiple peaks as HRV-A2 and other VLPs that were measured by the working group (but are not shown) do.

The overlay of the spectra of the liposomes with GFP-labeled P22 VLPs and the VLP stock (in an equal dilution as in the liposome sample) on the other hand is similar to the liposomes containing HRV-A2: The VLP graph lies below the liposome signal, meaning that the VLPs would not be detectable in the liposome signal with GEMMA.
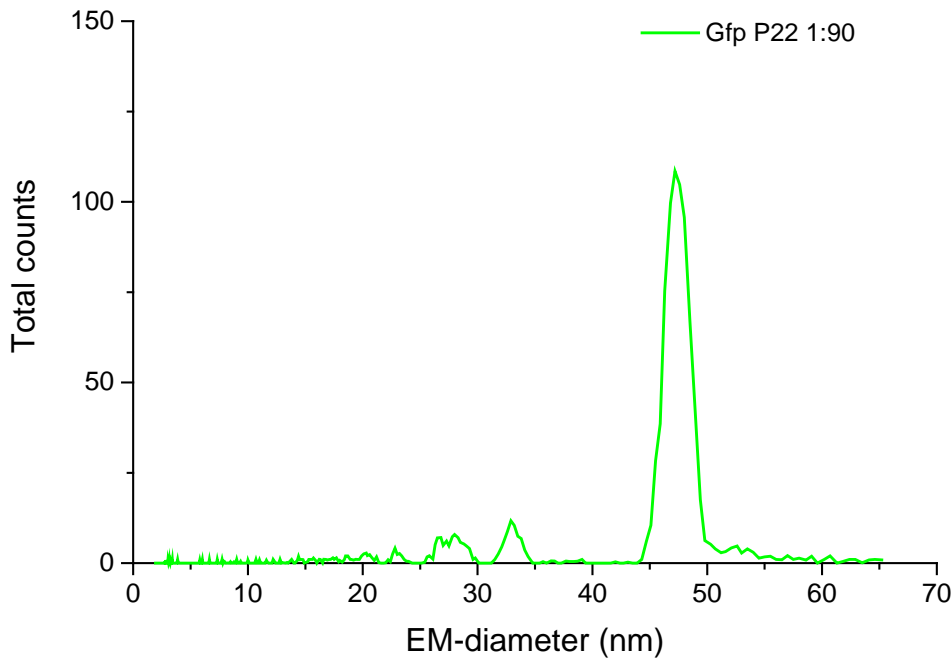
Parameters

40 mM NH_4COOCH_3 pH 7

Sheath flow: 2.5 l/min
Voltage: 2.00 kV
CO_2 in: 0.1 l/min

Air in: 1.0 l/min
PSID: 4.0
Scan time: 150 s
Retrace: 30 s
Capillary ID: 25 µm

Figure 41: GFP-labeled P22 VLP.
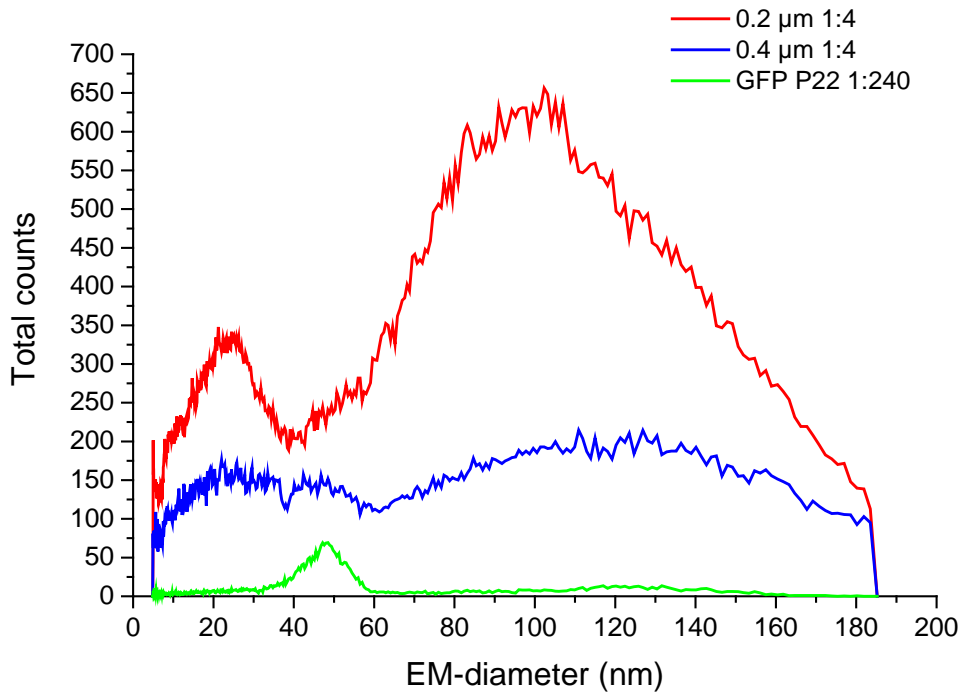
Parameters

40 mM NH_4COOCH_3 pH 7

Sheath flow: 2.5 l/min
Voltage: 2.00 kV
CO_2 in: 0.1 l/min

Air in: 1.0 l/min
PSID: 4.0
Scan time: 150 s
Retrace: 30 s
Capillary ID: 25 µm

Figure 42: Liposomes created with added P22 VLPs, plotted against the P22 VLP stock.

Fluorescence measurements with VLPs

The GFP-labeled P22 VLPs were also measured with a Typhoon FL 9500 laser scanner (GE Healthcare, Chalfont St. Giles, United Kingdom). This was done in order to determine up to which dilution fluorescence would be observable.

As samples the stock (1:3 dilution from the aliquot) and dilutions 1:30, 1:300, 1:3000, 1:30000, 1:300000 and 1:3000000 were pipetted on microscopy cover slides and measured.

Based on the size of the microscopy slides (23.8 x 40 mm) and the images (see Figure 43 and Figure 44) the area covered by the samples was calculated. It was approximately 2 mm², with the exception of the stock sample (1:3 dilution) with approximately 5 mm².

Pure ammonium acetate as blank (number 8 on the slides) and ultrapure water (number 9 on the first slide) were also applied. Two different methods were used. They are given together with the samples of interest mentioned above in the table below.

Table 9: Settings and samples for the absorbance measurements of the VLPs

Methods and filter	GDye 100: Laser 473 nm / Filter BPB1 (530DF20 nm) Alexa Fluor 488: Laser 473 nm / Filter LPB (Y510)						
Samples	1:3	1:30	1:300	1:3000	1:30000	1:300000	1:3000000
Number on slide	1	2	3	4	5	6	7
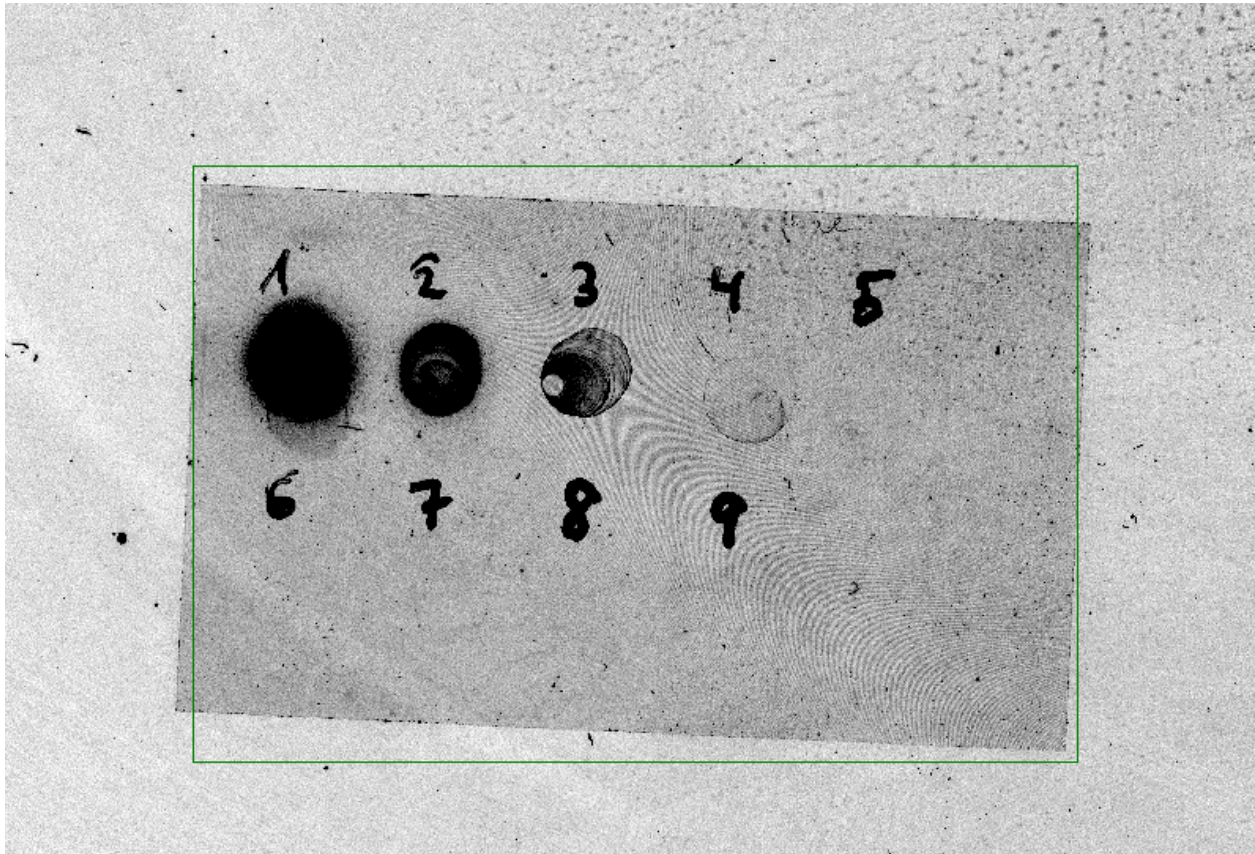
Figure 43: Fluorescence measurement of VLPs, method GDye 100. The sample dilutions applied were given a number (in round brackets): 1:3 (1), 1:30 (2), 1:300 (3), 1:3000 (4), 1:30000 (5), 1:300000 (6), 1:3000000 (7), blank (8), ultrapure water (9).

Figure 43 and Figure 44 both show that fluorescence signals are visible up to a dilution of 1:3000. A clear signal however is found only up to a dilution of 1:300. This in the range of a 1:5 dilution regarding the concentration of the liposomes containing the VLPs. Since the result is based on free VLPs, it was concluded that the level of fluorescence observed could be too low when the VLPs are inside the liposomes. Especially for the collection using GEMMA, lower than 1:5 diluted liposome preparations lead to problems with the electrospray as the capillaries are clogged.

Additional tests in the future, using a VLP or virus with more GFP attached to it or a scanner with higher sensitivity, should be done. Regarding the methods used, both GDye 100 and Alexa Fluor 488 are viable options.
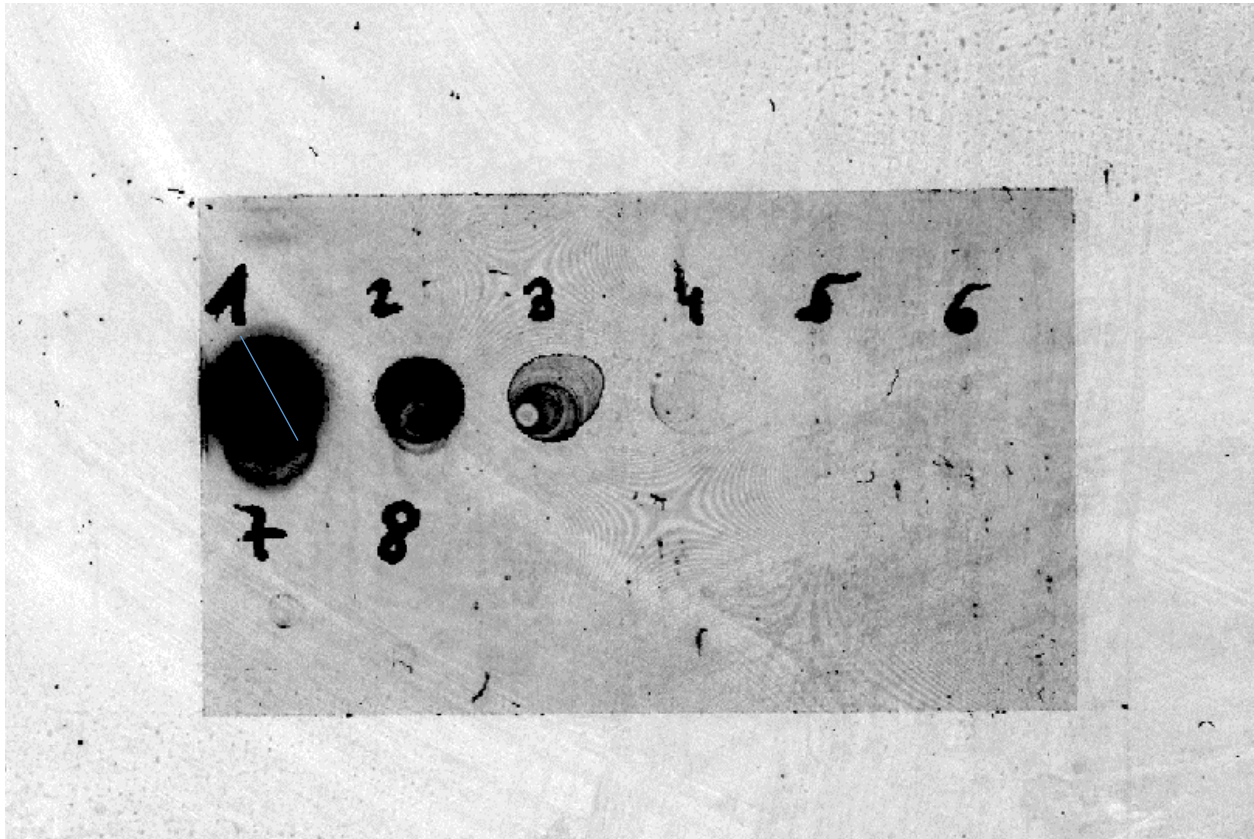
Figure 44: Fluorescence measurement of VLPs, method Alexa Fluor 488. The sample dilutions applied were given a number (in round brackets): 1:3 (1), 1:30 (2), 1:300 (3), 1:3000 (4), 1:30000 (5), 1:300000 (6), 1:3000000 (7), blank (8).

Collection of Liposomes on wafers and atomic force microscopy (AFM)

Atomic force microscopy (AFM) was performed with liposomes collected on wafers made of polished silicon. These wafers were stored in a closed box, taken out with tweezers and cleaned using isopropanol before collection. The liposomes were extruded using 0.1 µm pore diameter membranes and were either empty or contained GFP-labeled P22 VLPs. The instrument used was a Bruker MultiMode8 HR AFM (Billerica, MA, USA).

The settings of the device are found in Table 10 below. The instrument was running in "tapping mode".

Table 10: Settings of the AFM measurement

Scan	Feedback	Limits	Additional settings
• Scan size: 1 - 5 µm • Aspect ratio: 1 • X offset: 0 • Y offset: 0 • Scan angle: 0° • Scan rate: 1.99 Hz • Sample line: 512	• Integral gain: 3.00 • Prop. gain: 2.00 • Ampl. Setpoint: 250 mV (variable) • Drive frequency: 292.861kHz (variable) • Drive Amplitude: 18.31 mV	• Z Limit: 3.888 µm • Reduced Z delay: 2s • Z auto center Boundary: 0 %	• RMS: 0.41 Amplitude (Start) • Vert: -2.79 (Start) • Sum: 1.98 (Start) • Excitation frequency: 3 kHz

The collector was cleaned with isopropanol before usage. Then a waver was attached atop the electrode using double-sided tape as seen in Figure 45.

A GEMMA spectrum was measured prior to collecting the samples. Based on the spectrum the peak maximum in the area around 100 nm was determined. The voltage was manually adjusted so that only particles at the size maximum could exit. Then the tube connection between DMA and CPC was swapped to connect the DMA with the collector and the collector was turned on with a voltage of around 3 kV on the counter electrode.

Figure 45: Collector, left: electrode without waver, right: electrode with silicon waver attached.

Four different liposome preparations were collected. These are listed in Table 11. The collection time for the individual sample was dependent on the condition of the capillary, because clogging was found to be an issue with increasing collection time and the addition of GALA.

The number of particles collected on the wafers was calculated as well, based on the count number found in the GEMMA spectrum. This count number (in counts per nm) was then divided with the scan time per nm (0.8 s/nm), which is derived from the scan time for the spectrum of 150 s and an observed size range within this time of 185 nm. The resulting counts per second where then multiplied with the collection time in seconds, resulting in the theoretical number of particles that passed the DMA.

$$Number\ of\ particles\ = \frac{Counts\ in\ spectrum\ at\ collected\ size\ [\frac{particles}{nm}]}{0.8\ [\frac{s}{nm}]} * collection\ time\ [s]$$

Equation 2: Calculation of the relative count number based on total counts

75

Table 11: Samples for AFM, their collection time and theoretical particle number on the wafers

Sample	Collection time [h:mm]	Collected size [nm]	Theoretical particle number [10^6]
Liposomes 0.1 µm, pH 7	2:00	91.0	7.32
Liposomes 0.1 µm, pH 5, 5 µM GALA	2:30	95.2	8.25
Liposome 0.2 µm with VLP, pH 5	2:53	103.2	7.77
Liposome 0.2 µm with VLP, pH 5, GALA 5 µM	3:00	100.5	5.58

The pictures taken with the AFM are found below (Figure 46, Figure 49, Figure 50 and Figure 53). The GEMMA spectra belonging to the samples are also found below (Figure 47, Figure 48, Figure 51 and Figure 52).

The first figure shows empty liposomes that are disintegrated on the waver (splash-like shape) as well as potentially intact ones. The GEMMA spectrum of that collection shows that the number of liposomes detected after collection has decreased. A reason for that might be the sedimentation of the liposomes inside the Eppendorf tube over the course of the collection.

The GEMMA spectrum of the second collection, where GALA was added to the empty liposomes, show two almost identical curves with the same peak height. This is in contrast to the spectrum of the empty liposomes. Even more different is the spectrum of the liposomes containing VLPs with added GALA, where the count number is higher after the collection than before. In this case however, the capillary was flushed after collection using pure ammonium acetate.

A problem found with the AFM is seen in the AFM pictures of the three samples following the empty liposomes. There are strong artifacts found in all of them. A reason for these artifacts could be that the AFM needle that is gliding over the waver surface adsorbs material (i.e. lipids) from the waver, as the intensity of these artifacts increased over the measurement times. A solution would be to change the AFM needle after every sample. This, however, would be costly. As a result, electron microscopy was favored over AFM for visualization.
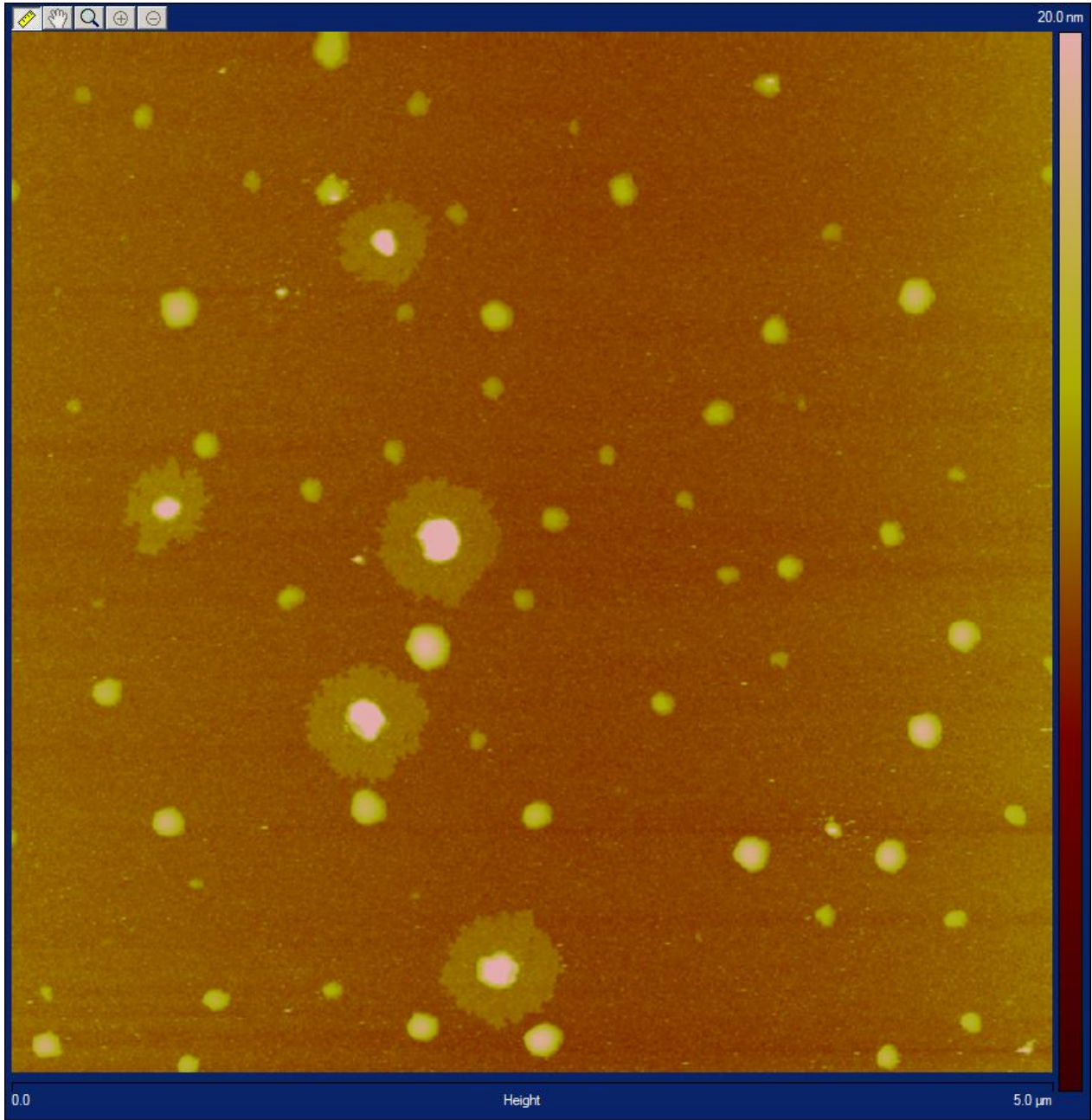
Figure 46: AFM picture of empty liposomes (pH 7)
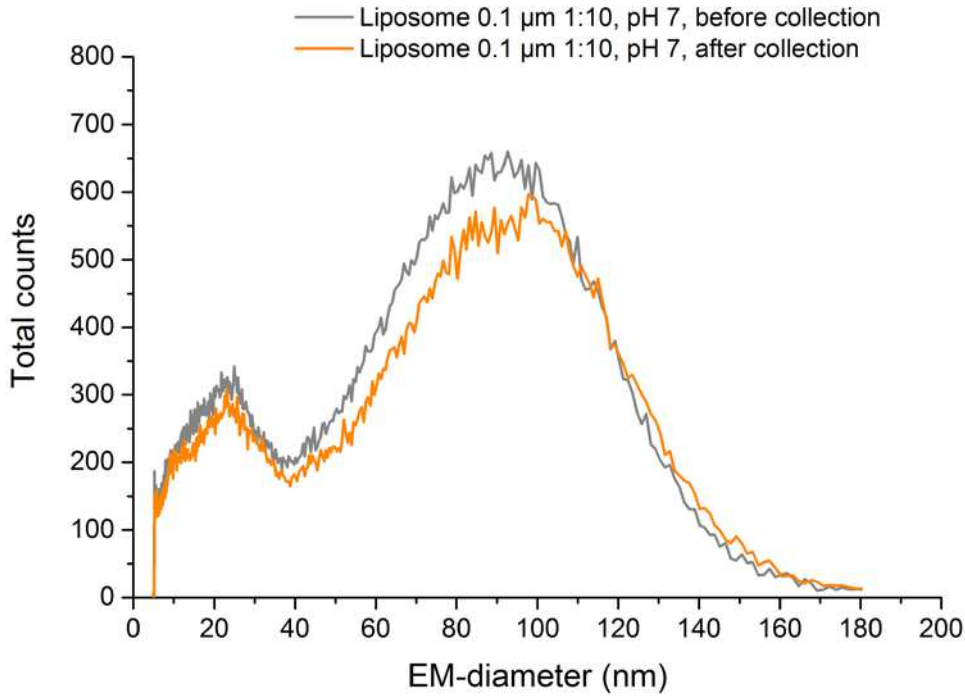
Parameters

40 mM NH_4COOCH_3 pH 7

Sheath flow:	2.5 l/min
Voltage:	1.99 kV
CO_2 in:	0.1 l/min
Air in:	1.0 l/min
PSID:	4.0
Scan time:	150 s
Retrace:	30 s
Capillary ID:	25 µm

Figure 47: Overlay of spectra of empty liposomes, before and after collection
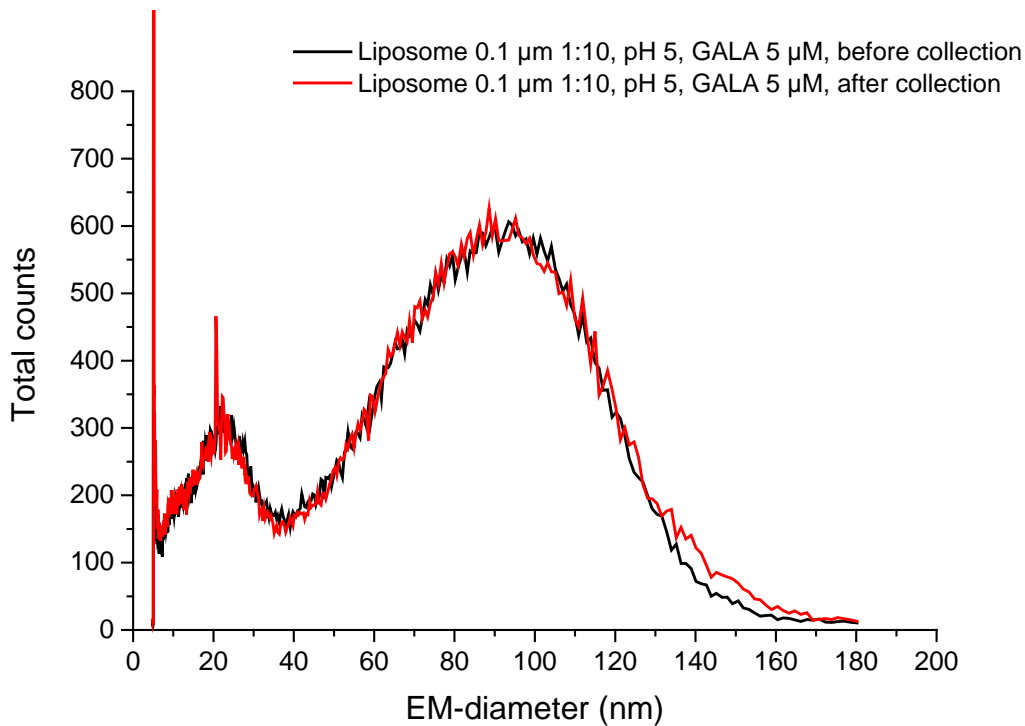
Parameters

40 mM NH_4COOCH_3 pH 5

Sheath flow:	2.5 l/min
Voltage:	1.93 kV
CO_2 in:	0.1 l/min
Air in:	1.0 l/min
PSID:	4.0
Scan time:	150 s
Retrace:	30 s
Capillary ID:	25 µm

Figure 48: Overlay of spectra of empty liposomes with added GALA, before and after collection
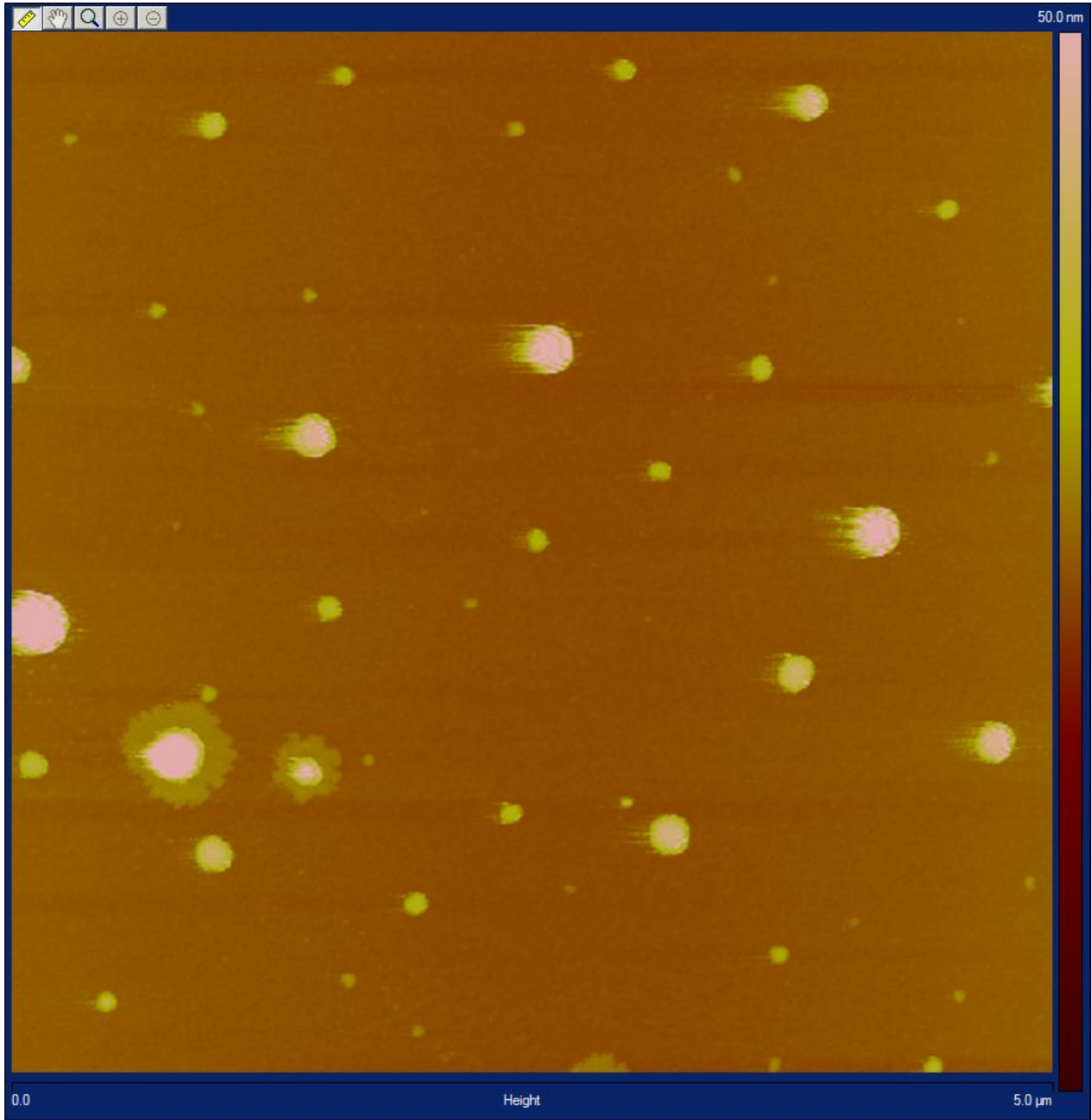
Figure 49: AFM picture of empty liposomes with added GALA (pH 5, 5 µM GALA).
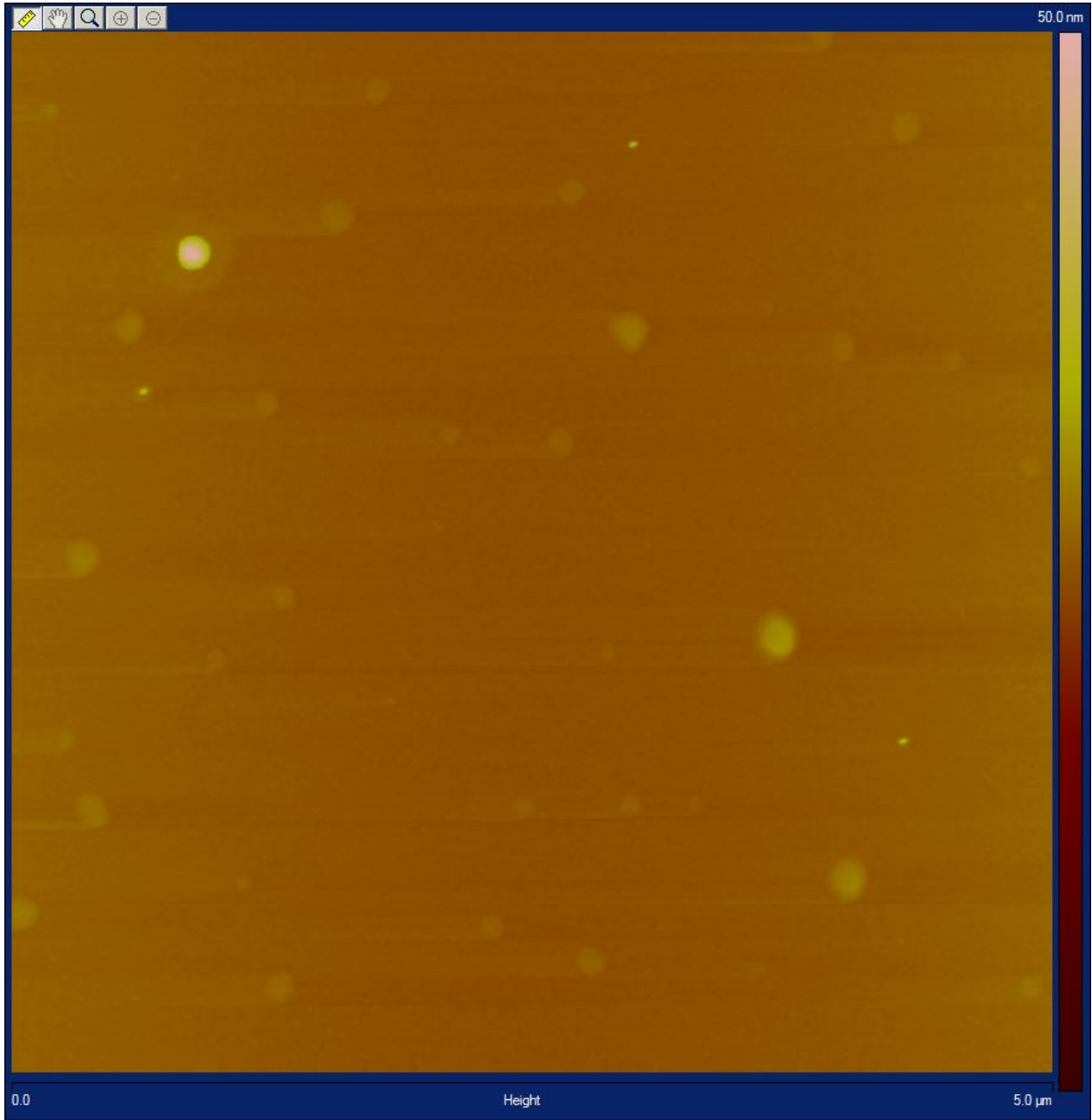
Figure 50: AFM picture of liposomes encapsulating GFP-labeled P22 VLPs.
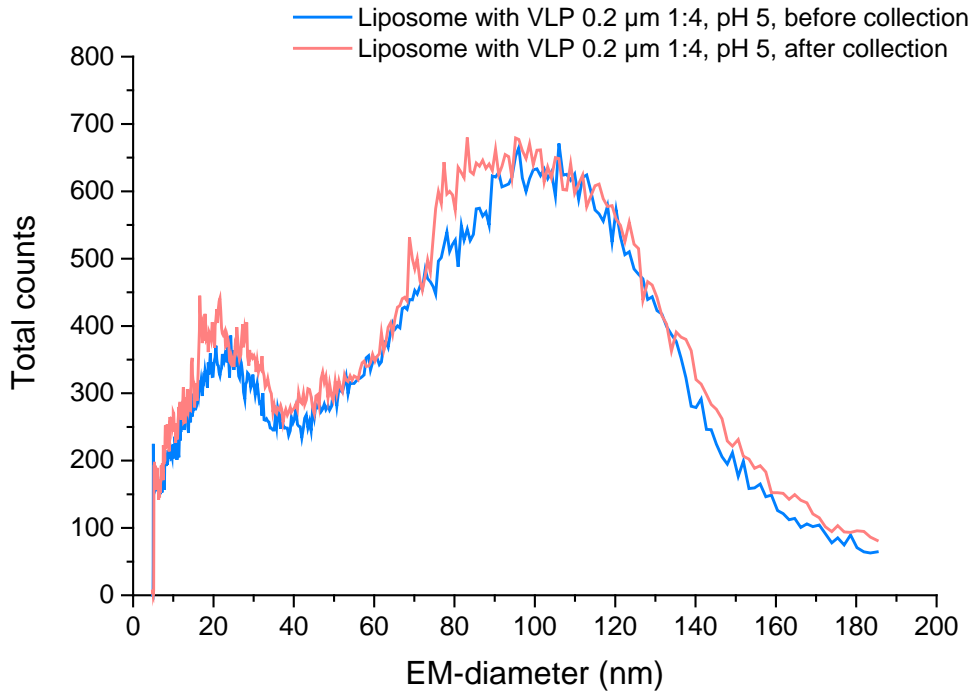
Parameters

40 mM NH_4COOCH_3 pH 5

Sheath flow:	2.5 l/min
Voltage:	1.86 kV
CO_2 in:	0.1 l/min
Air in:	1.0 l/min
PSID:	4.2
Scan time:	150 s
Retrace:	30 s
Capillary ID:	25 µm

Figure 51: Overlay of spectra of liposomes encapsulating GFP-labeled P22 VLPs, before and after collection
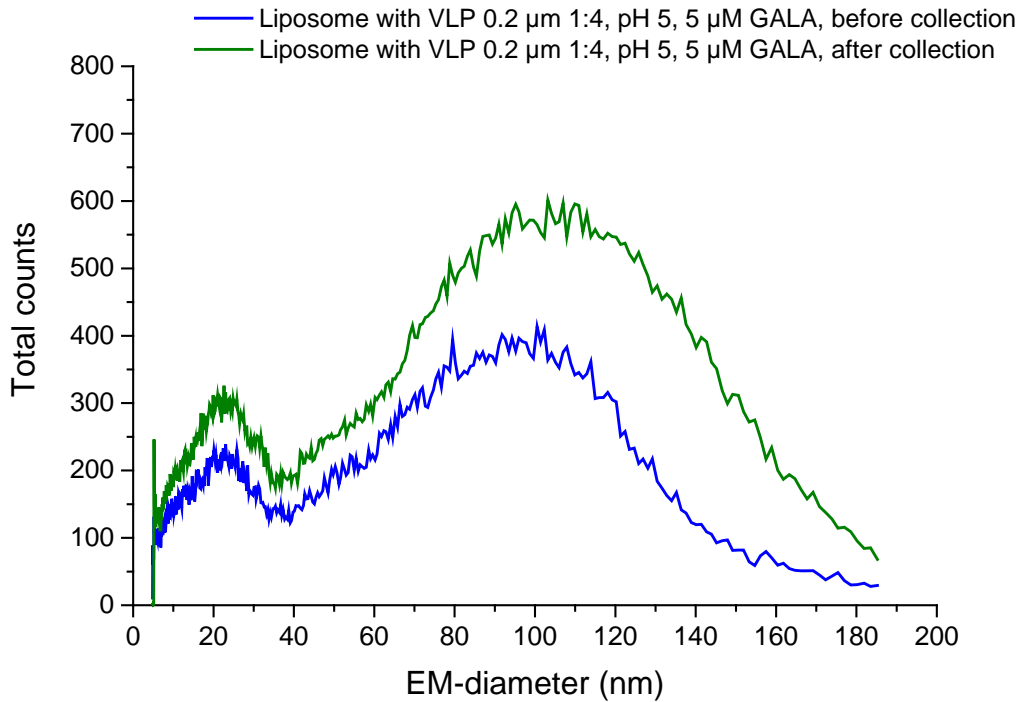
Parameters

40 mM NH_4COOCH_3 pH 5

Sheath flow:	2.5 l/min
Voltage:	1.88 kV
CO_2 in:	0.1 l/min
Air in:	1.0 l/min
PSID:	4.2
Scan time:	150 s
Retrace:	30 s
Capillary ID:	25 µm

Figure 52: Overlay of spectra of liposomes encapsulating GFP-labeled P22 VLPs with added GALA, before and after collection
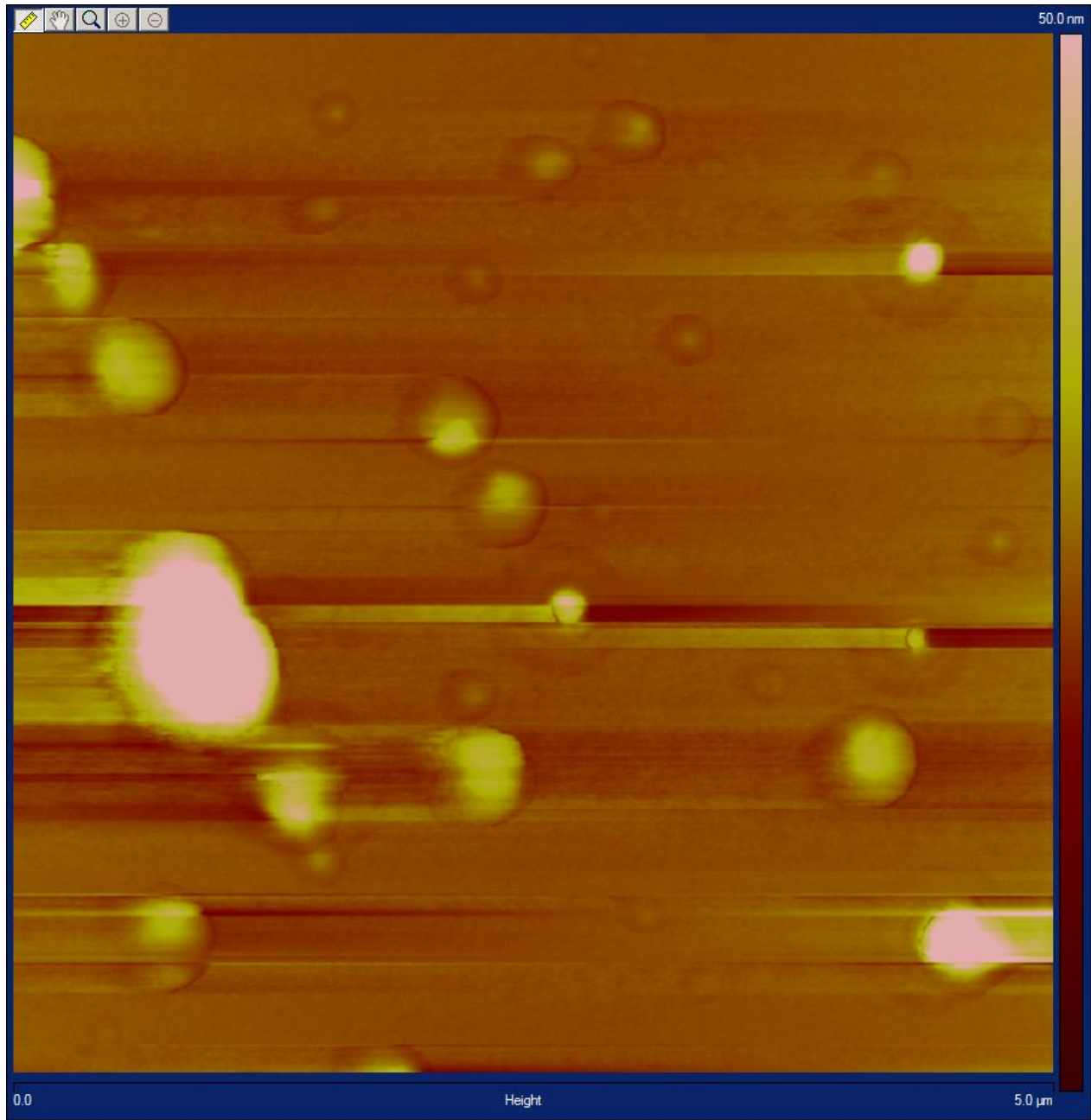
Figure 53: AFM picture of liposomes encapsulating GFP-labeled P22 VLPs (with 5 µM GALA added).

GEMMA: Variation of the tube length between Electrospray unit and DMA inlet

Additional tests were also done after changes in the overall setup of the GEMMA system. Variation of the tube length between the spray chamber and the DMA was suggested to influence the drying time of the particles. The GEMMA spectra of these tests are found below. Samples of empty liposomes and empty liposomes treated with GALA, both with a pH of 5, were used. The tube lengths used were 26.3 cm (shorter than the standard tube), 46.5 cm (standard tube length used for the other measurements), and 81.1 cm (longer than the standard tube). One sample of liposomes was used for all tube lengths, meaning that shifts in a single spectrum are derived from the variation of the tube alone.

Parameters
40 mM NH_4COOCH_3 pH 5

Sheath flow: 2.5 l/min
Voltage: 1.95 kV
CO_2 in: 0.1 l/min
Air in: 1.0 l/min
PSID: 4.0
Scan time: 150 s
Retrace: 30 s
Capillary ID: 25 μm
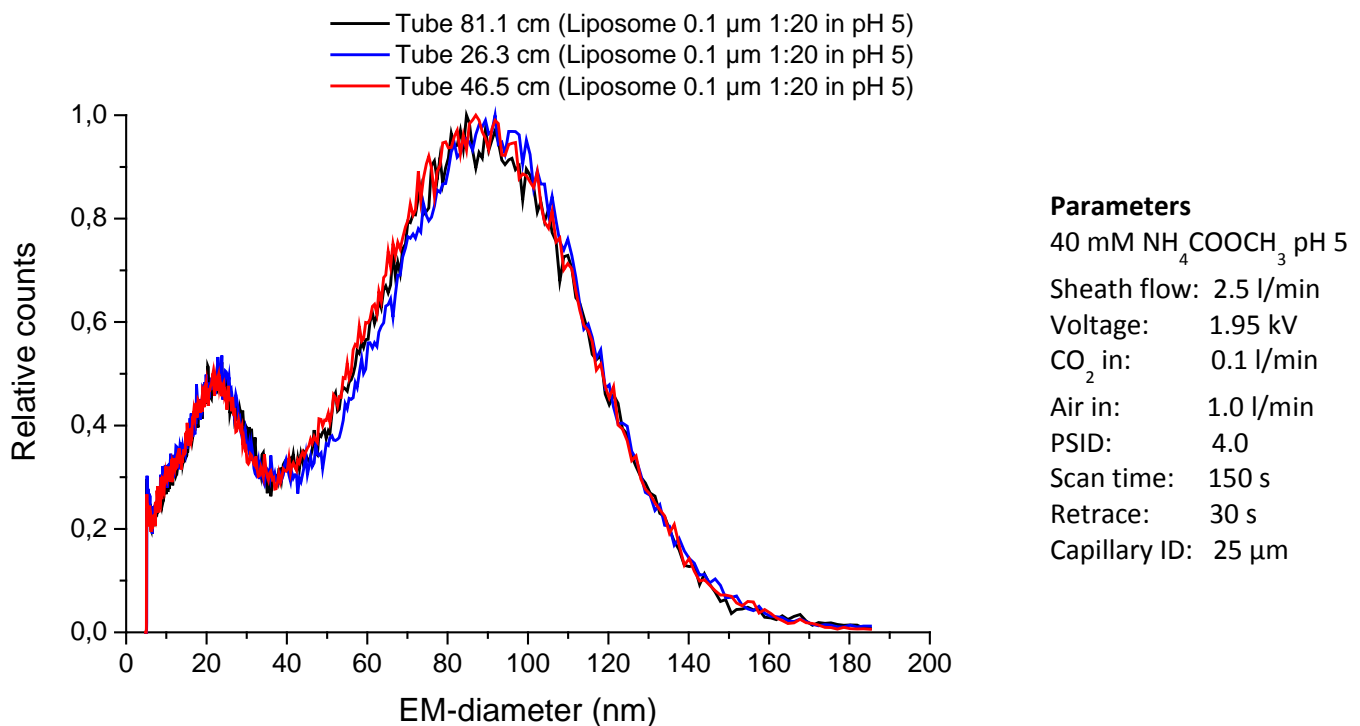
Figure 54: Variation of the tube length between spray chamber and DMA, empty liposomes.

As shown in Figure 54 the variation of the tube length does only show a difference in the spectrum when using a shorter tube than 46.5 cm. Here the size maximum is slightly shifted towards a higher EM-diameter. An explanation for this could be that less of the bigger liposomes are adsorbed in the shorter tube, or that the liposomes are not completely surface dry.

However, there is a more pronounced effect seen with different tube lengths when adding GALA as seen in the next figure.

83

First, by comparing the spectra of the 46.5 cm and the 81.1 cm tube length, the peak between 40 and 130 nm becomes sharper with the increasing tube length. Secondly, there is a shift of the peak front towards higher EM-diameters when decreasing the tube length from 46.5 cm to 26.3 cm. With it the size maximum also changes. This indicates that a shortening of the tube does have a general effect on the measurement, as this effect is also (to a lesser degree) seen in Figure 54. On the other hand, a longer tube length than 46.5 cm does not seem to have a considerable effect on the result, because the spectra only differed after adding GALA.

Parameters

40 mM NH_4COOCH_3 pH 5

Sheath flow: 2.5 l/min
Voltage: 1.98 kV
CO_2 in: 0.1 l/min
Air in: 1.0 l/min
PSID: 4.4
Scan time: 150 s
Retrace: 30 s
Capillary ID: 25 µm
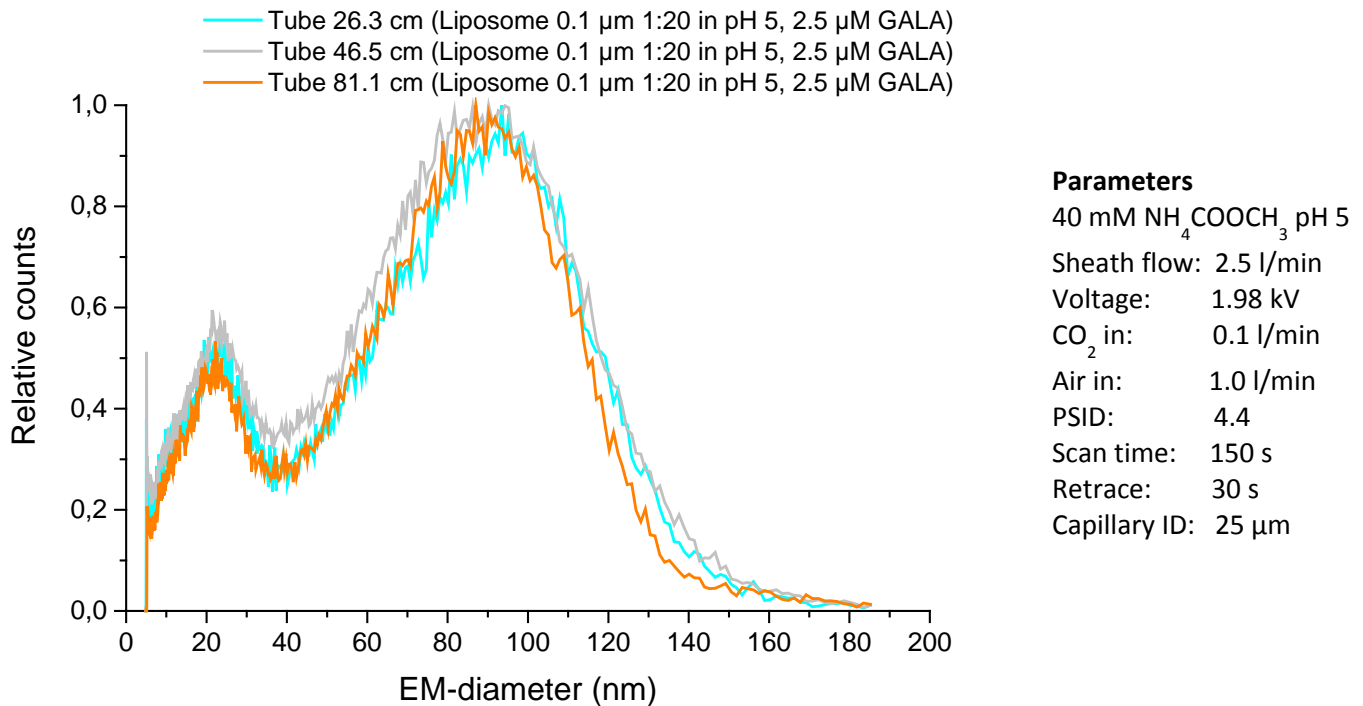
Figure 55: Variation of the tube length between spray chamber and DMA, empty liposomes treated with GALA.

Density gradient centrifugation – Additional centrifugations

The centrifugations number 3 / 4 and 5 / 6 did not show any liposome peaks in the GEMMA spectrum like centrifugation number 2 below, where only a peak front from residual sucrose can be seen. Two duplicates of centrifugations, i.e. number 8 (duplicate of 7) and 10 (duplicate of 9), were not further purified and measured as the approach was dismissed in favor of the first approach during the work. As the figures show there is a strong variation of count numbers found in the fractions from centrifugation to centrifugation.

Parameters	
40 mM NH_4COOCH_3 pH 8.4	
Sheath flow:	2.5 l/min
Voltage:	1.70 kV
CO_2 in:	0.1 l/min
Air in:	1.0 l/min
PSID:	3.6
Scan time:	150 s
Retrace:	30 s
Capillary ID:	40 µm
Centrifugation time:	3:30 h
Sample applied:	20 µL / bottom

Legend:
- 2A (0% Sucrose) 1:10
- 2B (first interphase) 1:10
- 2C (30% Sucrose) 1:10
- 2D (second interphase) 1:10
- 2E (60% Sucrose) 1:10
- 2F (bottom phase) 1:10
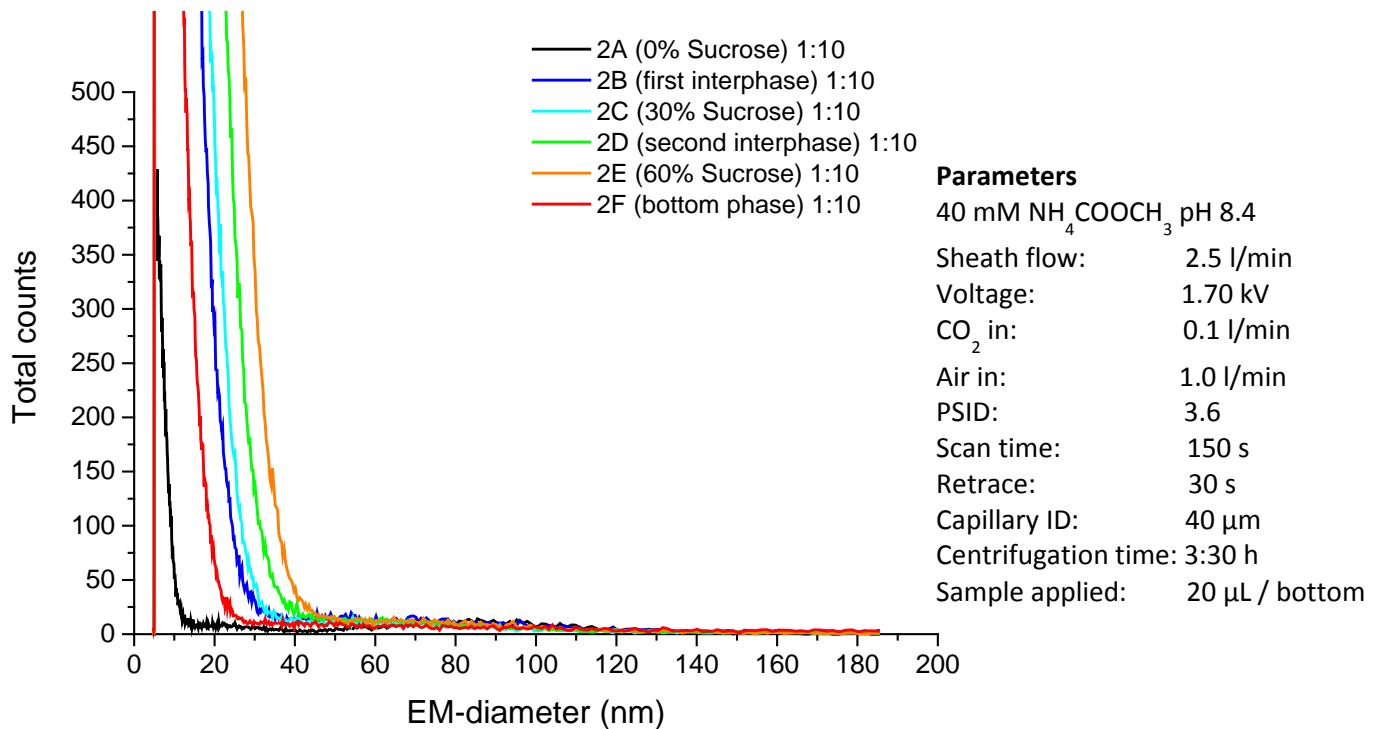
Figure 56: Density gradient centrifugation number 2, fractions after solvent exchange.

Parameters

40 mM NH_4COOCH_3 pH 8.4

Sheath flow:	2.5 l/min
Voltage:	1.89-1.96 kV
CO_2 in:	0.1 l/min
Air in:	1.0 l/min
PSID:	3.6
Scan time:	150 s
Retrace:	30 s
Capillary ID:	40 µm
Centrifugation time:	2:00 h
Sample applied:	60 µL / top
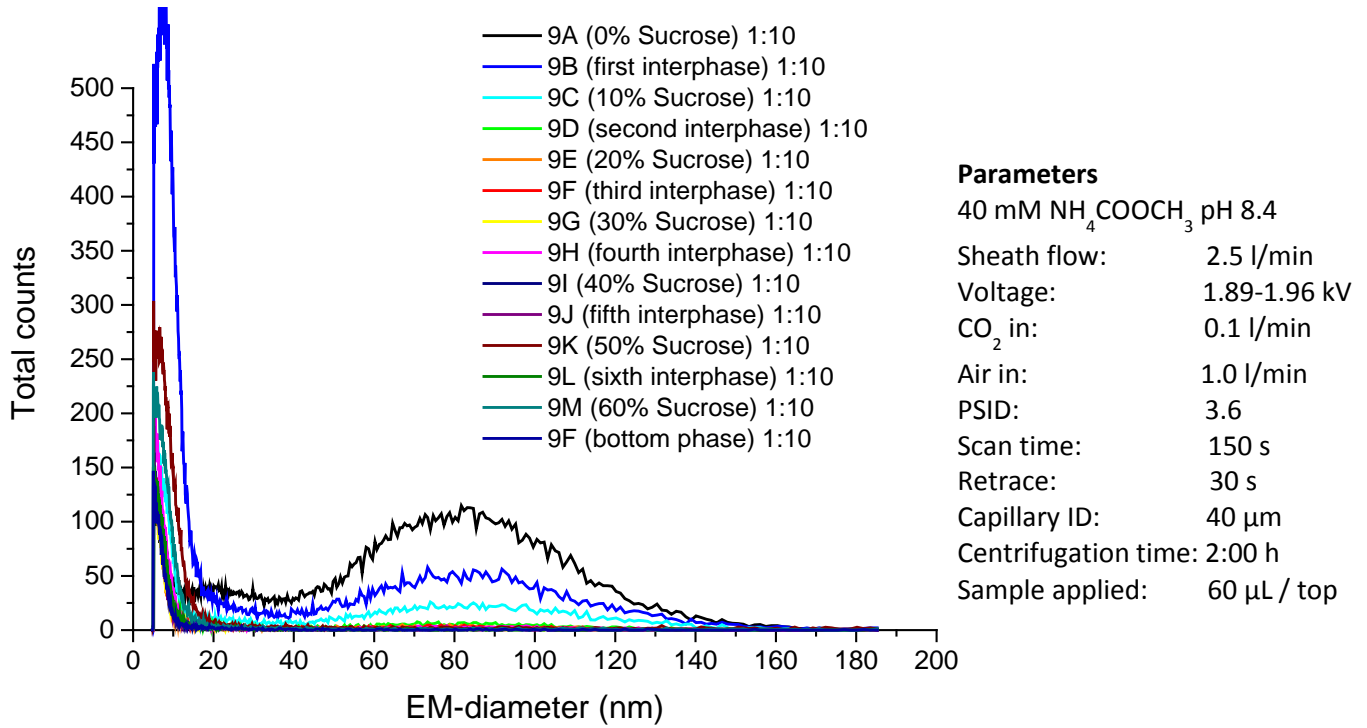
Figure 57: Density gradient centrifugation number 9, fractions after solvent exchange.

Parameters

40 mM NH_4COOCH_3 pH 8.4

Sheath flow:	2.5 l/min
Voltage:	1.75-1.80 kV
CO_2 in:	0.1 l/min
Air in:	1.0 l/min
PSID:	3.6
Scan time:	150 s
Retrace:	30 s
Capillary ID:	40 µm
Centrifugation time:	1:30 h
Sample applied:	50 µL / bottom
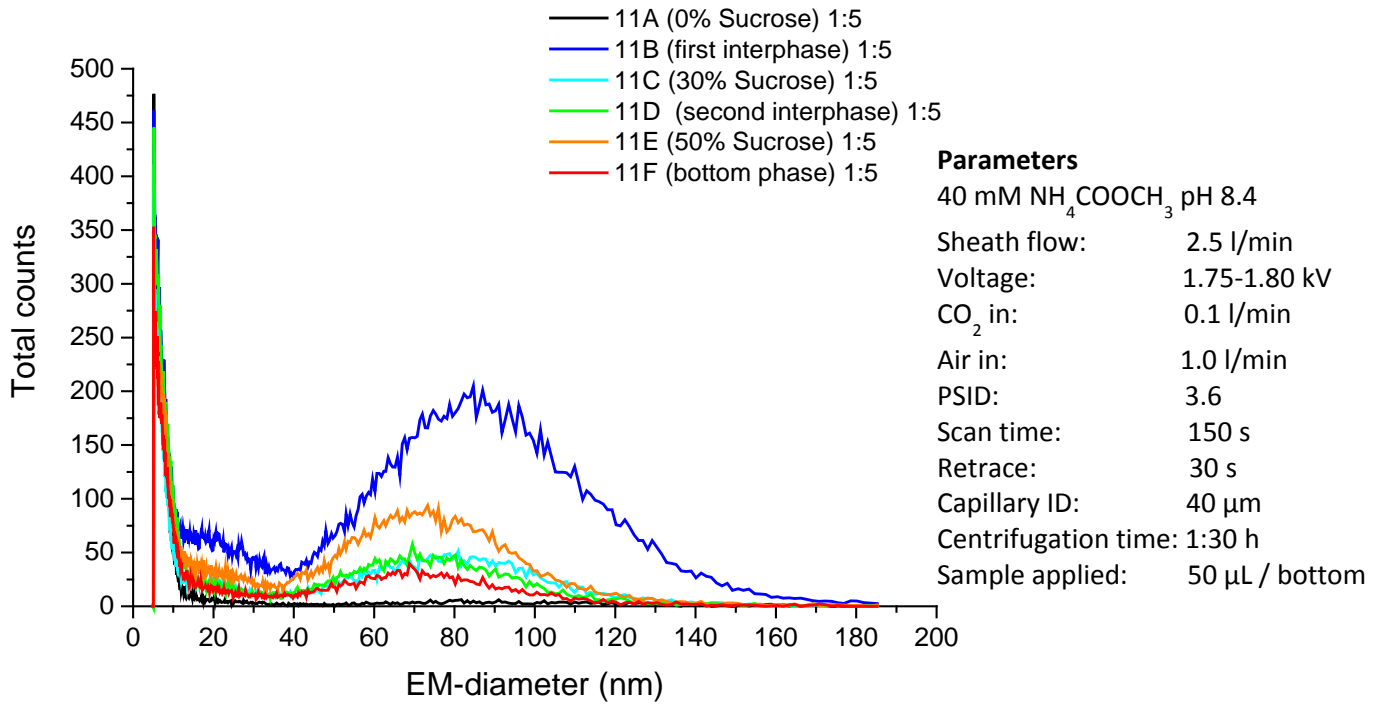
Figure 58: Density gradient centrifugation number 11, fractions after solvent exchange.

Parameters

40 mM NH_4COOCH_3 pH 8.4

Sheath flow:	2.5 l/min
Voltage:	1.75-1.80 kV
CO_2 in:	0.1 l/min
Air in:	1.0 l/min
PSID:	3.6
Scan time:	150 s
Retrace:	30 s
Capillary ID:	40 μm
Centrifugation time:	1:30 h
Sample applied:	50 μL / bottom
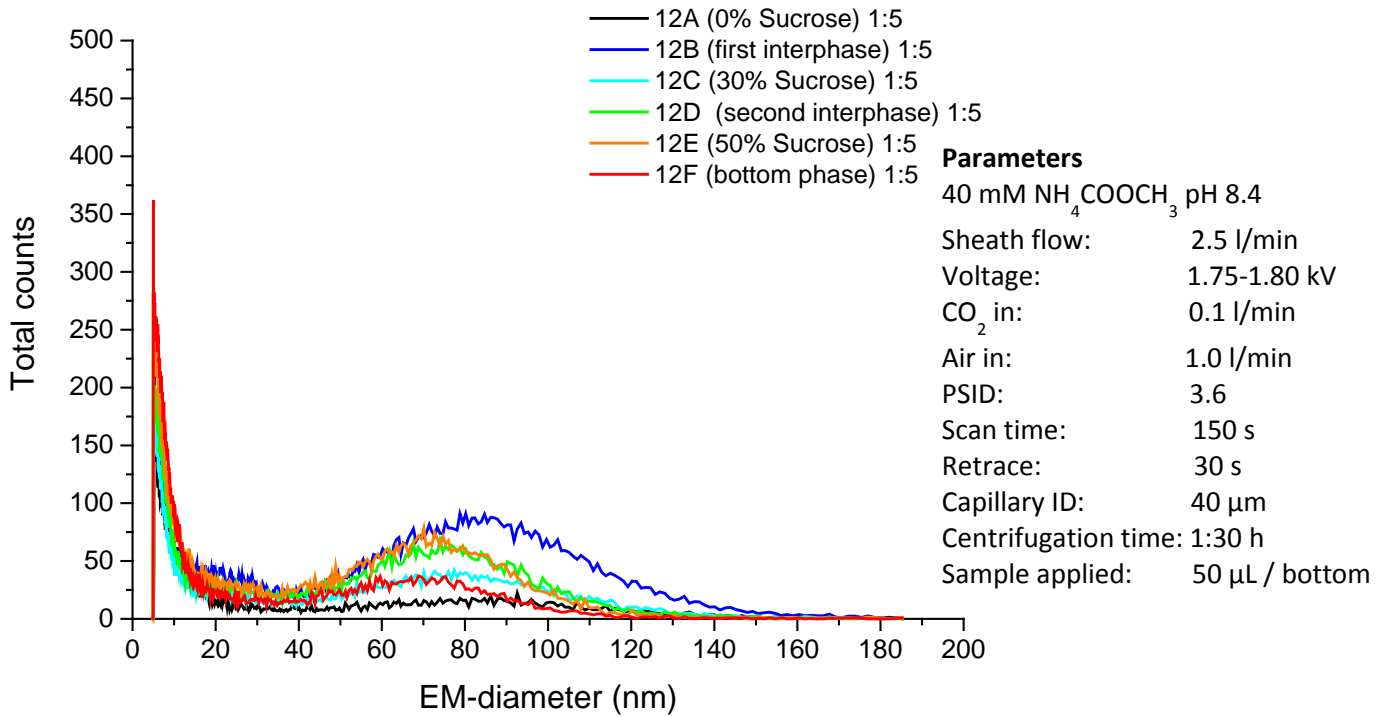
Figure 59: Density gradient centrifugation number 12, fractions after solvent exchange.

Parameters

40 mM NH_4COOCH_3 pH 8.4

Sheath flow:	2.5 l/min
Voltage:	1.75-1.80 kV
CO_2 in:	0.1 l/min
Air in:	1.0 l/min
PSID:	3.6
Scan time:	150 s
Retrace:	30 s
Capillary ID:	40 μm
Centrifugation time:	2:30 h
Sample applied:	50 μL / bottom
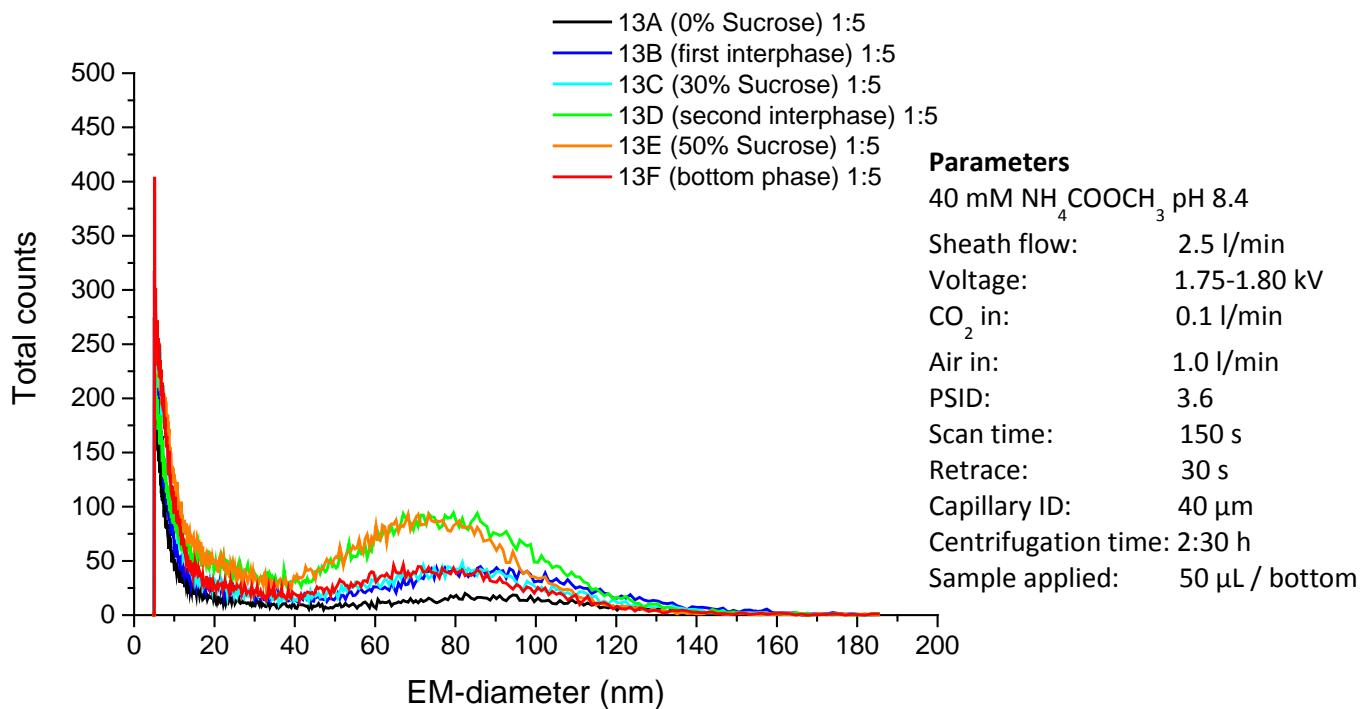
Figure 60: Density gradient centrifugation number 13, fractions after solvent exchange.
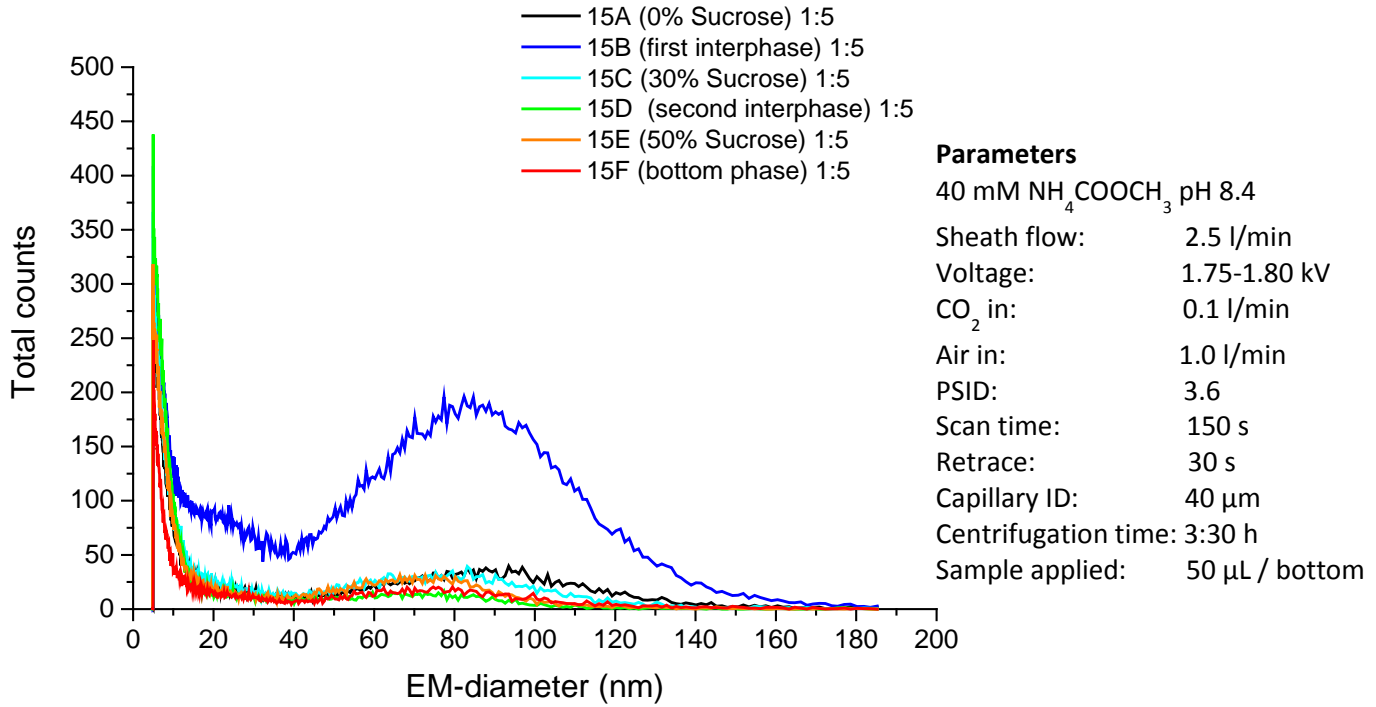
Figure 61: Density gradient centrifugation number 15, fractions after solvent exchange.
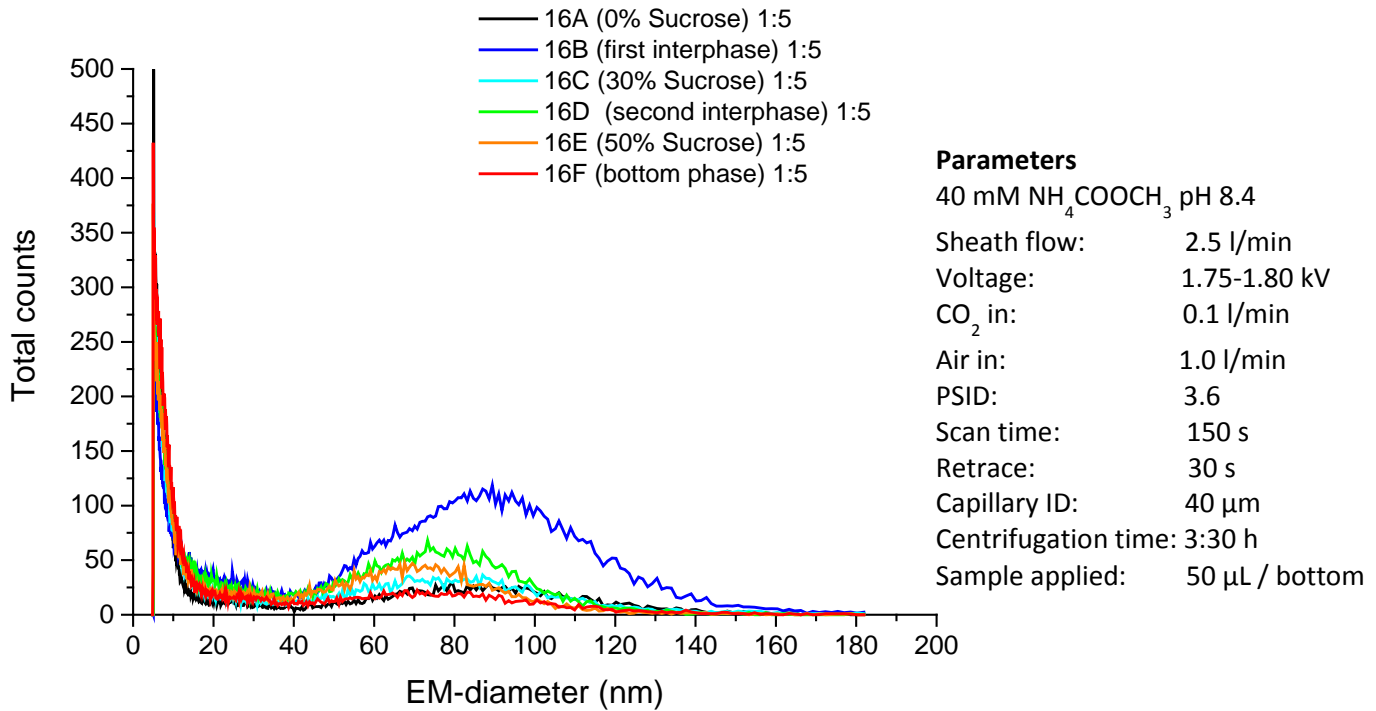
Figure 62: Density gradient centrifugation number 16, fractions after solvent exchange.

SDS-PAGE Gel migration pattern and protein bands of ladder

kDa

260
160
110
80
60
50
40
30
20
15
10
3.5

10 µL of Novex®
Sharp Pre-Stained
Protein Standard on
a NuPAGE® 4–12%
Bis-Tris Gel with
MES SDS Running
Buffer
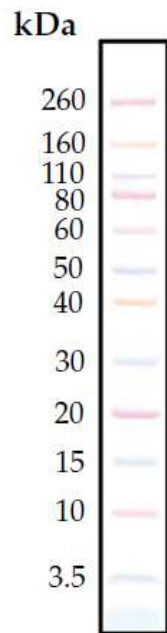
Figure 63: Novex Sharp Pre-stained Protein standard, protein bands on a 4-12 % Bis-Tris Gel with MES SDS running buffer.

Figure 64: Migration pattern of protein standards on Novex gels.

Abbreviations

AFM:	Atomic force microscopy
AgNO$_3$:	Silver nitrate
APS:	Ammonium persulfate
Asp:	Aspartic acid
Bis-Tris:	2-[Bis(2-hydroxyethyl)amino]-2-(hydroxymethyl)propane-1,3-diol
CDHR3 receptor:	Cadherin-related family member 3 receptor
CHCl$_3$:	Chloroform
CH$_3$COOH:	Acetic acid
CH$_3$OH:	Methanol
CO$_2$:	Carbon dioxide
CPC:	Condensation particle counter
Cys:	Cysteine
DLS:	Dynamic light scattering
DMA:	Differential mobility analyser
DSPE:	1,2-Distearoyl-sn-glycero-3-phosphoethanolamine
DTT:	Dithiothreitol
EM:	Electron microscopy
EM-diameter:	Electrophoretic mobility diameter
ENAS / ENPS:	Electrostatic nanometer aerosol sampler / Electrostatic nanoparticle sampler
FWHM:	Full width at half maximum (peak width at half maximum)
GALA:	Synthetic peptide with a repeat of amino acids glutamic acid - alanine - leucine - alanine
GEMMA:	Gas-phase electrophoretic mobility molecular analysis

GFP:	Green-fluorescent protein
Glu:	Glutamic acid
HEPES:	4-(2-hydroxyethyl)-1-piperazineethanesulfonic acid
His:	Histidine
HRV-A2 / HRV II / RV-A2:	Human rhinovirus serotype 2
Hydro-Soy PC:	L-α-phosphatidylcholine from soy
ICAM-1 receptor:	Intercellular adhesion molecule-1 receptor
KCl:	Potassium chloride
KH_2PO_4:	Potassium dihydrogen phosphate
LDL:	Low density lipoprotein
LDS:	Lithium dodecyl sulfate
Lys:	Lysine
MES:	2-(N-morpholino)ethane sulfonic acid
MW:	Molecular weight
NaCl:	Sodium chloride
$NaCO_3$:	Sodium carbonate
Na_2HPO_4:	Disodium hydrogen phosphate
$Na_2S_2O_3$:	Disodium thiosulfate
nES:	Nano-Electrospray
NH_4COOCH_3:	Ammonium acetate
PBTS:	Phosphate buffered saline
Po:	Polonium
Pt:	Platinum
PTA:	Phosphotungstic acid
PVDF:	Polyvinylidene difluoride

REM / SEM:	Rasterelektronenmikroskopie/Scanning electron microscopy
RNA:	Ribonucleic acid
SDS:	Sodium dodecyl sulfate
SDS-PAGE:	Sodium dodecyl sulfate polyacrylamide gel electrophoresis
SEC:	Size exclusion chromatography
STEM:	Scanning transmission electron microscopy
TEM:	Transmission electron microscopy
Tris:	Tris-(hydroxymethyl)-amino methane
Tris-HCl:	Mixture of tris-(hydroxymethyl)-amino methane and hydrochloric acid
VLP:	Virus-like particle

Equations

Figures

Tables

Literature

1.   Bruno, M.T., et al., *HPV16 persistent infection and recurrent disease after LEEP.* Virol J, 2019. **16**(1).
2.   Hu, Z., et al., *Mouse-adapted H9N2 avian influenza virus causes systemic infection in mice.* Virol J, 2019. **16**(1).
3.   Peiris, J.S., M.D. de Jong, and Y. Guan, *Avian influenza virus (H5N1): a threat to human health.* Clin Microbiol Rev, 2007. **20**(2): p. 243-67.
4.   Redding, D.W., et al., *Impacts of environmental and socio-economic factors on emergence and epidemic potential of Ebola in Africa.* Nat Commun, 2019. **10**.
5.   Tsang, T.K., et al., *Effects of infection history on dengue virus infection and pathogenicity.* Nat Commun, 2019. **10**.
6.   Jacobs, S.E., et al., *Human Rhinoviruses.* Clin Microbiol Rev, 2013. **26**(1): p. 135-162.
7.   Verdaguer, N., D. Blaas, and I. Fita, *Structure of human rhinovirus serotype 2 (HRV2).* J Mol Biol, 2000. **300**(5): p. 1179-1194.
8.   Blaas, D. and R. Fuchs, *Mechanism of human rhinovirus infections.* Mol Cell Pediatr, 2016. **3**(1).
9.   Akbarzadeh, A., et al., *Liposome: classification, preparation, and applications.* Nanoscale Res Lett, 2013. **8**(1).
10.   Sanchez-Lopez, V., J.M. Fernandez-Romero, and A. Gomez-Hens, *Evaluation of liposome populations using a sucrose density gradient centrifugation approach coupled to a continuous flow system.* Anal Chim Acta, 2009. **645**(1-2): p. 79-85.
11.   Bangham, A.D., M.M. Standish, and J.C. Watkins, *Diffusion of univalent ions across the lamellae of swollen phospholipids.* J Mol Biol, 1965. **13**(1): p. 238-52.
12.   Zhou, C., et al., *Novel Class of Ultrasound-Triggerable Drug Delivery Systems for the Improved Treatment of Tumors.* Mol Pharm, 2019. **16**(7): p. 2956-2965.
13.   Bilek, G., et al., *Liposomal nanocontainers as models for viral infection: monitoring viral genomic RNA transfer through lipid membranes.* J Virol, 2011. **85**(16): p. 8368-75.

14. Weiss, V.U., et al., *Liposomal leakage induced by virus-derived peptides, viral proteins, and entire virions: rapid analysis by chip electrophoresis.* Anal Chem, 2010. **82**(19): p. 8146-52.

15. Weiss, V.U., et al., *Nano electrospray gas-phase electrophoretic mobility molecular analysis (nES GEMMA) of liposomes: applicability of the technique for nano vesicle batch control.* Analyst, 2016. **141**(21): p. 6042-6050.

16. Hope, M.J., et al., *Production of large unilamellar vesicles by a rapid extrusion procedure: characterization of size distribution, trapped volume and ability to maintain a membrane potential.* Biochim Biophys Acta, 1985. **812**(1): p. 55-65.

17. MacDonald, R.C., et al., *Small-volume extrusion apparatus for preparation of large, unilamellar vesicles.* Biochim Biophys Acta, 1991. **1061**(2): p. 297-303.

18. Urey, C., et al., *Combining gas-phase electrophoretic mobility molecular analysis (GEMMA), light scattering, field flow fractionation and cryo electron microscopy in a multidimensional approach to characterize liposomal carrier vesicles.* Int J Pharmaceut, 2016. **513**(1-2): p. 309-318.

19. Bacher, G., et al., *Charge-reduced nano electrospray ionization combined with differential mobility analysis of peptides, proteins, glycoproteins, noncovalent protein complexes and viruses.* J Mass Spectrom, 2001. **36**(9): p. 1038-52.

20. Kaddis, C.S., et al., *Sizing large proteins and protein complexes by electrospray ionization mass spectrometry and ion mobility.* J Am Soc Mass Spectrom, 2007. **18**(7): p. 1206-1216.

21. Weiss, V.U., et al., *Size and molecular weight determination of polysaccharides by means of nano electrospray gas-phase electrophoretic mobility molecular analysis (nES GEMMA).* Electrophoresis, 2018. **39**(9-10): p. 1142-1150.

22. Konermann, L., *A simple model for the disintegration of highly charged solvent droplets during electrospray ionization.* J Am Soc Mass Spectrom, 2009. **20**(3): p. 496-506.

23. Liu, B.Y.H., D.Y.H. Pui, and B.Y. Lin, *Aerosol Charge Neutralization by a Radioactive Alpha-Source.* Part Part Syst Char, 1986. **3**(3): p. 111-116.

24. Levit, L., *A Study of the Static Discharging Power of a Decaying Alpha Source* in *Proc. ESA Annual Meeting on Electrostatics 2013.* 2013: Cocoa Beach, FL, US.

25. Fuchs, N.A., *On the stationary charge distribution on aerosol particles in a bipolar ionic atmosphere.* Geofis. Pura Appl., 1963. **56**(1): p. 185-193.

26. Wiedensohler, A., *An approximation of the bipolar charge distribution for particles in the submicron size range.* J. Aerosol Sci., 1988. **19**(3): p. 387-389.

27. Njuguna, J. and S. Sachse, *Measurement and sampling techniques for characterization of airborne nanoparticles released from nano-enhanced products.* Woodh Pub S Compos S, 2014(49): p. 78-111.

28. *TSI KNOWS NANOPARTICLE MEASUREMENT* 2019, 22nd October; Available from: https://www.tsi.com/getmedia/55863eb2-6850-4d1d-8407-43cc2296685c/Nano-Brochure_US_5001282_RevD_Web?ext=.pdf.

29. *Electrostatic Precipitator.* 2020, 24th January; Available from: https://www.sciencedirect.com/topics/earth-and-planetary-sciences/electrostatic-precipitator.

30. Jaworek, A., et al., *Two-stage electrostatic precipitators for the reduction of PM2.5 particle emission.* Prog Energ Combust, 2018. **67**: p. 206-233.

31. Li, C.J., S.S. Liu, and Y.F. Zhu, *Determining Ultrafine Particle Collection Efficiency in a Nanometer Aerosol Sampler.* Aerosol Sci Tech, 2010. **44**(11): p. 1027-1041.

32. *Brief Introduction to Coating Technology for Electron Microscopy.* 2019, 22nd October; Available from: https://www.leica-microsystems.com/science-lab/brief-introduction-to-coating-technology-for-electron-microscopy/.

33. Ohi, M., et al., *Negative Staining and Image Classification - Powerful Tools in Modern Electron Microscopy.* Biol Proced Online, 2004. **6**: p. 23-34.

34. Brenner, S. and R.W. Horne, *A Negative Staining Method for High Resolution Electron Microscopy of Viruses.* Biochim Biophys Acta, 1959. **34**(1): p. 103-110.

35. Switzer, R.C., 3rd, C.R. Merril, and S. Shifrin, *A highly sensitive silver stain for detecting proteins and peptides in polyacrylamide gels.* Anal Biochem, 1979. **98**(1): p. 231-7.

36. Chevallet, M., S. Luche, and T. Rabilloud, *Silver staining of proteins in polyacrylamide gels.* Nat Protoc, 2006. **1**(4): p. 1852-8.

37. Shevchenko, A., et al., *Mass spectrometric sequencing of proteins from silver stained polyacrylamide gels.* Anal Chem, 1996. **68**(5): p. 850-858.

38. Wong, A.Y.H., et al., *Fluorescent Silver Staining of Proteins in Polyacrylamide Gels.* J Vis Exp, 2019(146).

39. Towbin, H., T. Staehelin, and J. Gordon, *Electrophoretic Transfer of Proteins from Polyacrylamide Gels to Nitrocellulose Sheets - Procedure and Some Applications.* P Natl Acad Sci USA, 1979. **76**(9): p. 4350-4354.

40. *Western Blotting Principles and Methods.* 2019, 22nd October; Available from: https://www.sigmaaldrich.com/content/dam/sigma-aldrich/docs/Sigma-Aldrich/General_Information/1/ge-western-blotting.pdf.

41. Nakase, I., et al., *Application of a fusiogenic peptide GALA for intracellular delivery.* Methods Mol Biol, 2011. **683**: p. 525-33.

42. Li, W., F. Nicol, and F.C. Szoka, Jr., *GALA: a designed synthetic pH-responsive amphipathic peptide with applications in drug and gene delivery.* Adv Drug Deliv Rev, 2004. **56**(7): p. 967-85.

43. Segrest, J.P., et al., *Amphipathic Helix Motif - Classes and Properties.* Proteins, 1990. **8**(2): p. 103-117.

44. Parente, R.A., S. Nir, and F.C. Szoka, *Mechanism of Leakage of Phospholipid Vesicle Contents Induced by the Peptide Gala.* Biochemistry, 1990. **29**(37): p. 8720-8728.

45. Tycova, A., J. Prikryl, and F. Foret, *Reproducible preparation of nanospray tips for capillary electrophoresis coupled to mass spectrometry using 3D printed grinding device.* Electrophoresis, 2016. **37**(7-8): p. 924-930.

46. Weiss, V.U., et al., *Capillary Electrophoresis, Gas-Phase Electrophoretic Mobility Molecular Analysis, and Electron Microscopy: Effective Tools for Quality Assessment and Basic Rhinovirus Research.* Methods Mol Biol, 2015. **1221**: p. 101-128.

47. Allmaier, G., et al., *Monolithic anion-exchange chromatography yields rhinovirus of high purity.* J Virol Methods, 2018. **251**: p. 15-21.

48. *Sucrose Density Table.* 2019, 26th November; Available from: https://www.internetchemie.info/chemie-lexikon/daten/s/saccharose-dichtetabelle.php.

49. Skern, T., et al., *A Neutralizing Epitope on Human Rhinovirus Type-2 Includes Amino-Acid-Residues between 153 and 164 of Virus Capsid Protein-Vp2.* J Gen Virol, 1987. **68**: p. 315-323.

50. *Recombinant Mouse Anti-HRV2 VP2 Antibody (8F5).* 2019, 3rd December; Available from: https://www.creativebiolabs.net/Anti-HRV2-VP2-Antibody-23040.htm.

51. Zauner, W., et al., *Rhinovirus-Mediated Endosomal Release of Transfection Complexes.* J Virol, 1995. **69**(2): p. 1085-1092.